ISTANBUL TECHNICAL UNIVERSITY ★ GRADUATE SCHOOL

DETERMINATION OF EQUIVALENT ELASTIC PROPERTIES OF PRINTED CIRCUIT BOARDS

M.Sc. THESIS

Erdinç YAKUT

Department of Aeronautics and Astronautics Engineering

Aeronautics and Astronautics Engineering Programme

JULY 2024

ISTANBUL TECHNICAL UNIVERSITY ★ GRADUATE SCHOOL

DETERMINATION OF EQUIVALENT ELASTIC PROPERTIES OF PRINTED CIRCUIT BOARDS

M.Sc. THESIS

Erdinç YAKUT
(511141118)

Department of Aeronautics and Astronautics Engineering

Aeronautics and Astronautics Engineering Programme

Thesis Advisor: Prof. Dr. Aytaç ARIKOĞLU

JULY 2024

İSTANBUL TEKNİK ÜNİVERSİTESİ ★ LİSANSÜSTÜ EĞİTİM ENSTİTÜSÜ

BASKI DEVRE KARTLARININ EŞLENİK ELASTİK ÖZELLİKLERİN BELİRLENMESİ

YÜKSEK LİSANS TEZİ

Erdinç YAKUT
(511141118)

Uçak ve Uzay Mühendisliği Ana Bilim Dalı

Uçak ve Uzay Mühendisliği Programı

Tez Danışmanı: Prof. Dr. Aytaç ARIKOĞLU

TEMMUZ 2024

Erdinç YAKUT, a M.Sc. student of ITU Graduate School student ID 511141118 successfully defended the thesis entitled "DETERMINATION OF EQUIVALENT ELASTIC PROPERTIES OF PRINTED CIRCUIT BOARDS", which he prepared after fulfilling the requirements specified in the associated legislations, before the jury whose signatures are below.

Thesis Advisor :	**Prof. Dr. Aytaç ARIKOĞLU** Istanbul Technical University	....
Jury Members :	**Asst. Prof. Dr. Kaan YILDIZ** Istanbul Technical University	....
	Asst. Prof. Dr. Arif ULU Istanbul Aydın University	....

Date of Submission : 24 May 2024
Date of Defense : 10 July 2024

To my family,

FOREWORD

I would like to express my deepest gratitude to my advisor, Prof. Dr. Aytaç Arıkoğlu, for his unwavering support throughout my studies. His guidance and expertise have been invaluable in shaping my research.
I am also grateful to GUMUSH AeroSpace for their support of this study. Their resources and assistance have made my research possible. I appreciate my colleagues at GUMUSH AeroSpace for their encouragement and friendship during this process.
Lastly, I extend my heartfelt thanks to my family and friends for their constant love and support. I am especially thankful to my wife for her patience and understanding during the demanding times of my research. Her love and support have been my strength.
Thank you to everyone who has played a role in my academic and personal growth. I am truly humbled by your support.

July 2024 Erdinç YAKUT
Astronautical Engineer

TABLE OF CONTENTS

ABBREVIATIONS

3D : Three Dimensional
ANN : Artificial Neural Network
ASTM : American Society for Testing and Materials
BGA : Ball Grid Array
CAD : Computer Aided Design
CLT : Classical Lamination Theory
CSP : Chip Scale Package
CTE : Coefficient of Thermal Expansion
DQM : Differential Quadrature Method
DSB : Double Side Board
ECSS : European Cooperation for Space Standardization
Er : Dielectric Constant
FE : Finite Element
FEA : Finite Element Analysis
FEM : Finite Element Method
GB : Gigabyte
Hz : Hertz
IPC : Institute for Printed Circuits
MLB : Multi Layer Board
NEMA : National Electrical Manufacturers Association
mm : Millimeter
PCBA : Printed Circuit Board Assembly
PCB : Printed Circuit Board
PTH : Plated Through Hole
PWB : Printed Wiring Board
RAM : Random Access Memory
REF : Reference
RMS : Root Mean Square
SSB : Single Side Board
Td : Decomposition Temperature
Tg : Glass Transition Temperature

SYMBOLS

$\boldsymbol{a}, \boldsymbol{b}$	: Dimensions of the plate
$\boldsymbol{\alpha}, \boldsymbol{\beta}$	: Fractional-order time derivatives
C	: Halpin-Tsai equivalent model parameter
$\boldsymbol{\varepsilon}_{\mathbf{xx}}, \boldsymbol{\varepsilon}_{\mathbf{yy}}$	: Normal strain components
$\boldsymbol{E}$	: Young's modulus
$\boldsymbol{E}_1, \boldsymbol{E}_2$	: Young's modulus
$\boldsymbol{E}_{\mathrm{x}}, \boldsymbol{E}_{\mathrm{y}}, \boldsymbol{E}_{\mathrm{z}}$	: Young's modulus components
$\boldsymbol{E}_{eq}$	: Young's modulus of equivalent model
$\boldsymbol{E}_M$	: Young's modulus of matrices
$\boldsymbol{E}_V$	: Young's modulus of void
$\boldsymbol{G}$	: Shear modulus
$\boldsymbol{G}_{13}, \boldsymbol{G}_{12}, \boldsymbol{G}_{23}$	: Shear modulus
$\boldsymbol{G}_{\mathbf{xy}}, \boldsymbol{G}_{\mathbf{yz}}, \boldsymbol{G}_{\mathbf{xz}}$	: Shear modulus components
$\boldsymbol{h}$	: Thickness
$\boldsymbol{h}_i$	: Thickness of the ith layer
$\boldsymbol{\rho}$	: Density
$\boldsymbol{\sigma}_{\mathbf{xx}}, \boldsymbol{\sigma}_{\mathbf{yy}}$	: Normal stress components
$\boldsymbol{T}_{\mathbf{xy}}$	: Moment components
$\boldsymbol{\tau}_{\mathbf{xy}}, \boldsymbol{\tau}_{\mathbf{xz}}, \boldsymbol{\tau}_{\mathbf{yz}}$	: Shear stress components
$\boldsymbol{\theta}_k$	: Angle of lamination
$\boldsymbol{t}$	: Time
$\boldsymbol{\omega}$	: Natural frequency
$\boldsymbol{\gamma}_{\mathbf{xy}}, \boldsymbol{\gamma}_{\mathbf{xz}}, \boldsymbol{\gamma}_{\mathbf{yz}}$	: Shear strain components
$\boldsymbol{\phi}$	: Void fraction
$\boldsymbol{\phi}_M$	: Maximum packing fraction
$\mathbf{c}_{\mathbf{ik}}^{(\mathbf{p})}, \mathbf{d}_{\mathbf{jm}}^{(\mathbf{r})}$	: Weighting coefficients
$\boldsymbol{M}_{\mathbf{xx}}, \boldsymbol{M}_{\mathbf{yy}}$	: Moment components
$\boldsymbol{M}, \boldsymbol{N}$	: Number of grid points in x and y directions
$\boldsymbol{N}_{\mathbf{xx}}, \boldsymbol{N}_{\mathbf{yy}}$	: Components of section force
$\boldsymbol{\nu}$	: Poisson's ratio
$\boldsymbol{\nu}_{\mathbf{xy}}, \boldsymbol{\nu}_{\mathbf{yz}}, \boldsymbol{\nu}_{\mathbf{xz}}$	: Poisson's ratio components
$\boldsymbol{Q}_{\mathbf{xy}}, \boldsymbol{Q}_{\mathbf{yz}}, \boldsymbol{Q}_{\mathbf{xz}}$	: Components of shear force
$\boldsymbol{Q}_{mn}^{(k)}$	: Transformed stiffness coefficients for the k^{th} layer
$\boldsymbol{u}, \boldsymbol{v}, \boldsymbol{w}$	: Displacements in x, y, and z directions
$\boldsymbol{U}_k, \boldsymbol{V}_k, \boldsymbol{W}_k$	: Displacements field through k'th layer in x, y and z directions
$\boldsymbol{\nu}_f$	: Volume fraction

LIST OF TABLES

Page

LIST OF FIGURES

Page

DETERMINATION OF EQUIVALENT ELASTIC PROPERTIES OF PRINTED CIRCUIT BOARDS

SUMMARY

Printed Circuit Boards (PCBs) are indispensable components in modern electronic equipment. They are widely used in various fields such as aerospace, military and defense products, industrial, medical, automotive, telecommunications, maritime, and consumer electronics. Some of these products, the PCBs have a higher volume than other parts of the products. PCBs have significantly effects on these products design and mechanical durability.

PCBs are crucial components in the CubeSats and PocketQubes satellites. CubeSats have main six subsystems and these subsystem except one (that is structure) made from PCB or it is controlled from PCB. PocketQubes are made from PCB also structural system. In this application PCBs can affect other systems and be affected by the environment.

PCB contains various layers, which are substrate, conductive, solder mask, and silkscreen layers. Each layer has a specific duty. Substrate ensures mechanical and thermal durability, insulation between conductive layers. Solder mask, silkscreen layers are used to help for integrating PCB assemblies. The conductive layers are the main layers of the PCBs, and their number is named PCB. The main duty is conducting electronic parts with electronic ways or surfaces. PCBs are made up of layers that are stacked with epoxy.

Due to the variability in design and materials, the mechanical properties of PCBs must be thoroughly tested. However, considering budget and time constraints, this is not always feasible in engineering practice.

This study proposes an equivalent model to efficiently and accurately model the mechanical properties of PCBs used in CubeSats and PocketQubes. The study is divided into two main parts: creating a data pool for elastically equivalent model values and solving an optimization problem to assign coefficients to the equivalent model. Commercial software and software developed for other projects were used. Modal frequency analyses were performed for the equivalent models and detailed natural frequency analyzes were performed using package software. For the optimization problem, the natural frequencies of geometries simulating the primary structure were determined using the differential quadrature method.

The database was created with 2-layer, 4-layer, 6-layer, and 8-layer PCBs with two samples of each. Solid models of each conductive layer were extracted from Altium Designer and modeled in CATIA based on the stack-up design. Layer fill ratios were calculated based on maximum dimensions. Due to the small thickness of some conductive (starting at 0.0175 mm) and insulating layers (starting at 0.26 mm), layers were modeled as shells for finite element analysis. Detailed surface models were prepared in Ansys SpaceClaim and transferred to PATRAN for finite element analysis.

Results were obtained from NASTRAN and added to the data pool for optimization and validation.

To run the optimization code, the natural frequencies were calculated using the differential quadrature method. The material model was based on the Halpin-Tsai model, the normalized root mean square error between the database results and those calculated with quadrature method is minimized for optimization. A brute force approach was used to obtain the material parameters that minimize the selected objective function.

The final comparison showed an average difference of around 3.47% between the equivalent model results obtained with the differential quadrature method and detailed finite element analysis results. One PCB, with a non-rectangular geometry, was solved using finite element analysis due to the inability to use the differential quadrature method. The detailed analysis of the model, solved using a finite element analysis program, took 28,695.00 seconds on a computer with 24 cores and 64 GB of memory, while the analysis modeled with elastic equivalent material model took 1,583.00 seconds on a computer with 12 cores and 32 GB of memory. The solution time was reduced by 94.48% compared to the detailed finite element analysis with average 2.54% difference in results.

Further validation involved comparing the results with the Voigt model, the Halpin-Tsai model is more accurate than the Voigt model, with their differences being around 3% compared to detailed model. The primary goal of reducing analysis time was achieved with a 2.54% mode similarity. Future work could expand creating the database through material property tests and optimizing the equivalent model with more data from more analysis and resonance survey of PCBs with varying fill volumes.

BASKI DEVRE KARTLARININ EŞLENİK ELASTİK ÖZELLİKLERİN BELİRLENMESİ

ÖZET

Baskı devre kartları, günümüz elektronik ekipmanlarında vazgeçilmez bir bileşendir. Bu kartlar; askeri ve savunma sanayisi, endüstri, sağlık hizmetleri ekipmanları, uzay, enerji, telekomünikasyon ve tüketici ekipmanları gibi pek çok alanda sıklıkla kullanılan elektronik ekipmanların temel bileşenleridir. Bu alanların her birinde, baskı devre kartlarının güvenilirliği ve performansı, genel sistemin başarısı ve verimliliği açısından kritik öneme sahiptir. Pek çok ekipmanın içinde baskı devre kartının hacmi ve etkin alanı azdır. Ancak, bazı ekipman ve sistemlerde ise bu kartların varlığı, ekipmanı veya sistemi oluşturan diğer birimlere göre daha fazladır. Özellikle, yüksek performans ve dayanıklılık gerektiren uygulamalarda, baskı devre kartlarının doğru malzeme özellikleri ve tasarımları, sistemin genel başarısını doğrudan etkileyebilir. Bu varlık oranı, baskı devre kartının ekipman ve sistem üzerindeki etkisini veya sistemin ve ekipmanın baskı devre kartı üzerindeki etkisini dikkate alınması gereken bir seviyeye getirmektedir. Bu hacim ve kütle fazlalığı örnekleri arasında küp uydular ve cep uyduları önemli bir yer tutmaktadır. Bu uyduların görevleri sırasında maruz kaldıkları zorlu ortam koşulları ve titreşimler, baskı devre kartlarının dayanıklılığını ve güvenilirliğini daha da önemli hale getirmektedir. Küp uydularda, yapı alt sistemi haricinde elektronik içeren tüm alt sistemler, ağırlıklı olarak baskı devre kartları üzerine kurgulanmıştır. Cep uydularında ise durum, küp uydulara göre daha yüksek bir orandadır; yapısal alt sistem olarak da baskı devre kartları kullanılmaktadır. Bu tür uydularda, baskı devre kartlarının yapısal bütünlüğü, uydunun genel performansı ve misyon başarısı için kritik öneme sahiptir. Küp uydular ve cep uyduları yörüngeye yerleştirilirken fırlatma araçları kullanılmakta ve bu araçlar uydular üzerinde çeşitli yükler oluşturmaktadır: 10 g'lik ($g = 9.806 m/s^2$) karekök ortalama (RMS) değerine sahip rastgele titreşim, 2 g'lik ivmelenme, 125 Hz'e kadar 2.5 g'lik sinüzoidal titreşimler ve fırlatma araçlarının kademe ayrılışları ile ateşleme zamanlarındaki şok yükleri. Uyduların bu yüklere dayanımları test aşamasında belirlenir. Uydu projelerinde test aşaması, üretim aşamasından sonra gelmekte ve projelerin son safhalarına denk düşmektedir. Bu testlerden başarıyla geçemeyen uydular tekrar incelemeye alınmakta ve testten başarılı olana kadar tasarım ve üretim faaliyetlerindeki hatalar ayıklanarak devam ettirilmektedir.

Baskı devre kartları, birkaç farklı malzemenin birbirine yapıştırılması ve elektriksel bağlantıların ilgili yerlere sağlanması ile oluşturulur. Bu katmanlar; yalıtkan katman, iletken katman, lehim maskesi ve serigrafi gibi bileşenlerden oluşur. Her bir katmanın kendine özgü malzeme özellikleri ve işlevleri vardır, bu da baskı devre kartlarının genel performansını ve dayanıklılığını belirler. İletken katman genellikle bakır malzemeden folyo olarak kullanılır ve 0.5 oz (0.0175 mm) kalınlıktan başlayarak ihtiyaca göre 1.0, 1.5, ... ve 13.0 oz olarak değişir. Yalıtkan katmanın malzeme

yelpazesi geniştir. Örnek olarak FR4, Rogger, Mercurywave ve alüminyum gibi malzemeler verilebilir. Bu katmanın temel görevleri, baskı devre kartına dayanıklılık sağlamak ve katmanlar arasında yalıtkanlık görevi görmektir. Katmanlar arası iletimi, via olarak adlandırılan delik içi iletken kaplamaları ile sağlanmaktadır. Bu via'lar, baskı devre kartlarının elektriksel bütünlüğünü sağlar ve katmanlar arasında güvenilir bağlantılar oluşturur. Yalıtkan katman, baskı devre kartının ihtiyaçlarına uygun olarak seçilir. Üretim esnasında da hazır olarak kullanılan ve standartlara uygun prepregler ile elektriksel yalıtım, mekanik ve termal dayanıklılık sağlanmaktadır. Baskı devre kartları, ekipmanların elektronik gereksinimlerine ve tasarımlarına göre şekillenir. Bu sebeple, tasarlanan ve üretilen tüm alt sistemler eşlenik olamaz. Eşlenik olmaması ve sürekli değişen tasarım ve malzeme çeşitliliğinden dolayı, baskı devre kartının mekanik özelliklerinin detaylı belirlenmesi için örneklerinin malzeme özellikleri belirleme testlerine girmesi gerekmektedir. Ancak, bunun bütçesel ve zaman maliyeti düşünüldüğünde, uygulaması mühendislik açısından uygun değildir.

Uyduların maruz kaldıkları ortamları doğru modellemek ve uyduları doğru malzeme özellikleriyle modelleyip analizlerini yapmak, başarım oranını artıracaktır. Aslının aksine aşırı dayanıklı olarak analiz sonuçları elde edilmiş baskı devre kartları testlerde başarısız sonuçlara yol açabilirken, düşük dayanımlı olarak analiz sonuçları elde edilmiş baskı devre kartları ise gereksiz yere fazla mühendislik çabası gerektirecektir. Daha az bilgisayar gücü ve zaman ile daha yüksek doğrulukta modellenmiş bir baskı devre kartı, en optimum çözümün oluşmasına olanak sağlayacaktır.

Bu çalışmada, küp ve cep uydularında kullanılan boyutlardaki baskı devre kartlarının mekanik özelliklerini daha ayrıntılı bir şekilde yansıtmak, ancak zaman verimli bir şekilde modellemek için eşlenik bir model önerilmiştir. Çalışma prensipte iki temel parçadan oluşmaktadır. Birinci kısım, eşlenik modele yönelik değerlerin belirlenmesi için bir veri havuzu oluşturulmasıdır. İkinci kısım ise, bu veri havuzundan alınan verilerin eşlenik modele atanacak katsayıların belirlenmesi için bir optimizasyon probleminin çözülmesidir. Çalışmada, ticari yazılımlar ve başka projelerde geliştirilmiş yazılımlar kullanılmıştır. Optimizasyon çalışmasında, eşlenik modellere ilişkin doğal frekans analizleri gerçekleştirilmiş ve veri havuzu için paket yazılımlar ile belirli koşullar altında detaylı doğal frekans analizleri yapılmıştır. Optimizasyon probleminin çözümü için, asıl geometrinin dış boyutlarını kapsayacak şekilde benzetilmiş geometrilerin doğal frekansları diferansiyel kuadratür yöntemi kullanılarak belirlenmiştir.

Veri havuzu, 2 katlı, 4 katlı, 6 katlı ve 8 katlı baskı devre kartlarının her çeşidinden ikişer adet olmak üzere toplamda sekiz farklı baskı devre kartı ile oluşturulmuştur. Öncelikle, baskı devre kartlarının bilgisayar destekli modellendiği baskı devre kartı tasarım programı Altium Designer'dan her iletken katmanın katı model çıktısı alınmıştır. Bu çıktılar, baskı devre kartının katman yığını tasarımına göre katı modelleme yazılımı olan CATIA ile modellenmiştir. Bu modelleme esnasında, katmanların doluluk hacim oranları hesaplanmıştır. Doluluk hacim oranları diferansiyel kuadratür yönteminde kullanılan maksimum uzunluklara göre hesaplanmıştır. Sekiz katlı ikinci modelde ise doluluk hacim oranı baskı devre kartının maksimum boyutlarına göre hesaplanmıştır. Modellenen baskı devre kartlarının bazı iletken katmanlarının kalınlıkları 0.0175 mm'den, yalıtkan katmanların kalınlıkları ise 0.26 mm'den başlamasından dolayı, sonlu elemanlar analizleri için katmanlar kabuk olarak modellenmiştir. Ek olarak, modelin detayında 0.1 milimetre x 0.1 milimetre uzunluk ve genişliğe sahip yüzeylerin

detaylarından ötürü, katı modeller sonlu elemanlar yazılımına hazırlanmak için Ansys SpaceClaim yazılımında orta yüzeyleri oluşturularak düzenlenmiştir. Düzenlenen yüzey modeller sonlu elemanlar yazılımı PATRAN yazalımına aktarılmıştır. PATRAN yazılımında, analizlerin sonlu elemanlar modeli malzeme özelliklerinin atanması ve sınır koşullarının belirlenmesi ile oluşturulmuştur. PATRAN yazılımında oluşturulan sonlu elemanlar modellerin analizleri NASTRAN yazılımında çözülmüş ve sonuçların ve görselleştirilmesi yine PATRAN yazılımında gerçekleştirilmiştir. 2 katlı ve 4 katlı baskı devre katlarının doğal frekans analizi modelleri ve sonuçları veri havuzuna optimizasyon adımında kullanılması için eklenmiştir. 6 katlı ve 8 katlı baskı devre kartlarının modelleri ve sonuçları ise veri havuzuna doğrulamadaki analizlerde kullanılmak üzere veri havuzuna eklenmiştir.
Eşlenik malzeme modelinin oluşturulmasında Halpin-Tsai modeli baz alınmış ve doluluk üzerine kurgulanan formülasyonu üzerine doluluk hacim oranına istinaden bir formülasyon önerilmiştir. Formülasyonda yer alan eşleme parametresi optimizasyon için kullanılan parametre olmuştur. Optimizasyon parametresinin doğal frekans hesaplamasında kullanımını kolaylaştırmak adına doğal frekanslar optimizasyon adımında da diferansiyel kuadratüre metodu kullanılmış ve doğal frekanslar bu yöntem ile hesaplanmıştır. Halpin-Tsai modeline göre veri havuzu sonuçları ile kuadratüre metot ile hesaplanan sonuçları normalleştirilmiş kök ortalamalarının toplamı en aza indirilecek şekilde optimize edilmiştir. Brute force yaklaşımıyla ile veri havuzu ve malzeme özellikleri değiştirilerek fark optimizasyonu gerçekleştirilmiştir.
Bu çalışmaların sonunda, baskı devre kartlarının eşlenik malzeme modelinin diferansiyel kuadratür yöntemi ile elde edilen analiz sonuçları ile detaylı modellenmiş sonlu elemanlar yöntemi analiz sonuçları kıyaslanmıştır. Kıyaslama sonucu, tüm diferansiyel kuadratür yöntemi ile elde edilmiş doğal frekans analizleri sonuçları arasındaki farkın ortalamasının %3.47 civarında olduğu bulunmuştur. Geometrisinin dikdörtgen olmaması nedeniyle bir baskı devre kartı, diferansiyel kuadratür yöntemi ile çözülememiş ve doğal frekans belirlemesi sonlu elemanlar yöntemi ile yapılmıştır. Bu baskı devre kartında, Halpin-Tsai ve Voigt modellerine göre elastik özellikleri değiştirilmiş ve her katman ayrı yüzey olarak modellenip çözülmüştür. Detaylı doğal frekans analizi sonucuyla eşlenik model analizi sonucu arasında Halpin-Tsai ile elde edilen malzeme modeline göre ortalama %2.54'lük bir fark bulunmuştur. Detaylı model analiz sonuçlarına göre, Voigt ve Halpin-Tsai modelleri arasındaki fark, Halpin-Tsai modelinin sonuçlarının Voigt modeline göre %3 daha iyi olduğunu göstermektedir. Sonlu elemanlar analiz programı ile çözümlenen modelin detaylı analizi, 24 çekirdekli ve 64 GB bellekli bir bilgisayarda 28,695.00 saniye sürerken, elastik eşlenik malzeme ile modellenen analiz, 12 çekirdekli ve 32 GB bellekli bir bilgisayarda 1,583.00 saniye sürmüştür. Çözüm süresi, detaylı sonlu elemanlar analizine göre %94.48 azaltılmıştır. Çalışmanın temel hedeflerinden biri olan analiz süresinin kısaltılması, %2.54'lük bir analiz sonuç benzerliği ile gerçekleştirilmiştir. Gelecek çalışmalarda veri havuzunun genişletilmesi, detaylı modellenmiş analiz sonuçları ile olan benzerliği arttırmaya yardımcı olacaktır. Veri havuzu, malzeme özelliklerini belirleme testleri, daha fazla detaylı analiz modelleri ve sonuçları ile genişletilebilir. Farklı doluluk hacim oranlarına sahip baskı devre kartlarının rezonans taraması yapılarak doğal frekansları belirlenip, diferansiyel kuadratür yöntemi ile eşlenik modelin optimizasyonunda daha fazla veriden yararlanılabilir.

1. INTRODUCTION

The thesis study is done to help the next generation of space technologies. Every smart equipment has an Printed Circuit Board (PCB). PCBs are needed to have good model. When designing an equipment, there is not enough time to model a detailed PCB for each iterate.

1.1 Purpose Of Thesis

Satellites heavily rely on PCBs. However, the intricate details of PCBs in CubeSats and PocketQubes make it time-consuming to model them for analyzing their durability under launch vehicle loads experienced during launch and orbit transfer phases. This study proposes an optimized solution for modeling PCBs during analysis to determine their readiness for these harsh environments.

1.1.1 Printed circuit board

PCBs are used in various applications. These applications can be headlined Aerospace, Defense, Industrial, Medical, etc. PCBs are stacked up by using the conductor and insulation layer to create a pad and a way to connect electronic components and create electronic equipment. PCB has numerous different designs because each application has its own positioning electronic components. They are named for the number of conductor layers. The two-layer PCB has two conductor layers. The layer number can start from one to infinite number. Generally, six and eight conductor number layers used in CubeSat, pocket cube satellite applications. An example of PCB stack-up is given in Figure 1.1.

- Conductor layers (yellow): These are the thin metal layers (usually copper) that carry electrical signals.

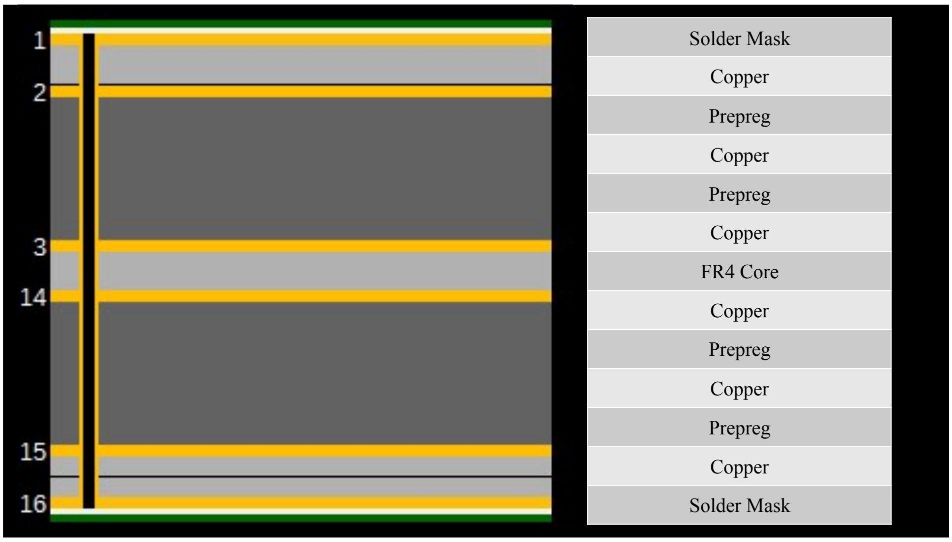

Figure 1.1 : PCB stack-up example.

- Insulating layers (gray): These are the thin layers of non-conductor material (likely epoxy resin) that separate the conductor layers and prevent unwanted electrical connections. Figure 1.1 depicts multiple gray layers, indicating a multilayered PCB.
- Silkscreen (green): This is the non-conductor green layer applied on the outer surface of the PCB for labeling components, reference designators, and other markings.
- The via hole is a plated hole (likely copper-plated) that goes through multiple gray insulating layers, electrically connecting the conductor layers on either side. [1]

Electronic components are placed on top or bottom side of the PCB. A PCB with electronic components is named PCB assembly. An example of the PCB assembly is given in Figure 1.2 [2].

1.1.1.1 Materials of insulating layers

FR-4 is a flame-retardant epoxy resin laminate developed by the National Electrical Manufacturers Association (NEMA) in 1968 [3]. It is the most commonly used PCB dielectric and core layer material [4]. FR-4 is reinforced with woven fiberglass cloth, providing excellent strength-to-weight ratios and near-zero water absorption, making it an effective electrical insulator with significant mechanical strength, suitable for various applications even in humid conditions.

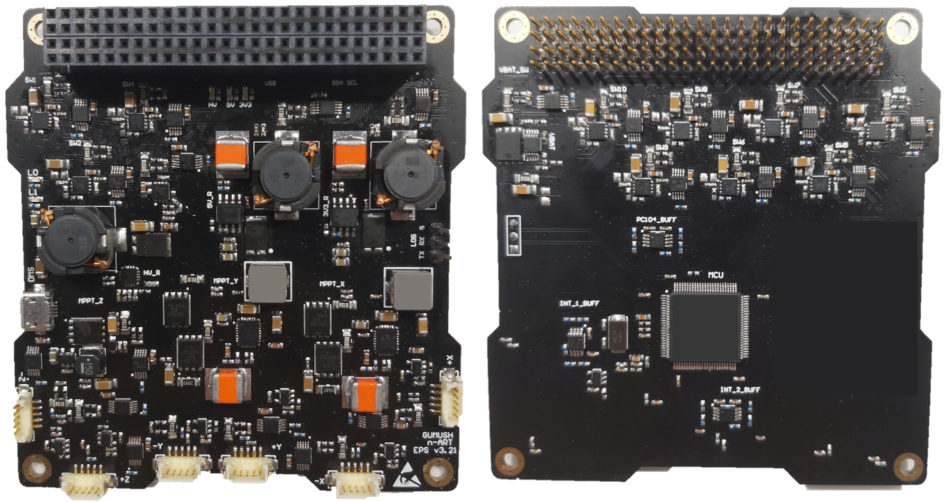

Figure 1.2 : PCB assembly example.

FR-4 materials are defined by the Institute for Printed Circuits (IPC) standards at Base Materials for Printed Boards, which specify different types of woven laminate. Common weave styles for FR-4 laminate materials include 1080, 2116, and 7628, as defined by IPC standards. Grade designations for glass epoxy laminates are G-10, G-11, FR-4, FR-5, and FR-6. Of these, FR-4 is the most widely used today. G-10, the predecessor to FR-4, lacks the self-extinguishing flammability characteristics of FR-4 and has been largely replaced by FR-4 in most applications.

FR-4 is extensively used in the production of rigid PCBs. A thin layer of copper foil is laminated to one or both sides of an FR-4 glass epoxy panel, creating “copper-clad laminates.” These sheets are etched to form circuitry, producing single or multilayer PCBs.

Additional PCB materials and properties

- **CEM-3:** Similar to FR-4 but uses a different type of glass fabric, resulting in a milky white, smooth material.

- **Prepreg:** Epoxy-coated glass fabric used as a dielectric in multilayer PCBs and as raw material for FR-4. Prepreg layers are laminated together to form the adhesive bonds in the PCB.

- **Flexible and Rigid-Flex PCBs:** Made using materials like Kapton, these boards can fold and twist, making them ideal for compact packaging. Kapton variants include Pyralux LF, Pyralux FR, and Pyralux AP.

- **RF/Microwave/High-Speed PCB Materials:** High-frequency PCBs use specialized materials such as Rogers' series (5870/5880, 3003/3006/3010, etc.) and Arlon's DiClad and CuClad series.

- **Hybrid PCBs:** Combine standard FR-4 laminate with other RF/microwave/high-speed laminates to balance performance and cost.

Key material characteristics

- **Coefficient of Thermal Expansion (CTE):** Measures material expansion with temperature changes, crucial for maintaining PCB integrity under thermal cycling.

- **Glass Transition Temperature (Tg):** The temperature at which material properties change from brittle to rubbery, affecting the material's suitability for different soldering processes.

- **Decomposition Temperature (Td):** Indicates the temperature at which a material starts to degrade, useful for assessing thermal stability.

- **Dielectric Constant (Er):** Determines signal propagation speed in a dielectric material, impacting the design of impedance-controlled signals.

- **Dissipation Factor (Loss Tangent):** Measures the percentage of transmitted power lost in the laminate material.

1.1.1.2 Classification of printed wiring boards

There are two primary methods for forming conductors on printed wiring boards (PWBs):

- Subtractive: This process removes unwanted copper foil from a base substrate, leaving the desired circuit pattern behind.

- Additive: This process creates the conductor pattern by adding copper to a bare substrate in specific locations. This can be achieved through copper plating, screening conductive paste, or laying down insulating wires onto the predetermined conductor paths.

Figure 1.3 categorizes PWBs based on several factors, including fabrication processes and substrate material [5]. Here's how to interpret the figure:
Column 1: Classifies PWBs by their substrate material.
Column 2: Classifies PWBs by the method used to create the conductor pattern image.
Column 3: Classifies PWBs by their physical form (rigid, flexible, etc.).
Column 4: Classifies PWBs by the method used to actually form the conductors.
Column 5: Classifies PWBs by the number of conductor layers they contain.
Column 6: Classifies PWBs by the presence or absence of plated-through-hole (PTH).
Column 7: Classifies PWBs by their production method.

1.1.1.3 Standards of printed circuit boards

One main organization creates standards for designing, producing, and testing the printed circuit boards. The organization is IPC as Association Connecting Electronics Industries, Bannockburn, IL. The IPC offers a comprehensive suite of standards that encompass various aspects of PCB design and manufacturing. Some of standards are:

- IPC-T-50 : Terms and Definitions
- IPC-222x Series : This series encompasses various generic standards that provide guidelines for designing different types of printed board, including flexible and multi-chip modules.
- IPC-2611 : Documentation Requirements
- IPC-A-600 and IPC-A-610 : Inspection and Evaluation
- IPC-601x Series : Specification and Qualification

The simplified standard tree is shown in Figure 1.4 [6].

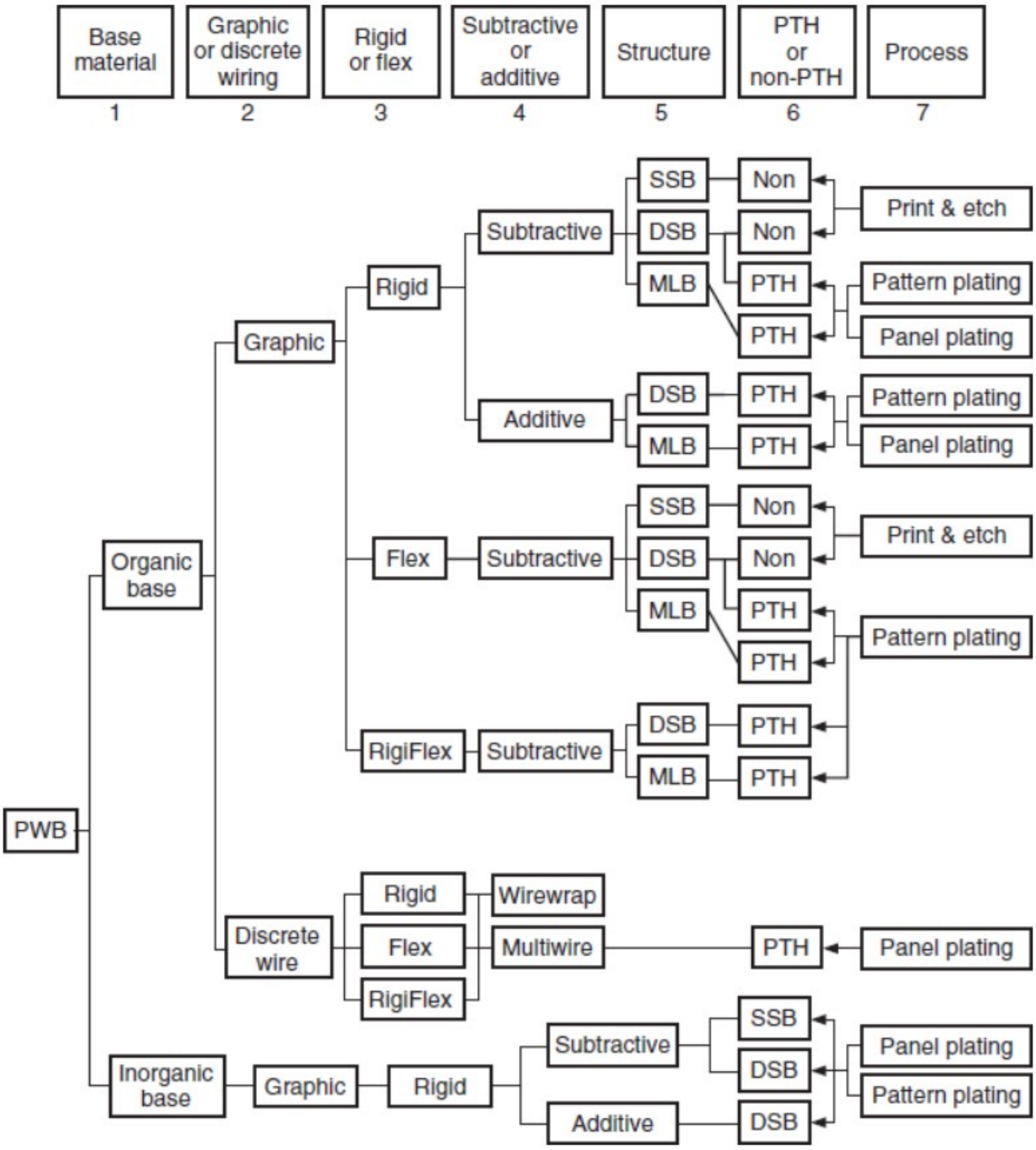

Figure 1.3 : Classification printed wiring boards.

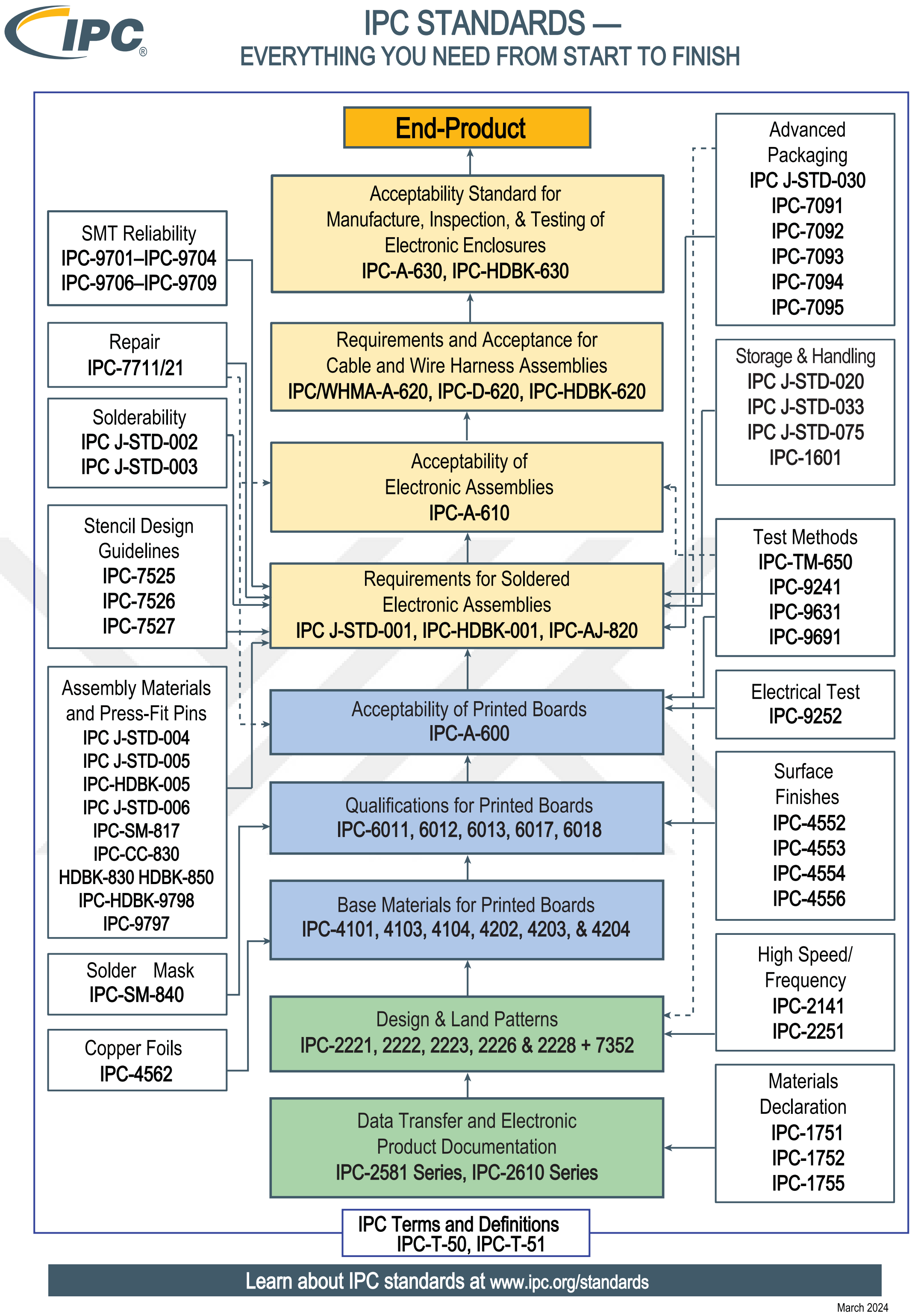

Figure 1.4 : IPC simplified tree.

1.1.1.4 Classification of board according to application and producibility

Each design and application should have a classification. There are three classes and levels for board classification. Figure 1.5 gives classes and levels of application and producibility [5].

Firstly, classes of board application specify according to the failure what cause. Class 1 consists toys, games, and general products. If these products fail, they don't cause any important issue for life threatening and the application can be stopped. Class 2 consists of desired electronic service products. These applications products are used for an important issue. If this issue cannot be performed, some problems occur; however, there is no life-threatening. Final Class 3 uses for high reliability electronics, such as military, aerospace, medical areas. This class should not fail, because it can be caused life threading.

There are three level about producibility of PCB. They are classified according to complexity. Level A has less complexity and a general design. Level B is standard. Level C has the highest complexity in these levels.

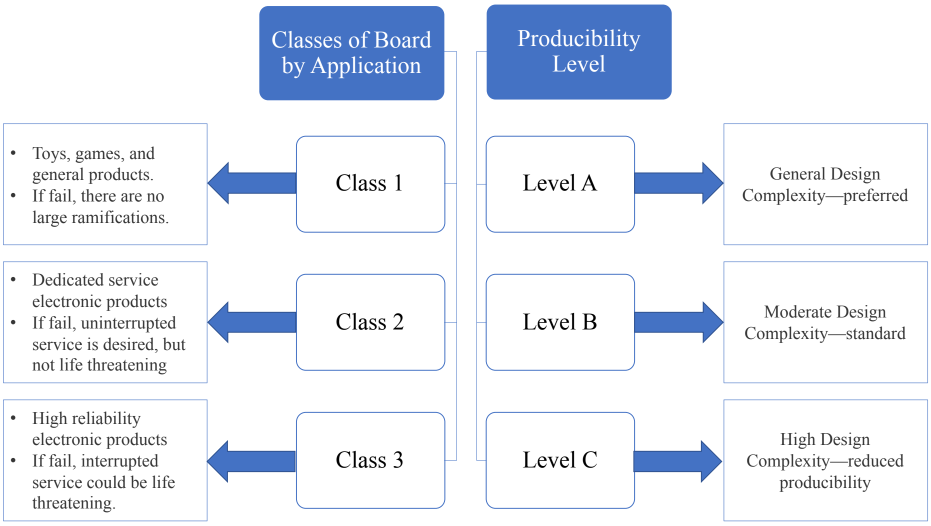

Figure 1.5 : Classes of board application and producibility levels.

1.1.1.5 Mechanical test for material characterization of PCB

Mechanical testing is crucial for qualifying copper-clad laminates before using them in PCB manufacturing. These tests provide valuable information for engineers to select materials suitable for the intended application. There are three common tests for determining the PCB's mechanical properties. These tests are tensile test, flexural test and copper peel strength test. Tensile Test: Measures the modulus (stiffness) and tensile strength (maximum load) of the laminate under tension.

Flexural Strength Test: Evaluates the laminate's resistance to bending forces.

Copper Peel Strength Test: Assesses the bond strength between the copper foil and the laminate before and after exposure to thermal stress.

Modulus and Tensile Strength (Tensile Test)

This test method, based on ASTM D 882, determines the Young's modulus and yield stress of copper-clad laminates. It aligns with industry standards like IPC-TM-650 for both rigid and flexible laminates.

Flexural Strength Test

This test, based on ASTM D 790 and IPC-TM-650 method 2.4.4B, determines the flexural strength of the laminate, which is its resistance to bending forces.

Copper Peel Strength Test

For copper peel strength testing, refer to Section 15.4.2 of the original text. This section likely describes the test method and potentially provides space to record results. Additional tests might be necessary after specific thermal stress exposure (solder dip, reflow profiles) or plating solutions to evaluate the impact on the copper-laminate bond strength.

1.1.2 Usage of PCBs at space application

PCBs are used in all kind of space applications. Class 3 PCBs are used most of the time. The user demands high durability, reliability, and affordable properties from PCBs. These PCBs design, manufacture requirements are standardized by European Cooperation for Space Standardization (ECSS). ECSS is standardized all space activity for European Space Community and is a follower of the ECSS standards. Basically, there are four branches for grouping standards. This tree is shown in Figure 1.6 [7].

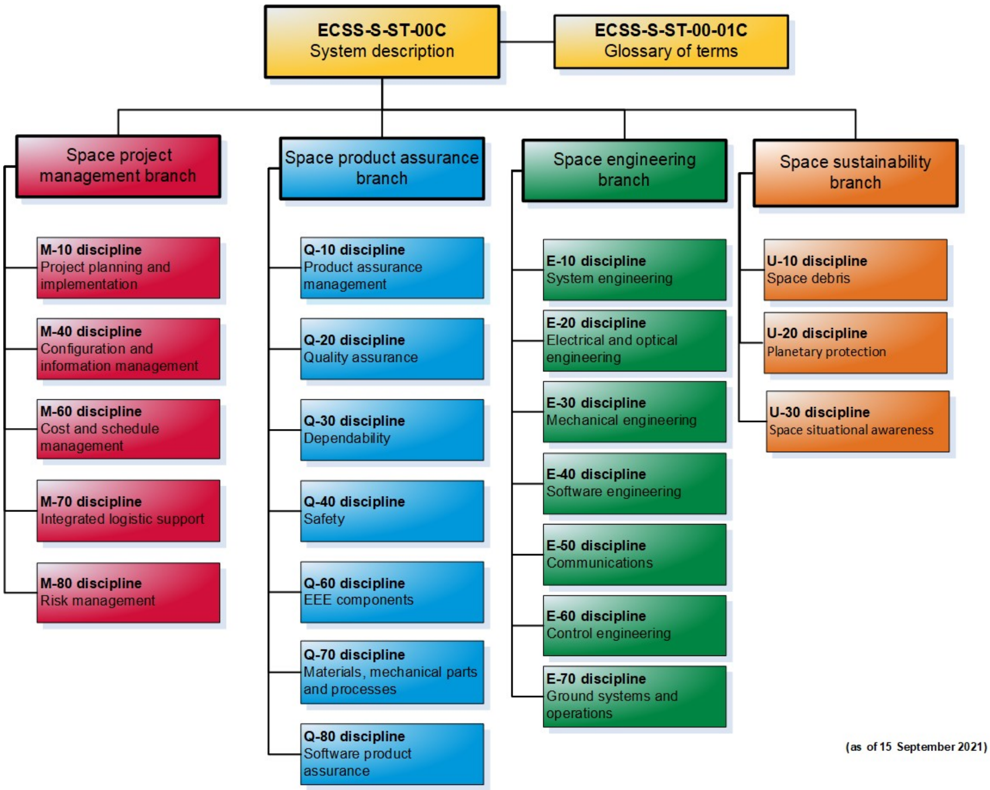

Figure 1.6 : ECSS disciplines.

If an application is related with PCB, the standard gives advice to who follower of the standards. There are two standards related with PCB totally, ECSS-Q-ST-70-12C and ECSS-Q-ST-70-60C. ECSS-Q-ST-12C is related about PCB design rules. The other standard is related about PCB procurement. The Q-70 discipline details tree is given in Figure 1.7 [8].

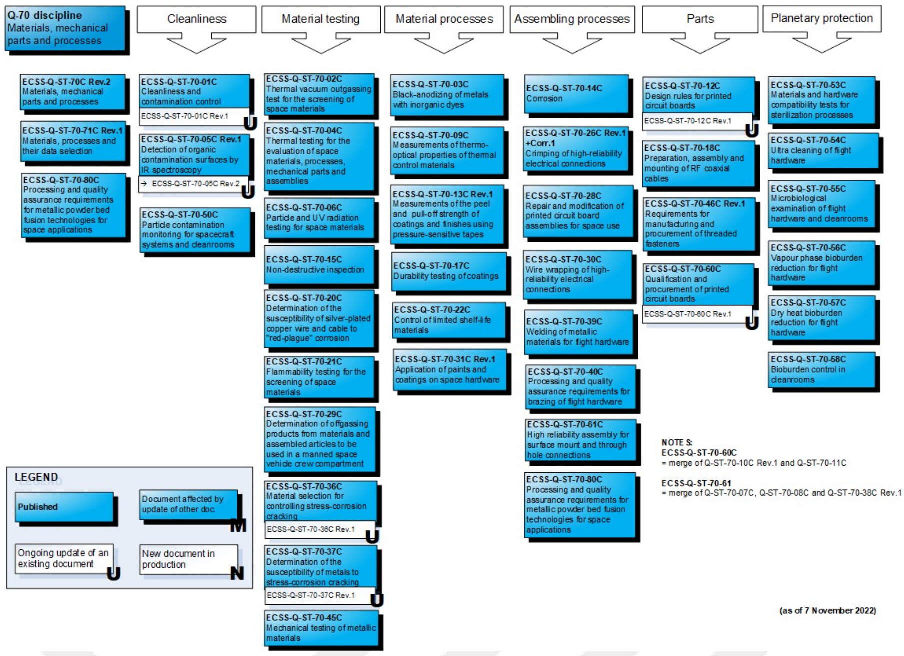

Figure 1.7 : ECSS Q70 discipline tree.

1.1.3 Example of PCBs at space application

In space applications there are numerous spacecraft and they are working in harsh conditions in the space environment. Also, there are many things for specified and classified spacecraft and satellites. Basically, spacecrafts are classified by eight types. These are listed below.

- Flyby spacecraft
- Orbiter spacecraft
- Atmospheric spacecraft
- Lander spacecraft
- Penetrator spacecraft
- Rover spacecraft
- Observatory spacecraft
- Communications and Navigation spacecraft

Spacecraft can be classified according to orbit, mass and volume, payloads, and missions. According to mass classification is shown Table 1.1 [9].

Table 1.1 : Spacecraft classification according to mass.

Definition	Platform Mass, kg
Large Spacecraft	=>1000
Medium Spacecraft	=>500 and <1000
Small Spacecraft	<500
Mini Spacecraft	=>100 and <500
Micro Spacecraft	=>10 and <100
Nano Spacecraft	=>1 and <10
Pico Spacecraft	=>0.1 and <1
Femto Spacecraft	=<0.1

Subsystems of CubeSat and PocketQube satellites are mainly focused satellites are this thesis. Standard size of CubeSats dimensions are given in Table 1.2 [10]. These dimensions are basic dimensions and those are can be changed according to launcher deployer.

Table 1.2 : Dimensions of CubeSats' standard size.

Size	Dimensions, mm x mm x mm
1U	100 x 100 x 113.5
1.5U	100 x 100 x 170.2
2U	100 x 100 x 227
3U	100 x 100 x 340.5
6U	113 x 226 x 340.5
12U	226 x 226 x 340.5

The standard size of the PocketQubes dimensions is given in Table 1.3 [11].

Table 1.3 : Dimensions of PocketQubes' standard size.

Standard Size	Dimensions, mm x mm x mm
1P	50 x 50 x 50
2P	50 x 50 x 114
3P	50 x 50 x 178

PCBs fractions are inverse propagation with satellite mass and volume. While the satellite mass and volumes decrease, the PCB fractions are increase. This relationship, give us an idea about the importance of the PCBs modelling increases at small satellites.

CubeSats are mainly fit in to categories of micro, nano, and pico satellites. PCBs also affect to CubeSat systems. It is not more then PocketQube; however, the effectiveness should be taken into account for launch vehicle analysis. Some examples of the CubeSats are shown in Figure 1.8. KILICSAT [12] is 3U CubeSat, BeEagleSat [13] is 2U CubeSat, BDSAT [14] is 1U CubeSat and SPACEBEE [15] is 0.25U CubeSat. All CubeSats has PCB based solar panels and interior of the BeEagleSat is shown in figure and it shows, number of PCB is also high inside of the satellites.

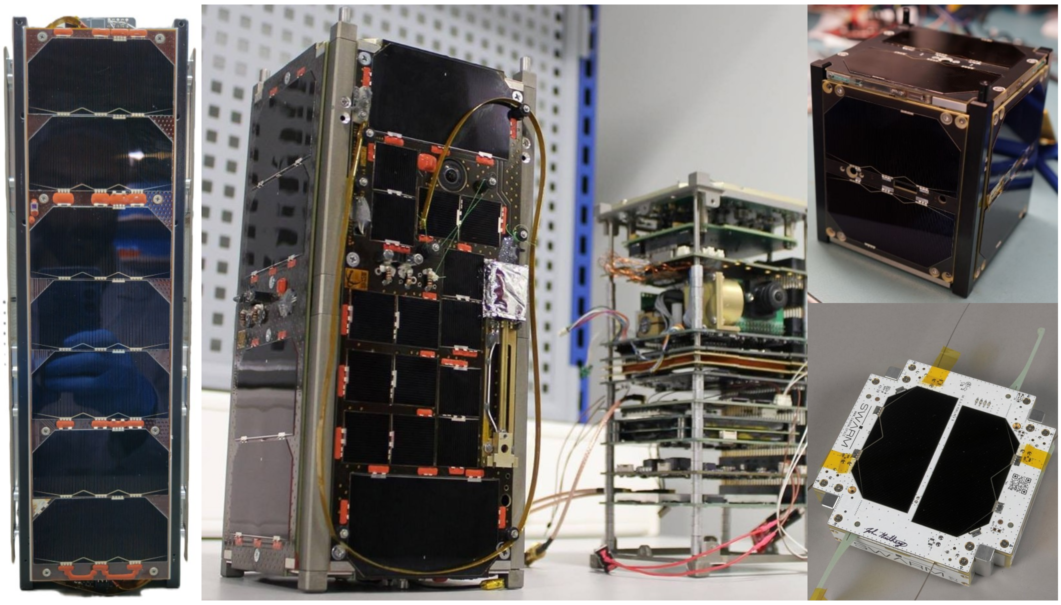

Figure 1.8 : Examples of CubeSats (KILICSAT, BeEagleSat, BDSAT, SPACEBEE).

PocketQubes are nowadays most used satellites at femto and pico satellite categories. PocketQubes nearly made from fully PCB. Structural system main focus is supporting the PCBs. Some PocketQubes examples are given in Figure 1.9. FOSSASAT-1 [16] is 1P PocketQube, FOSSASAT-2 [17] is 2P PocketQube, Delfi-PQ [18] and MRC-100 [19] are 3P PocketQubes. Delfi-PQ's interior design also shown in the figure and number of PCBs is high inner and outer design. This number of the PCB has important effective on the satellite.

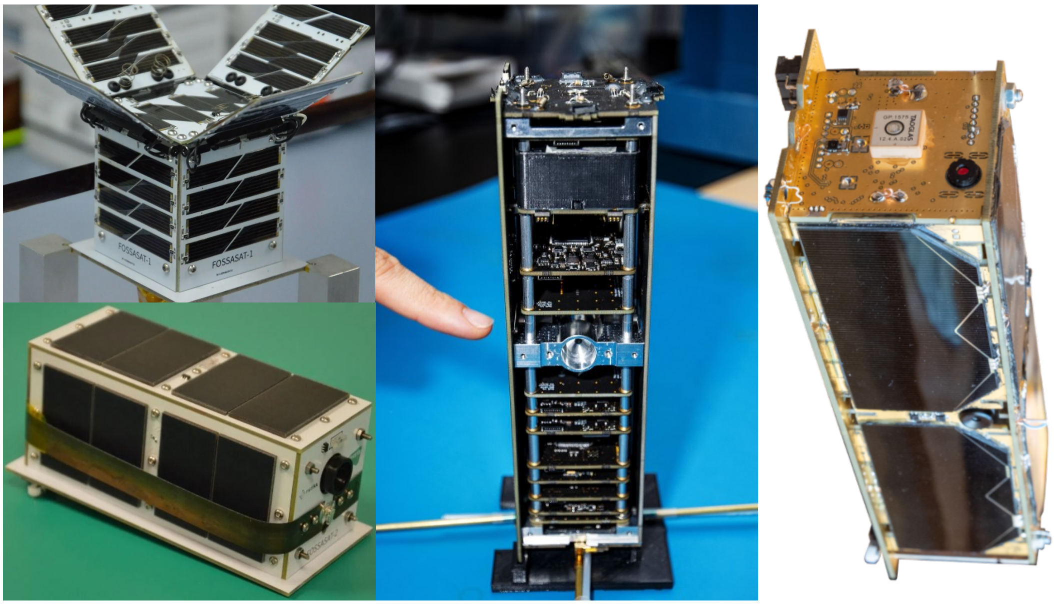

Figure 1.9 : Examples of PocketQubes (FOSSASAT-1 , FOSSASAT-2 , DELFI-PQ , MRC-100).

From this basic idea, PCBs should have good model for all kind of activity on modelling. All of these project cost-effective project and modelling process should be decreased more then now. In this study, 4 case are created with designed and produced PCBs. At the final stage, some numbers will found for without modelling detailed of PCBs.

1.2 Framework

This thesis explores a method to determine the equivalent homogenized mechanical properties for each layer of a PCB without explicitly modeling the entire PCB. The process begins with a finite element method (FEM) analysis focused on modal analysis, which examines the natural vibration frequencies of the PCB. The detailed modal analysis results from the FEM analysis are then stored in a database for optimization. Since we are dealing with sandwich plates, the Differential Quadrature Method (DQM) is a well-suited approach for solving for the natural frequencies. The optimization process aims to achieve the desired modal results obtained from the detailed FEM model by adjusting the material's elastic properties. The Halpin-Tsai material model is employed, and the optimization is based on this model. This method is applied to optimize the modal responses of four different PCBs. The complete workflow of the thesis is illustrated in Figure 1.10.

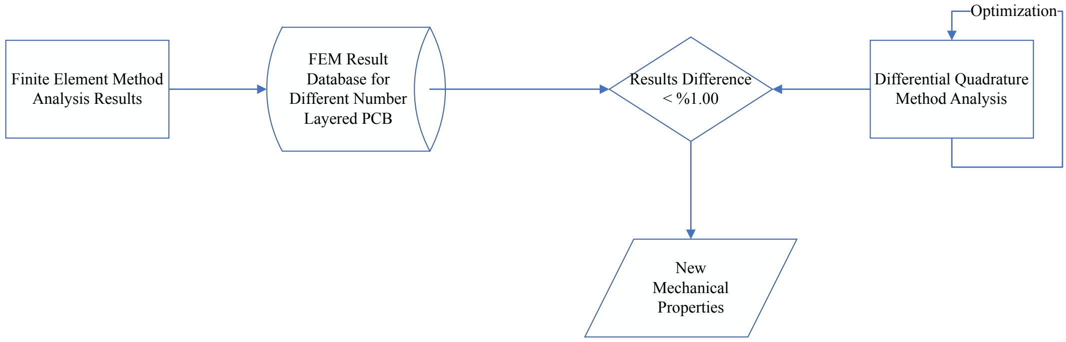

Figure 1.10 : Workflow of thesis is defined by diagram.

1.3 Thesis Outline

The thesis aims that finding an affordable equivalent model for solving behavior of PCBs at environmental loads. PCBs and their classifications, standards, usage of them at space application, satellites, and their importance on satellites are explained in Chapter 1. Also, outlines are figured the main objective of this study.

Following the introduction, Chapter 2 provides a comprehensive literature review exploring existing research on PCB modeling for mechanical load analysis.

After the literature review section, detailed PCB modeling is described. Because there are so many different PCB designs, conducting the analysis on a computer is more convenient for creating a database for this thesis. Therefore, Finite Element Analysis (FEA) is selected for developing the database. All steps of modelling and obtaining results of the PCBs are outlined in Chapter 3. Eight PCB models are prepared with all details for the thesis.

Chapters 4, 5, and 6 focus on the mathematical framework. Chapter 4 explains origin of the proposed material models and derivation of the associated equations. Chapter 5 introduces a mathematical model specifically developed for the Differential Quadrature Method (DQM), which is then elaborated upon in Chapter 6. Notably, DQM is an efficient method for use in optimization code. While optimization involves changing equivalent material properties, DQM is able to obtain analysis results faster than FEA. Additionally, DQM models are presented in this chapter.

Chapter 7 describes the optimization strategy, detailing how DQM is used alongside the detailed FEM results to determine the optimal material model for each PCB layer.

Finally, Chapter 8 presents the results of all analyses and validates the study's findings. The thesis concludes with a summary of the key takeaways and potential future directions in Chapter 9.

2. LITERATURE REVIEW

The review is divided into two parts. The first focuses on PCB modeling approaches, considering whether electronic components are included. Some researchers focus on modeling the entire PCB assembly, including electronic parts. Others focus solely on modeling the PCB itself. The second part explores how researchers select and justify the values used for analysis and modeling.

2.1 Material Property Determination

Numerous studies have been conducted about the modeling of PCBs for using mechanical and thermal analysis. Study of Pitarresi examines experimental and computational methods employed in PCB vibration analysis [20]. It also addresses the validation of the modeling results and the impact of the simplification of material properties on modeling.

Researchers are conducting various studies on the determination of PCB mechanical properties. Determination of PCBs mechanical properties studies can be categorized by two way. The first way is to use test methods and determine the mechanical properties of the PCB for implementing the analysis. The other way is estimation of mechanical properties according to analysis criteria with using composite plate theory. If two ways are not used for FEM analysis, each stacked layer is implementing to analysis. Due to the complexity of the modeling, FEM analysis takes a lot of time. The tests are very expensive because of the high number of PCB designs.

Bhavsar et al. propose a method to determine equivalent single-layer material properties for PCBs [21]. Their study highlights the importance of material properties in PCB analysis and the impact of variations on the board's response. The method utilizes Classical Lamination Theory (CLT) to estimate the average properties of the FRP laminate and validates the results through simulations with using Ansys and Sherlock software. Chippalkatti et al. addressed the challenge of characterizing the complex

material properties of PCBs [22]. Their study aimed to estimate equivalent single-layer properties using finite element (FE) analysis, testing, and calculations. Five PCBs with different thicknesses, dimensions, and copper layers were chosen for analysis. By varying boundary conditions, damping values, and other factors, they estimated Young's modulus and Poisson's ratio for each PCB. The obtained equivalent properties were validated by comparing the first modal frequency from simulations with experimental results, demonstrating good agreement. Gharaibed proposed a method using FEA and the response surface method (RSM) to identify the unknown in-plane material properties of PCBs [23]. Their approach involves comparing resonant frequencies and mode shapes from FEA with experimental data, iterative refining the model using RSM to achieve good agreement, and validating the estimated material properties. Gharaibed also propose an artificial neural network (ANN) approach to estimate the equivalent in-plane material properties of PCBs in recent his research [24]. Their method utilizes FEA data to train the ANN to identify the relationship between natural frequencies and mechanical properties. The ANN-predicted properties are then used in FEA simulations, resulting in good agreement with experimental data, highlighting the potential of this AI-based methodology.
Morettini et al. addressed a critical gap in CubeSat design by proposing a method to model PCBs alongside their electronic components [25]. Vibrations during launch are a major cause of CubeSat failure, highlighting the need for accurate modeling. Traditional methods neglect components, leading to unreliable predictions. Authors were determined mechanical properties of PCB from studies of Wei and Xu [26] and Bell et al. [27]. Also, study shows that equivalent mechanical properties of PCB is useful satisfied by test and analysis comparing.

2.2 Material Effectiveness Determination Studies

Fuchs et al. emphasize the importance of considering direction-dependent material properties in FEA simulations of PCBs [28]. This can lead to significant differences in predicted stress and deformation fields compared to using isotropic material models. This study demonstrates that considering the direction-dependent material properties of PCB layers is crucial for accurate stress analysis via finite element simulations.

Although these properties significantly affect stress in the insulating layers, their impact on the conducting layers is minimal, highlighting the importance of accurate material characterization for a reliable PCB design.

Study handled by Haugan and Dalsjo investigated the material properties of two FR-4 laminates commonly used in PCBs [29]. By measuring various properties like elasticity and thermal expansion, the research aimed to improve understanding of how these laminates behave under different temperatures, including those experienced during soldering processes. The findings provide valuable data for selecting appropriate laminates based on their end-use application.

Guoquan et al. investigated the impact of PCB thickness on natural frequencies using finite element modeling (ANSYS) and modal analysis [30]. Their findings demonstrated a positive correlation between thickness and natural frequency, particularly for higher-order modes. This highlights the importance of considering thickness during PCB design, but it's important to note that their model likely used FR-4 material properties and excluded copper layers, potentially affecting the real-world behavior.

2.3 Dynamic Analysis and Modeling Methods

Study of Lim the dynamic characteristics of PCBs supported by edge retainers and plug-in connectors were analyzed, and a method for maximizing the fundamental frequency of vibrating structures was proposed [31].

While many studies focus on material properties during PCB modeling, Wei and Xu specifically developed a dynamic model for PCBs using FR-4's orthotropic properties [26]. Their work emphasizes the importance of considering not only material properties but also boundary conditions and component placement for accurate vibration analysis through finite element modeling.

Dash et al. investigated the impact of component stiffness on PCB dynamics using FR-4 as the base material [32]. Their study compared detailed component modeling with a time-saving "local smearing" approach, finding good agreement for natural frequencies and frequency response functions. This suggests local smearing is suitable for these aspects, while detailed modeling remains necessary for stress analysis at component interfaces.

Al-Araji et al. proposed a methodology for preliminary vibration analysis of PCBs during the design phase [33]. To improve design efficiency, they compared finite element simulations (using "concentrated weight" elements for components) with experimental results, demonstrating good agreement. This approach allows for faster modeling and reduces design iterations by identifying potential vibration issues early.

Bachoo et al. explored how component properties like mass, location, and stiffness influence a PCB's resonant behavior [34]. Using a combination of experimental testing and finite element modeling (FEM) with FR-4 material, they observed that sparsely populated PCBs have lower natural frequencies compared to bare boards, while densely populated ones experience an increase. This finding suggests that designers can strategically place components during the design phase to achieve desired vibration characteristics for the PCB.

Overall, research of Amy presents a new design process with validated tools that can significantly improve the efficiency and effectiveness of designing spacecraft electronic equipment for vibration resistance [35]. The research successfully delivered the proposed design tools. These tools provide a good level of design optimization with minimal effort and are likely to be adopted due to their ease of use. Even if a design fails the qualification test (which is now less likely), the upfront optimization reduces the need for a complete redesign, allowing for simpler and faster corrective actions. The main focus of the research was on validating the processes for creating these tools, rather than the tools themselves. This involved significant advancements in response prediction (modeling accuracy and influencing factors) and failure criteria (identifying local curvature as the primary failure cause). This not only validates the proposed design tools but also provides valuable insights for developing more efficient future models. In summary, the research achieves its goals and offers valuable contributions in design tools, process validation, response prediction, and failure criteria, all of which can improve the design process for spacecraft electronic equipment. Model PCB by testing. Researcher determined that, PCB's properties is not given properly from manufacturer.

Tinca et al. address the challenge of modeling PCBs with unique material compositions [36]. Their study focuses on a 9-layer PCB with a ceramic-filled composite layer, commonly used in automotive radar applications. Standard material models might not accurately capture the behavior of such PCBs. The authors propose an FEA calibration method that leverages low-cost experiments to determine the material properties. They create three main FEA models: a homogeneous model with different material definitions (isotropic, transverse isotropic, and orthotropic), a trace reinforcement model, and a mapped model. Through optimization, they achieve an excellent overall fit (1%) between the calibrated model and experimental data. Notably, the transverse isotropic material formulation (DP2) and the mapped trace model (DP5) demonstrate the best accuracy (4% error), highlighting their effectiveness for modeling PCBs with unique material compositions.

2.4 Model Calibration and Validation

The article studied by Zhang et al. is about modal analysis of a board-level electronic package subjected to drop impact [37]. The model of PCB taken from a private company. They created a theoretical model of a PCB with three chip size packages (CSPs) mounted on it. They analyzed this model to determine the mode shapes and natural frequencies. They built a FE model of the PCB and CSPs and performed modal analysis on it. They conducted a modal test using an impulse hammer to measure the actual mode shapes and natural frequencies. They compared results from the theoretical model, FE model, and modal test.

Zhang et al. used a laser-based interferometric technique to measure the modal parameters of a board-level package at another study [38]. They then built an equivalent finite element model of the board-level package and used the Taguchi method to optimize the equivalent material properties. The optimized material properties were then used to improve the accuracy of the finite element model. In other words, they built a model of a circuit board and figured out the best way to represent the materials the board is made of in the model. This will allow them to more accurately predict how the board will behave in different situations.

Fuchs et al. highlights the importance of accurate, direction-dependent material properties in FEA simulations of PCBs, demonstrating significant differences in stress and deformation fields compared to isotropic material models [28].

Mukind's thesis evaluated FR-4 and Mercurywave, common PCB materials, for Nano satellites through tensile tests [39]. FR-4 emerged as the superior choice due to its improved strength, stiffness, and ductility, offering a more cost-effective and structurally sound option for these miniature spacecraft. The study also satisfy PCBs mechanical properties for researcher. The results of this study also evaluated at Table 2.1 and Table 2.2.

Study of Fontana et al. investigates various numerical models for analyzing the dynamics of two-layer PCBs [40]. The goal is to identify efficient models for future studies on Printed Circuit Board Assemblies (PCBAs). The authors compare five models of varying complexity with experimental data. Interestingly, simpler models based on analytical relationships ("Equivalent Copper" and "Uniform Layers") achieved good accuracy for both static and dynamic behavior. These models offer a favorable balance between accuracy and ease of use compared to more complex models requiring specific software or extensive data. The study suggests these simpler models as promising candidates for further investigations on PCBAs populated with components.

This article studied by Lall et al. discusses a model for predicting the reliability of ball grid array (BGA) and chip scale package (CSP) assemblies used in automotive underhood applications [41]. The authors compare their model to existing damage relationships and find that their model provides more accurate predictions for BGA and CSP assemblies on high-Tg printed circuit boards. They modelled PCB as the organic laminates are modeled as orthotropic and that the temperature dependence of their Coefficient of Thermal Expansion (CTE) and elastic modulus is taken into account suggests that the material properties of the PCB material are incorporated into the finite element models in a way that accounts for their anisotropy and temperature dependence.

2.5 Used PCB Properties

Tables 2.1 and 2.2 in this thesis summarize PCB properties based on the evaluated literature for this study.

Table 2.1 : Mechanical properties of PCBs have FR-4 dielectric material in literature.

# Layer	h, mm	ρ, kg/m^3	E_x, MPa	E_y, MPa	E_z, MPa	G_{xy}, MPa	G_{yz}, MPa	G_{xz}, MPa	ν_{xy}	ν_{yz}	ν_{xz}	REF
2	1.5	1970.00	17200	-	-	-	-	-	0.40	-	-	[34]
2	1.6	2074.07	22000	-	-	-	-	-	0.20	-	-	[22]
4	1.6	2201.88	28919	28919	3750	13740	1	1	0.15	0.10	0.10	[21]
4	1.4	2960.98	27000	-	-	-	-	-	0.20	-	-	[22]
4	1.6	2278.66	24500	27400	15000	10800	6400	6300	0.20	0.39	0.39	[25]
4	1.6	-	6800	-	-	-	-	-	0.80	-	-	[39]
6	1.6	-	16824	16824	7404	7590	3310	3310	0.11	0.39	0.39	[41]
6	2.1	1984.76	20000	-	-	-	-	-	0.12	-	-	[32]
8	0.9	1910.00	15000	-	-	-	-	-	0.39	-	-	[37]
14	2.2	2170.00	20150	23180	-	5600	-	-	0.25	-	-	[23]
14	2.2	2170.00	20980	25160	-	5750	-	-	0.20	-	-	[24]
-	1.6	1870.00	17000	-	-	-	-	-	0.12	-	-	[31]
-	1.7	1820.00	24000	20000	-	4400	-	-	0.30	-	-	[35]
-	3.5	1900.00	11100	-	-	-	-	-	0.28	-	-	[30]
-	-	1850.00	39000	8400	3200	4200	3900	3900	0.26	0.28	0.28	[26]

Table 2.2 : Mechanical properties of PCBs have various or undefined dielectric material in literature.

# Layer	h, mm	ρ, kg/m^3	E_x, MPa	E_y, MPa	E_z, MPa	G_{xy}, MPa	G_{yz}, MPa	G_{xz}, MPa	ν_{xy}	ν_{yz}	ν_{xz}	REF
2	1.6	-	16824	16824	7404	7590	3310	3310	0.11	0.39	0.39	[41]
4	1.6	-	16824	16824	7404	7590	3310	3310	0.11	0.39	0.39	[41]
4	2.0	5007.45	18400	-	-	-	-	-	0.12	-	-	[33]
4[1]	1.6	-	5900	-	-	-	-	-	0.90	-	-	[39]
5[2]	1.2	-	20726	20563	5843	14383	10722	9150	0.28	0.26	0.25	[36]
8	1.0	1910.00	16900	16900	7400	7600	3300	3300	0.11	0.39	0.39	[38]

[1] 4-Layer PCB's dielectric material is Mercurywave.
[2] 5-Layer PCB's dielectric material is Rogers.

3. FINITE ELEMENT ANALYSIS of PCBs

Designed and produced PCBs are selected for creating a database according to the volume fraction, the number of layers. Eight cases created. 2 Layer PCBs and 4 Layer PCBs are used for optimization, 6 Layer PCBs and 8 Layer PCB are used for validation. FEM analyses of all PCBs are solved in the same way as in the workflow. A database was created from FEA that has all details included in FEA models.

3.1 Workflow of Creating Detailed PCB's Modal Frequency Database

Firstly, each layers are generated by using PCB design software that is Altium Designer [42]. After generating each layer, Computer Aided Design (CAD) models created detailed. Each layer is assembled according to the PCBs design. This process is carried out using the CAD software that is CATIA [43]. This process aims to obtain a detailed model of PCBs.

After this process, another CAD software is used to prepare the CAD model for FEM analysis. At this point, Ansys SpaceClaim [44] software is used and a mid-surface 2D surface generated is generated to decrease the solution time in FEM analysis.

Finally, the FEM analysis model is created by using PATRAN [45] software. The mesh size of the analysis model defines one course size. After FEM analysis model creation, analysis performing by MSC NASTRAN [46]. After getting result, mesh size is divided half of that and model re-created for performing analysis. Two analysis results are compared and if the difference of the results is average less than 1.00 %, the first six natural frequency modes of the PCBs are satisfied under defined boundary conditions.

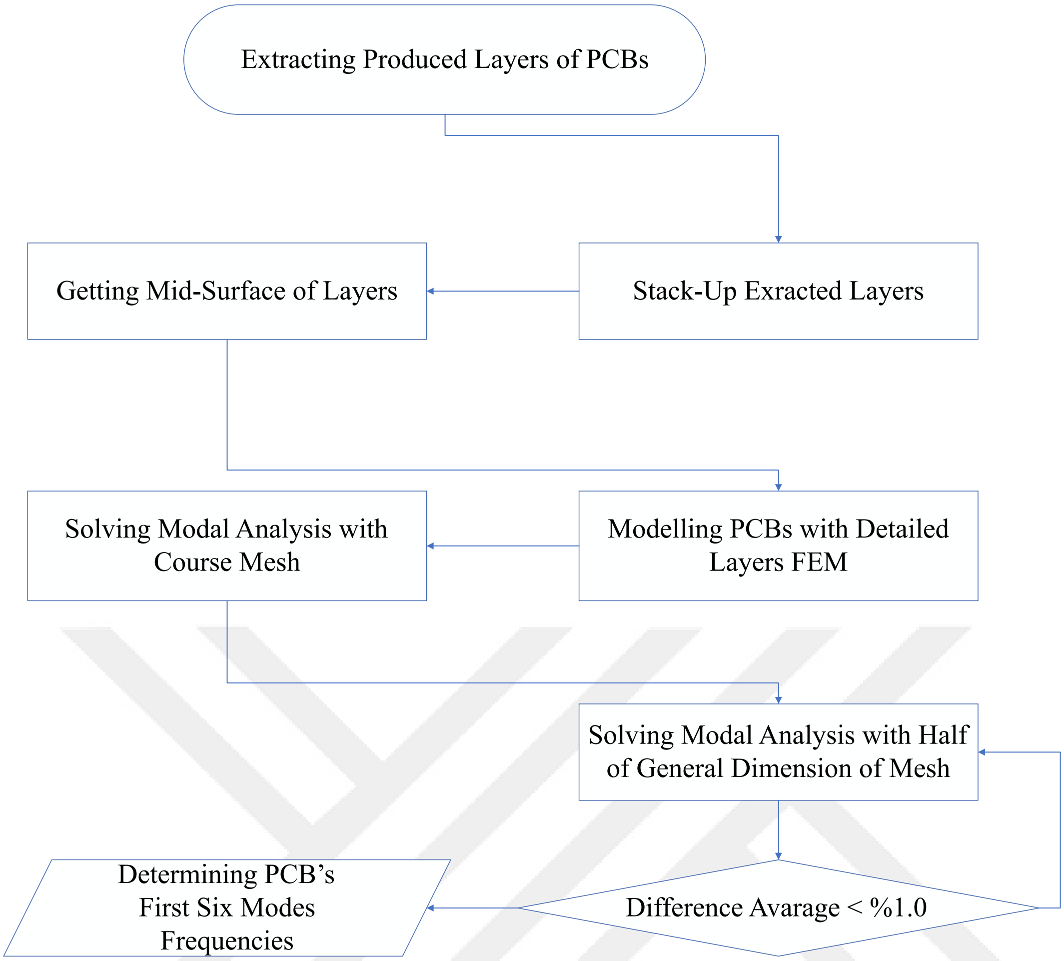

Figure 3.1 : Workflow of FEM analysis.

3.1.1 Volume fraction of PCBs calculation

Volume fractions are used in the calculation of equivalent elastic properties. Two methods are used for calculating volume fractions. The first volume fraction calculation method is used in the DQM code, while the second method is used for solving the equivalent model in FEA software. The volume fraction of each layer is calculated individually. The maximum dimensions are considered mutual. The first volume fraction calculation model and its equivalent model illustration is shown in Figure 3.2. The first volume fraction calculation method is defined as follows:

1. Define the maximum length (a) and width (b) as a rectangular shape.

2. Calculate the maximum surface area based on the length and width.

3. Determine the volume of the layer occupied by voids and material by multiplying the maximum surface area by the layer thickness, defined as $V_{Maximum}$.

4. Determine the layer's volume occupied by material from CAD software, defined as V_{Layer}.

5. Calculate the volume fraction by dividing the calculated volume of the layer by the maximum volume of that layer $v_f = V_{Layer}/V_{Maximum}$.

The second calculation method differs only in the second step. The maximum area is calculated using CAD software based on all maximum edges, and the shape can differ from a rectangular shape. The other steps are the same as in the first method. The second volume fraction calculation model and its equivalent model illustration is shown in Figure 3.3.

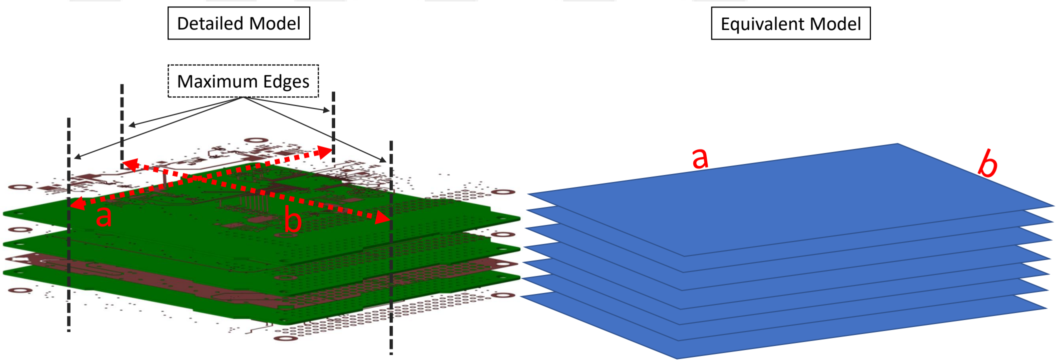

Figure 3.2 : Volume fraction calculation example for first calculation method.

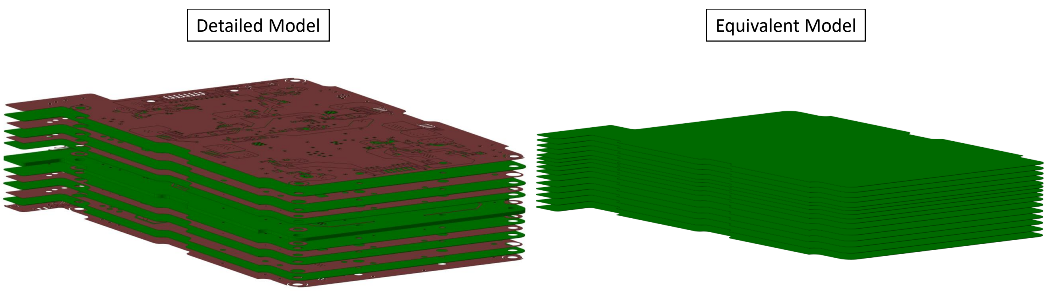

Figure 3.3 : Volume fraction calculation example for second calculation method.

3.2 CAD Models of PCBs

In total, eight different CAD models are created using the Altium Designer software export tool. The copper layers are exported inside of the Parasolid file. All Parasolid files are converted to STEP file. After this convert application, the layers are ready for stack-up and build PCB in computer environment.

Figure 3.4 and Figure 3.5 are shown first group PCBs models. There are three layers; bottom and top sides have copper material. Middle side has FR-4 material. The stacking materials, thicknesses and volume fractions of these PBCs are defined in Table 3.1 and Table 3.2.

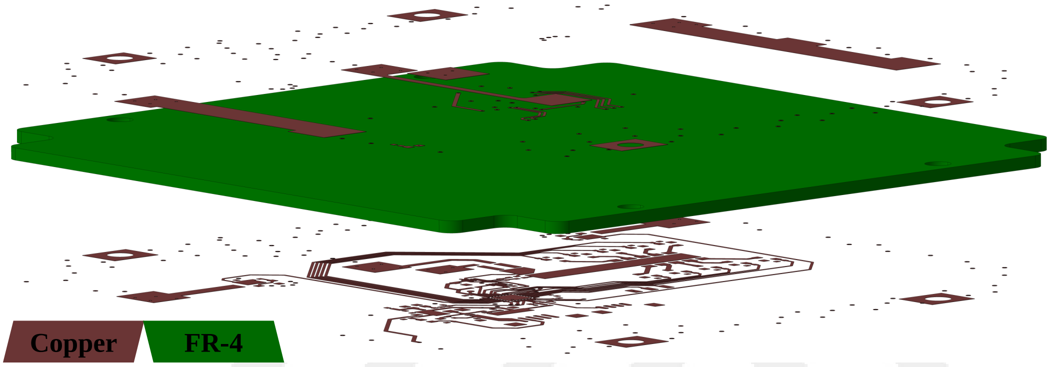

Figure 3.4 : CAD model of 2-Layer PCB-001.

Table 3.1 : Model information of 2-Layer PCB-001.

Layer Number	Material	Thickness, mm	Volume Fraction
1	Copper	0.035	0.094
2	FR-4	1.500	0.962
3	Copper	0.035	0.109

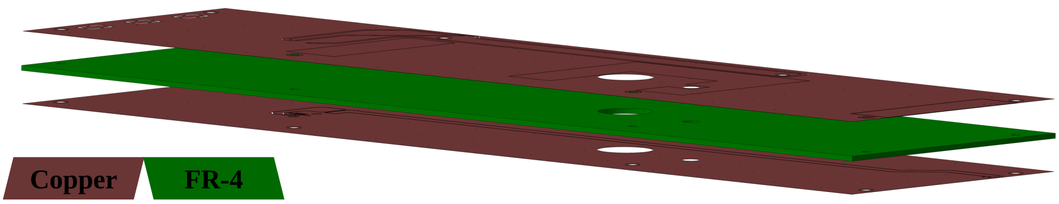

Figure 3.5 : CAD model of 2-Layer PCB-002.

Table 3.2 : Model information of 2-Layer PCB-002.

Layer Number	Material	Thickness, mm	Volume Fraction
1	Copper	0.035	0.983
2	FR-4	1.500	0.991
3	Copper	0.035	0.988

The second group of PCBs are 4 layer PCBs. They have 4 items copper layers and 3 items FR-4 layers. Their CAD models are shown in Figure 3.6 and Figure 3.7. Their properties are given in Table 3.3 and Table 3.4.

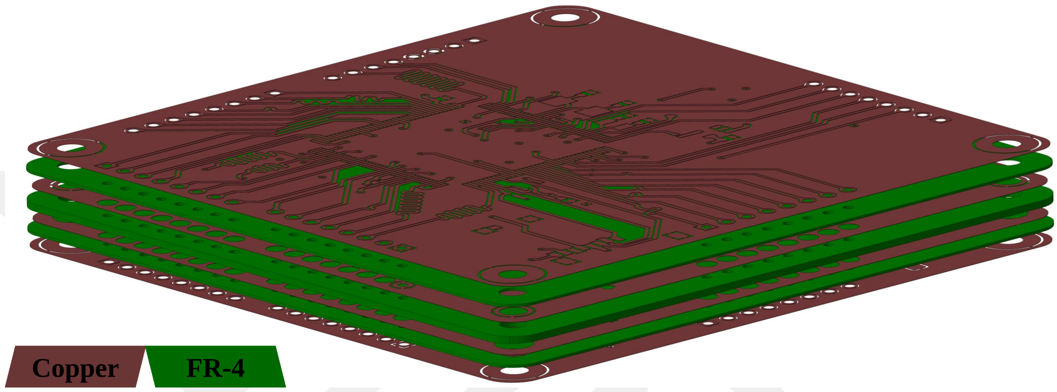

Figure 3.6 : CAD model of 4-Layer PCB-001.

Table 3.3 : Model information of 4-Layer PCB-001.

Layer Number	Material	Thickness, mm	Volume Fraction
1	Copper	0.035	0.863
2	FR-4	0.260	0.986
3	Copper	0.035	0.914
4	FR-4	0.700	0.986
5	Copper	0.035	0.913
6	FR-4	0.260	0.968
7	Copper	0.035	0.914

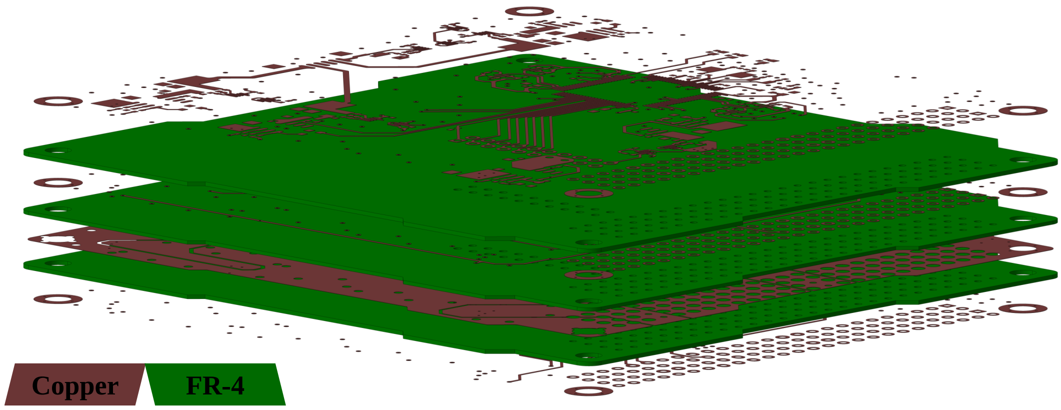

Figure 3.7 : CAD model of 4-Layer PCB-002.

Table 3.4 : Model information of 4-Layer PCB-002.

Layer Number	Material	Thickness, mm	Volume Fraction
1	Copper	0.035	0.147
2	FR-4	0.500	0.935
3	Copper	0.035	0.068
4	FR-4	0.440	0.935
5	Copper	0.035	0.839
6	FR-4	0.500	0.935
7	Copper	0.035	0.058

Third group of PCBs are 6 Layer PCBs. They have 6 items copper layers and 5 items FR-4 layers. Their CAD models are shown in Figure 3.8 and Figure 3.9. Their properties are given at Table 3.5 and Table 3.6.

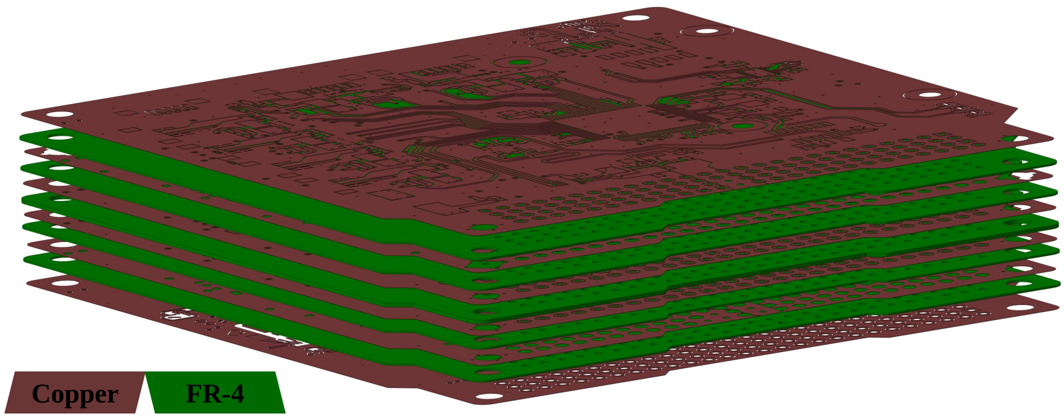

Figure 3.8 : CAD model of 6-Layer PCB-001.

Table 3.5 : Model information of 6-Layer PCB-001.

Layer Number	Material	Thickness, mm	Volume Fraction
1	Copper	0.035	0.844
2	FR-4	0.230	0.965
3	Copper	0.035	0.898
4	FR-4	0.230	0.965
5	Copper	0.035	0.920
6	FR-4	0.460	0.965
7	Copper	0.035	0.918
8	FR-4	0.230	0.965
9	Copper	0.035	0.889
10	FR-4	0.230	0.965
11	Copper	0.035	0.895

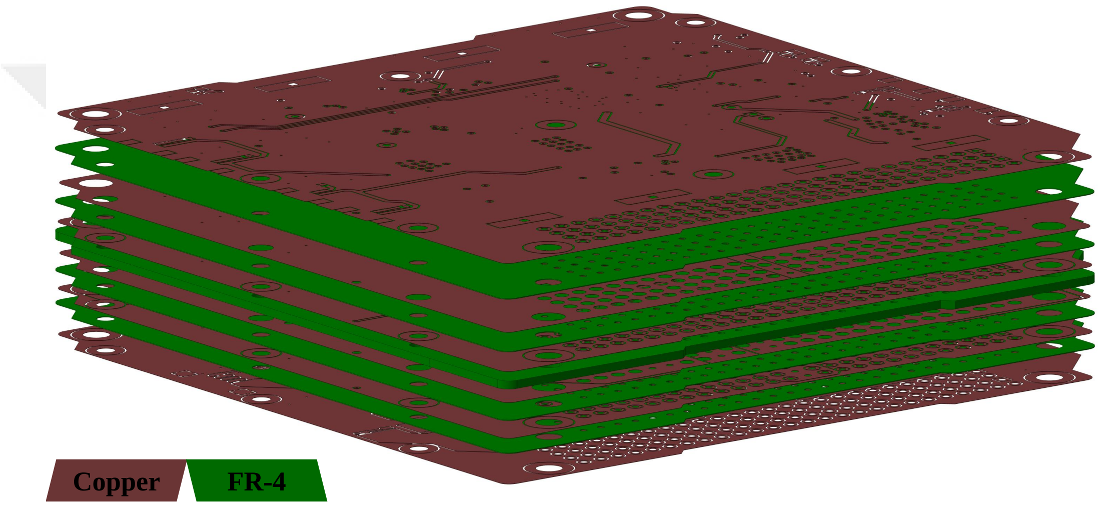

Figure 3.9 : CAD model of 6-Layer PCB-002.

Table 3.6 : Model information of 6-Layer PCB-002.

Layer Number	Material	Thickness, mm	Volume Fraction
1	Copper	0.035	0.893
2	FR-4	0.100	0.957
3	Copper	0.035	0.879
4	FR-4	0.100	0.957
5	Copper	0.035	0.892
6	FR-4	1.000	0.957
7	Copper	0.035	0.901
8	FR-4	0.100	0.957
9	Copper	0.035	0.873
10	FR-4	0.100	0.957
11	Copper	0.035	0.842

The final group of PCBs are 8 layer PCBs. They have 8 items copper layers and 7 items FR-4 layers. Their CAD models are shown in Figure 3.10 and Figure 3.11. Their properties are given at Table 3.7 and Table 3.8.

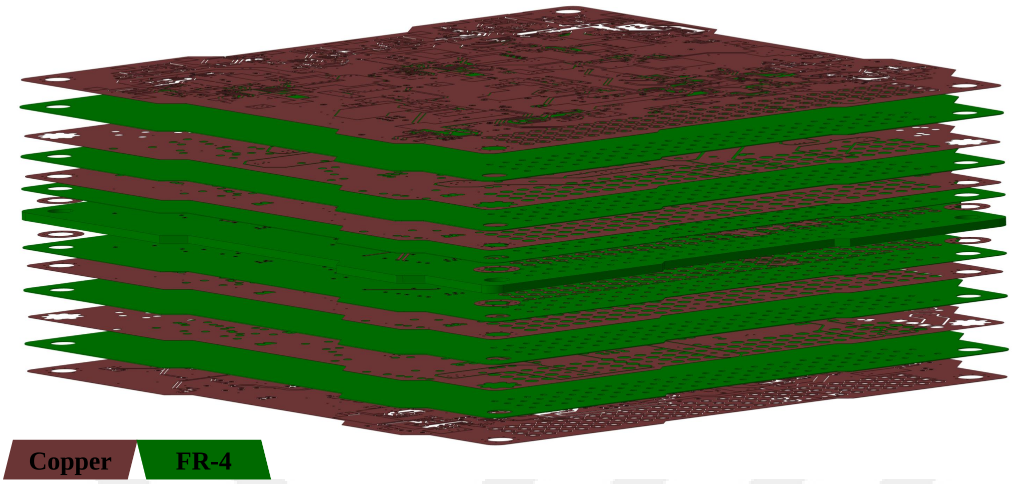

Figure 3.10 : CAD model of 8-Layer PCB-001.

Table 3.7 : Model information of 8-Layer PCB-001.

Layer Number	Material	Thickness, mm	Volume Fraction
1	Copper	0.035	0.788
2	FR-4	0.107	0.937
3	Copper	0.018	0.822
4	FR-4	0.107	0.937
5	Copper	0.035	0.853
6	FR-4	0.071	0.937
7	Copper	0.018	0.121
8	FR-4	1.000	0.937
9	Copper	0.018	0.104
10	FR-4	0.071	0.937
11	Copper	0.035	0.853
12	FR-4	0.107	0.937
13	Copper	0.018	0.817
14	FR-4	0.107	0.937
15	Copper	0.035	0.795

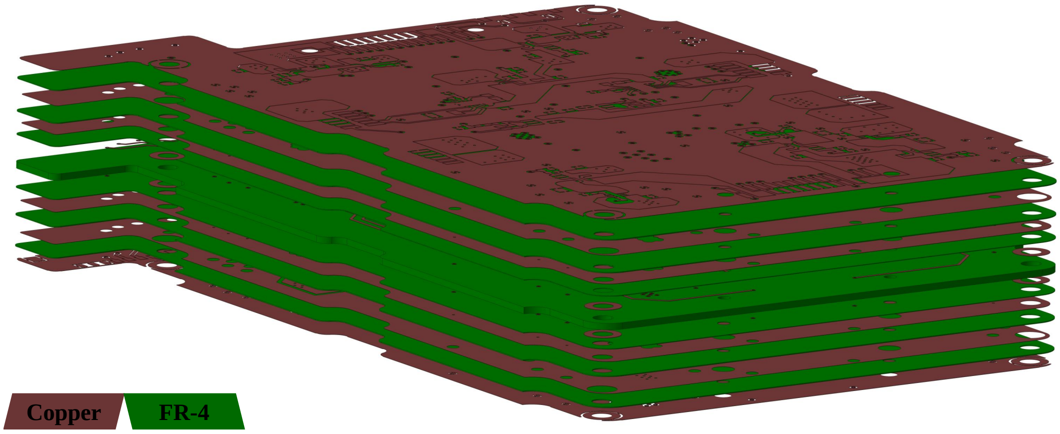

Figure 3.11 : CAD model of 8-Layer PCB-002.

Table 3.8 : Model information of 8-Layer PCB-002.

Layer Number	Material	Thickness, mm	Volume Fraction
1	Copper	0.035	0.915
2	FR-4	0.107	0.996
3	Copper	0.018	0.924
4	FR-4	0.107	0.996
5	Copper	0.035	0.908
6	FR-4	0.071	0.996
7	Copper	0.035	0.071
8	FR-4	0.720	0.996
9	Copper	0.035	0.030
10	FR-4	0.071	0.996
11	Copper	0.035	0.902
12	FR-4	0.107	0.996
13	Copper	0.018	0.914
14	FR-4	0.107	0.996
15	Copper	0.035	0.923

PCBs general dimensions are given at Table 3.9.

Table 3.9 : General dimensions of PCBs.

PCB Code	Width, mm	Length, mm	Thickness, mm
2-Layer PCB-001	97.000	98.000	1.570
2-Layer PCB-002	87.000	327.500	1.570
4-Layer PCB-001	70.000	70.000	1.360
4-Layer PCB-002	87.000	92.700	1.580
6-Layer PCB-001	90.000	93.700	1.590
6-Layer PCB-002	93.000	93.700	1.610
8-Layer PCB-001	88.000	94.000	1.781
8-Layer PCB-002	72.000	99.000	1.534

3.3 FEM Models of PCBs

In this section, FEM models are described. Firstly, the materials and properties are defined. After this subsection, the boundary conditions and contact are described in the next subsection. The mesh information section concludes the mesh models and their quality for analysis according to the NASTRAN limits in the last subsection.

3.3.1 Materials and properties

Two materials, FR-4 and copper, are used to create all models [47]. All analysis models are used same value of the materials. PCBs are modeled with using shells(2D). FR-4 material is defined as orthotropic material, and the defined properties of FR-4 are given in Table 3.10 [47]. The copper material is defined as an isotropic material, and the defined properties of copper are given in Table 3.11 [47].

Table 3.10 : FR-4 defined properties.

Property Item	Quantity
ρ	1900.00 kg/m^3
E_x	20400.00 MPa
E_y	18400.00 MPa
E_z	15000.00 MPa
G_{xy}	9200.00 MPa
G_{yz}	8400.00 MPa
G_{xz}	6600.00 MPa
ν_{xy}	0.11
ν_{yz}	0.09
ν_{xz}	0.14

Table 3.11 : Copper defined properties.

Property Item	Quantity
ρ	8942.00 kg/m^3
E	126000.00 MPa
G	46840.00 MPa
ν	0.345

3.3.2 Boundary conditions and contacts

Same boundary conditions are used for all models. All edges of PCBs are clamped. This boundary condition is defined because the DQM code's requirement for solving modal frequency is that all edges of plate should be clamped. Contacts between layers are defined as glue contact. They move totally together.

The boundary conditions of 2-layer PCB-001 and 2-layer PCB-002 are shown in Figure 3.12. 2-Layer PCBs contain one FR-4 layer and two copper layers, totally it is made up three layers. The boundary conditions of 4-layer PCB-001 and 4-layer PCB-002

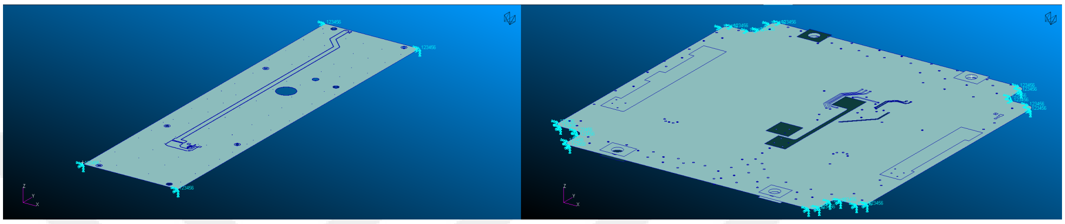

Figure 3.12 : Boundary conditions of 2-Layer PCBs.

are shown in Figure 3.13. 4-Layer PCBs contain three FR-4 layers and four copper layers, totally it is made up seven layers. The boundary conditions of 6-layer PCB-001

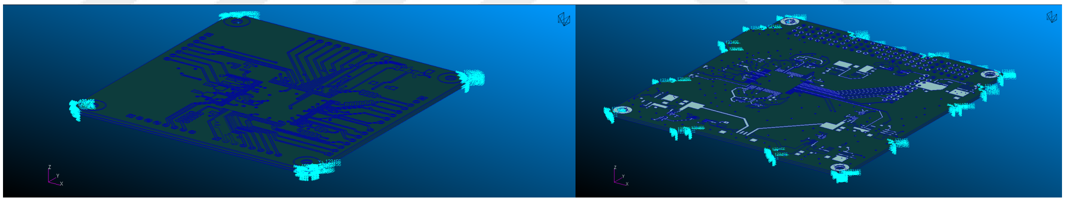

Figure 3.13 : Boundary conditions of 4-Layer PCBs.

and 6-layer PCB-002 are shown in Figure 3.14. 6-Layer PCBs contain five FR-4 layers and six copper layers, totally it is made up eleven layers. The boundary conditions of

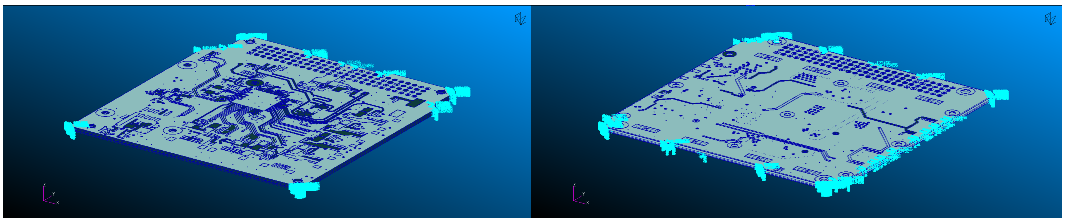

Figure 3.14 : Boundary conditions of 6-Layer PCBs.

8-layer PCB-001 and 8-layer PCB-002 are shown in Figure 3.15. 8-Layer PCBs contain seven FR-4 layers and eight copper layers, and are made up of fifteen layers.

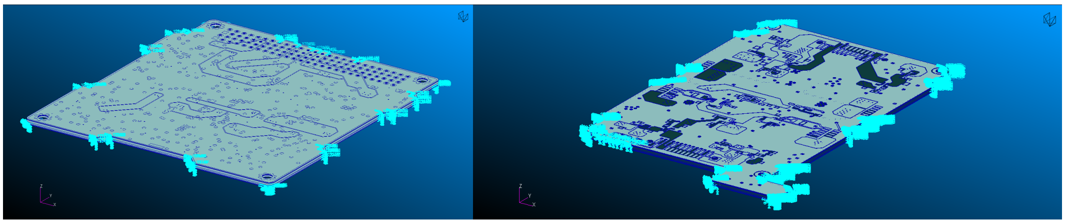

Figure 3.15 : Boundary conditions of 8-Layer PCBs.

3.3.3 Mesh information

Eight models' mesh are represented in this section. Figures show mesh with two perspectives. The one in which all of the PCB is shown, other one is focused somewhere on the surface. All of the models except 4-layer PCB-001 model are meshed with using tria elements. The 4-layer PCB-001 model is configured hybrid with tria and quad elements.

The final model of the 2-layer PCB-001 model (mesh size: 0.50 mm) is meshed with 98296 tria elements. The mesh model information is shown in Table 3.12 and its visual is shown in Figure 3.16.

Table 3.12 : 2-Layer PCB-001's mesh properties information.

Property	Failed Quantity	Worst Case	Criteria
Aspect Ratio	1204	Max=29.191139	5
Skew Angle	1004	Min=2.2663233	10
Normal Offset	0	Max=0.	0.15
Tangent Offset	0	Max=0.	0.15
Jacobian Ratio	0	Max=1.	-
Jacobian Zero	0	Min=0.00070767989	-

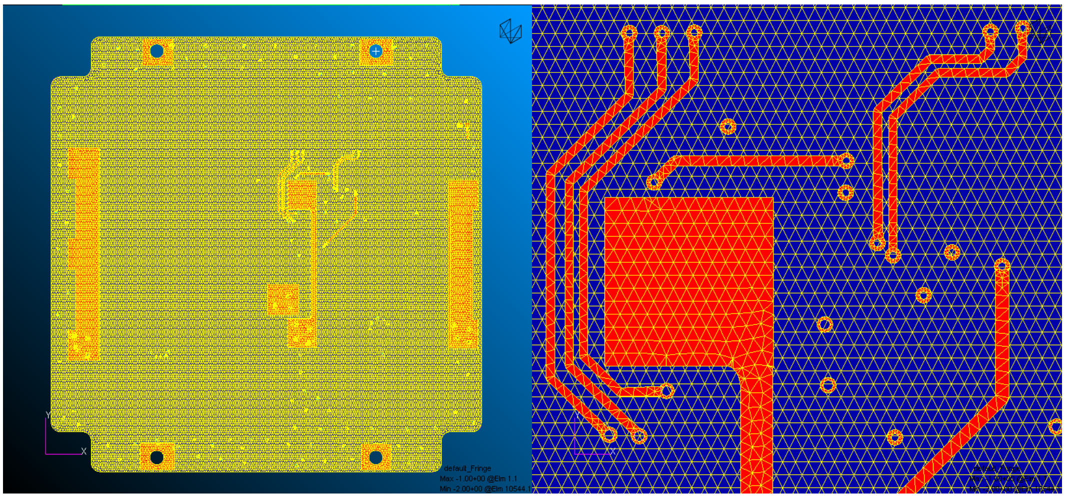

Figure 3.16 : Mesh figure of 2-layer PCB-001 model.

The final model of the 2-layer PCB-002 model (mesh size: 0.25 mm) is meshed with 2674982 tria elements. The mesh model information is shown in Table 3.13 and its visual is shown in Figure 3.17.

Table 3.13 : 2-Layer PCB-002's mesh properties information.

Property	Failed Quantity	Worst Case	Criteria
Aspect Ratio	1193	Max=1E+10	5
Skew Angle	1126	Min=0.015001139	10
Normal Offset	0	Max=0.	0.15
Tangent Offset	0	Max=0.	0.15
Jacobian Ratio	0	Max=1.	-
Jacobian Zero	0	Min=4.2561442E-07	-

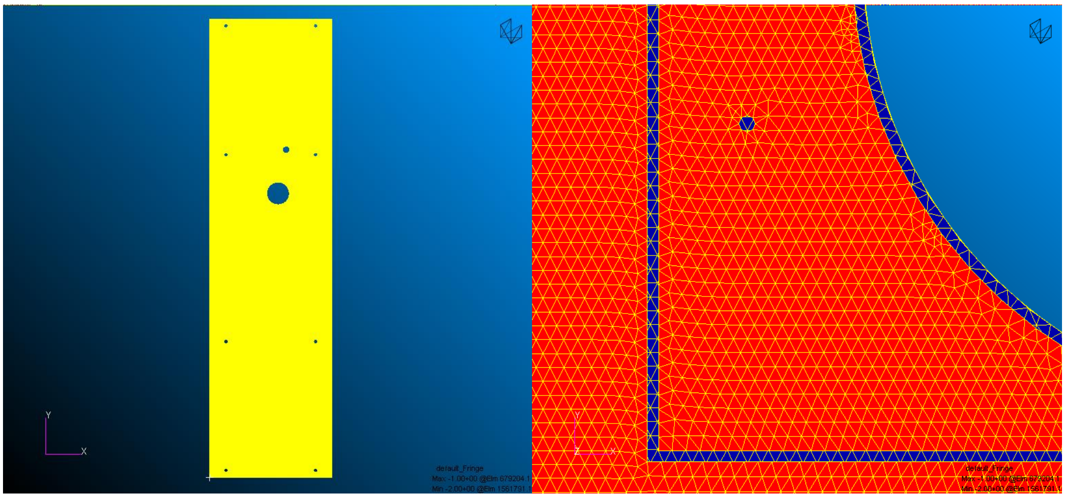

Figure 3.17 : Mesh figure of 2-layer PCB-002 model.

The final model of the 4-layer PCB-001 model (mesh size: 0.25 mm) is meshed with 15930 tria and 429604 quad elements, totally 445534 elements. The mesh model information is shown in Table 3.14 and its visual is shown in Figure 3.18.

Table 3.14 : 4-Layer PCB-001's mesh properties information.

Property	Failed Quantity	Worst Case	Criteria
Aspect Ratio	100	Max=10.394914	5
Skew Angle	0	Min=11.116948	30
Normal Offset	0	Max=0.	0.15
Tangent Offset	0	Max=0.	0.15
Jacobian Ratio	0	Max=7.4496489	-
Jacobian Zero	0	Min=0.0011810388	-
Taper	453	Max=0.76330376	0.5
Warp Angle	0	Max=0.	0.05

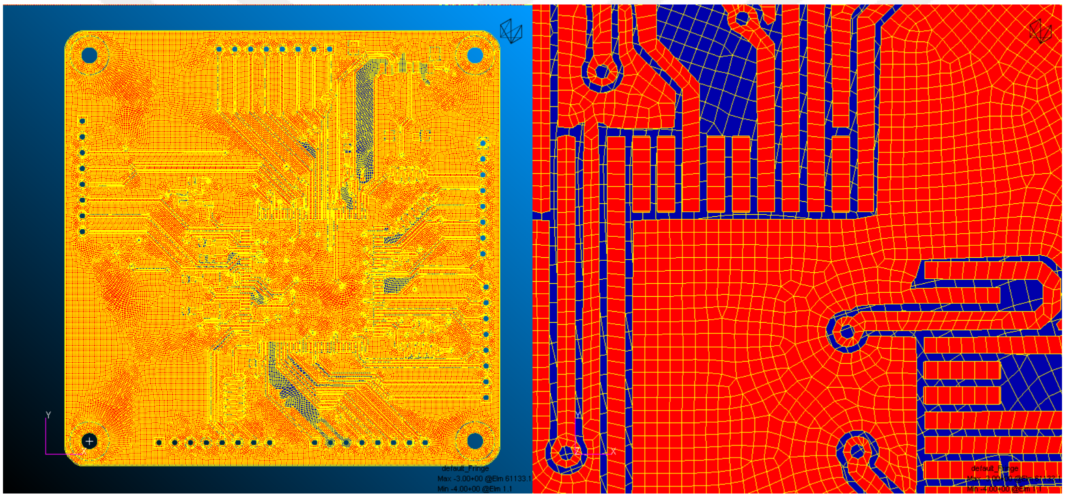

Figure 3.18 : Mesh figure of 4-layer PCB-001 model.

The final model of the 4-layer PCB-002 model (mesh size: 0.25 mm) is meshed with 1025566 tria elements. The mesh model information is shown in Table 3.15 and its visual is shown in Figure 3.19.

Table 3.15 : 4-Layer PCB-002's mesh properties information.

Property	Failed Quantity	Worst Case	Criteria
Aspect Ratio	76	Max=14.111297	5
Skew Angle	46	Min=4.7177963	10
Normal Offset	0	Max=0.	0.15
Tangent Offset	0	Max=0.	0.15
Jacobian Ratio	0	Max=1.	-
Jacobian Zero	0	Min=0.0023775399	-

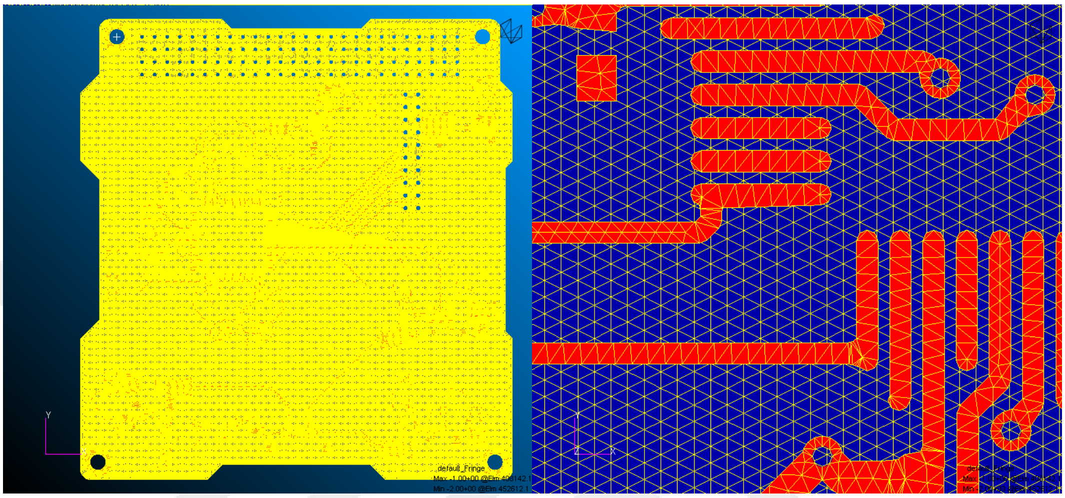

Figure 3.19 : Mesh figure of 4-layer PCB-002 model.

The final model of the 6-layer PCB-001 model (mesh size: 0.25 mm) is meshed with 2781861 tria elements. The mesh model information is shown in Table 3.16 and its visual is shown in Figure 3.20.

Table 3.16 : 6-Layer PCB-001's mesh properties information.

Property	Failed Quantity	Worst Case	Criteria
Aspect Ratio	4165	Max=86.538559	5
Skew Angle	2239	Min=0.76422298	10
Normal Offset	0	Max=0.	0.15
Tangent Offset	0	Max=0.	0.15
Jacobian Ratio	0	Max=1.	-
Jacobian Ratio	0	Max=1.	-
Jacobian Zero	0	Min=0.00017426652	-

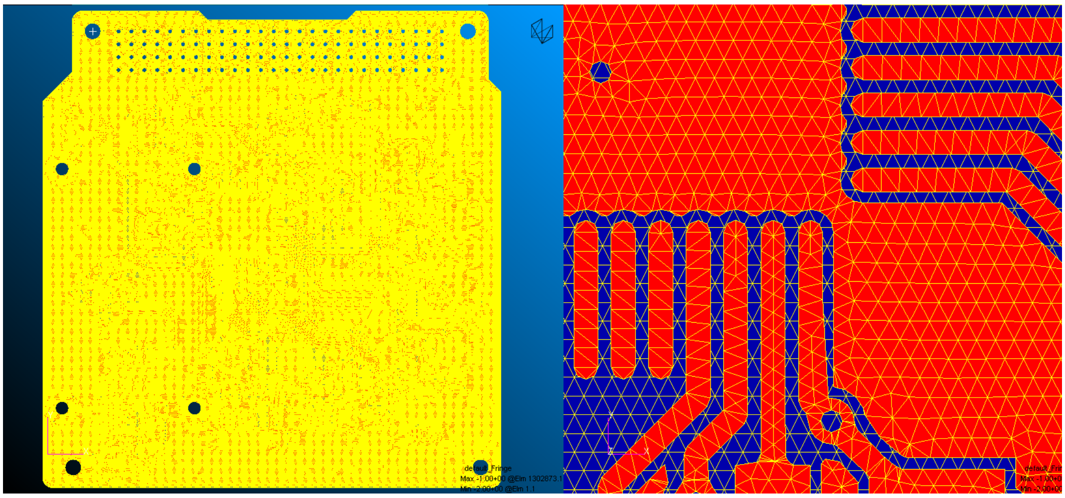

Figure 3.20 : Mesh figure of 6-layer PCB-001 model.

The final model of the 6-layer PCB-002 model (mesh size: 0.25 mm) is meshed with 2846523 tria elements. The mesh model information is shown in Table 3.17 and its visual is shown in Figure 3.21.

Table 3.17 : 6-Layer PCB-002's mesh properties information.

Property	Failed Quantity	Worst Case	Criteria
Aspect Ratio	2093	Max=42.872265	5
Skew Angle	1094	Min=1.5715505	10
Normal Offset	0	Max=0.	0.15
Tangent Offset	0	Max=0.	0.15
Jacobian Ratio	0	Max=1.	-
Jacobian Zero	0	Min=0.00035483204	-

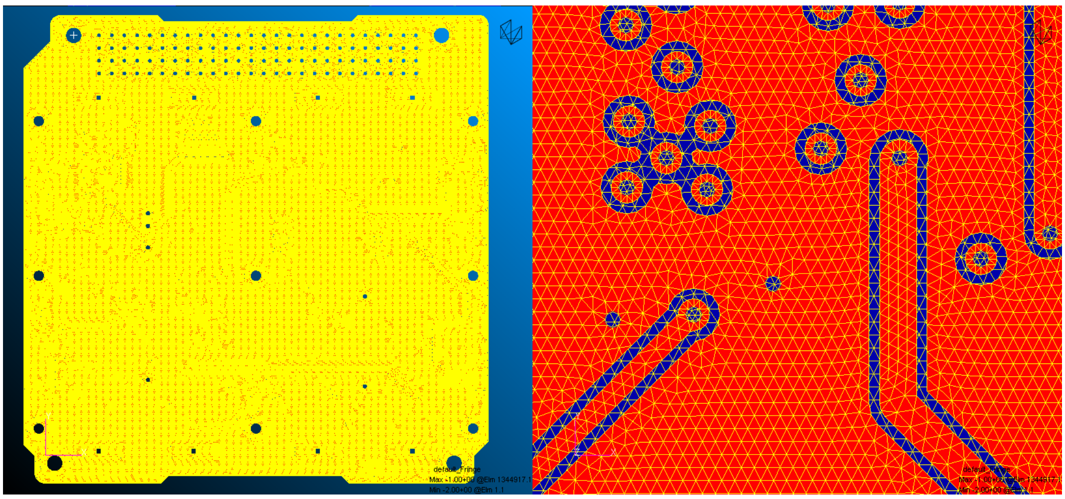

Figure 3.21 : Mesh figure of 6-layer PCB-002 model.

The final model of the 8-layer PCB-001 model (mesh size: 0.50 mm) is meshed with 1851163 tria elements. The mesh model information is shown in Table 3.18 and its visual is shown in Figure 3.22.

Table 3.18 : 8-Layer PCB-001's mesh properties information.

Property	Failed Quantity	Worst Case	Criteria
Aspect Ratio	276	Max=86.094185	5
Skew Angle	157	Min=0.76816118	10
Normal Offset	0	Max=0.	0.15
Tangent Offset	0	Max=0.	0.15
Jacobian Ratio	0	Max=1.	-
Jacobian Zero	0	Min=0.00064299442	-

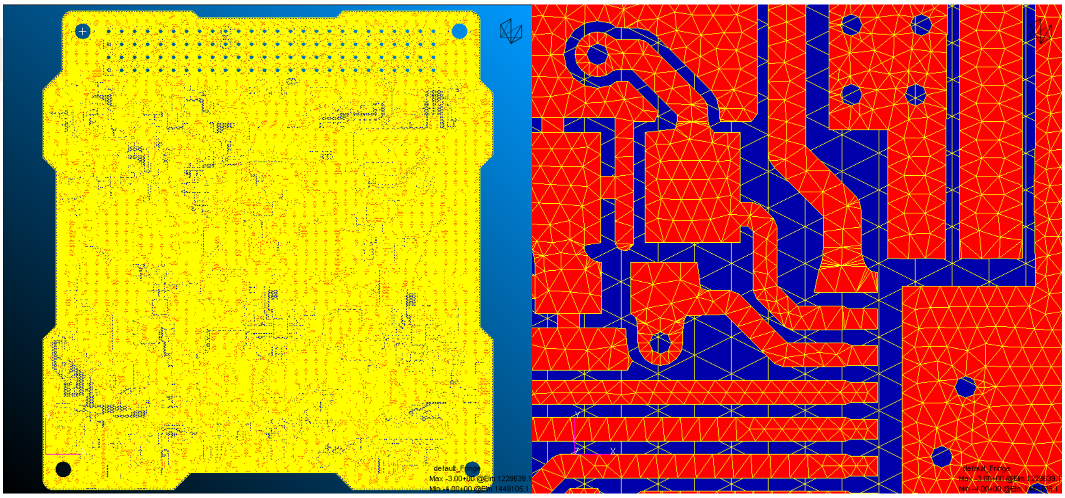

Figure 3.22 : Mesh figure of 8-layer PCB-001 model.

The final model of the 8-layer PCB-002 model (mesh size: 0.50 mm) is meshed with 835982 tria elements. The mesh model information is shown in Table 3.19 and its visual is shown in Figure 3.23.

Table 3.19 : 8-Layer PCB-002's mesh properties information.

Property	Failed Quantity	Worst Case	Criteria
Aspect Ratio	1967	Max=226.79768	5
Skew Angle	970	Min=0.29176819	10
Normal Offset	0	Max=0.	0.15
Tangent Offset	0	Max=0.	0.15
Jacobian Ratio	0	Max=1.	-
Jacobian Zero	0	Min=0.00018080747	-

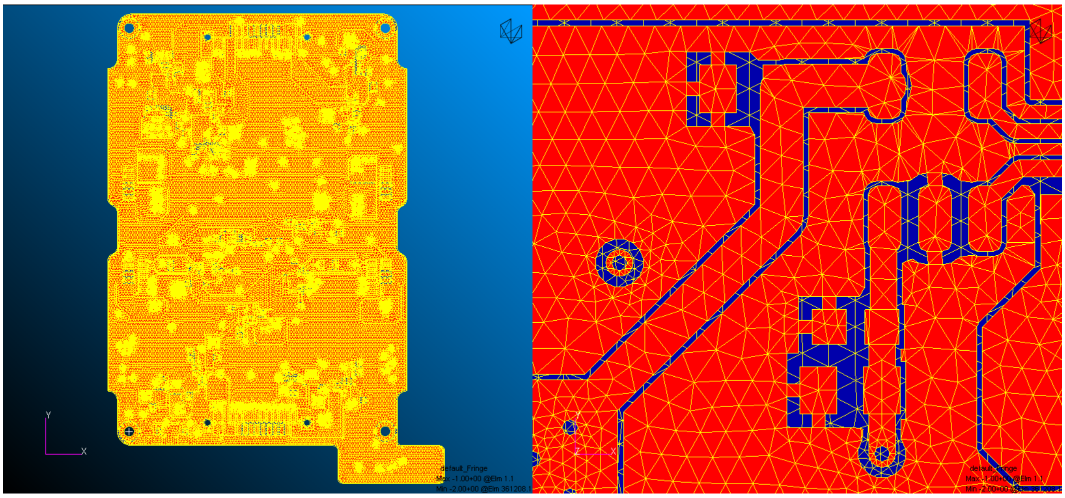

Figure 3.23 : Mesh figure of 8-layer PCB-002 model.

4. EQUIVALENT MATERIAL MODEL

An equivalent material model is proposed from study of Tognana et. al. [48]. Four material models are examined on this study. Those material models are Halpin-Tsai, mixture law, Foam, and Mori Tanaka. Halpin-Tsai, Foam and Mori Tanaka's models were good fitted. The Foam model is based on densities. The Mori-Tanaka is more complex model. In conrast, the mixture law was a poor fit. The Halpin-Tsai model was good fitted with experimental data. The Halpin-Tsai equation generalized by Kerner [49], the foam model, and the Mori-Tanaka method work well because they consider the material's composite nature and internal structure. The mixture law, however, fails because it oversimplifies the material properties, ignoring the effects of the internal infill. The study is based for 3D printed models.

In this study, the proposed models of Halpin-Tsai and Mixture Law models are adapted according to volume fractions of the PCB's layers.

Before equation adaptation, the study is used the Halpin-Tsai approach by generalized form by Kerner. The equations is started by:

$$E = E_M \frac{(1 + CB\phi)}{1 - B\psi} \tag{4.1}$$

where C and B are fitting parameters, and B can be calculated as:

$$B = \frac{\frac{E_V}{E_M} - 1}{\frac{E_V}{E_M} + C} \tag{4.2}$$

Void elasticity modulus is defined by E_V. And It is equal to 0 and it makes $B = -1/C$. E_M is the modulus of the matrix, and the parameter ψ can be estimated from:

$$\psi = 1 + \frac{1 - \phi_M}{\phi_M^2} \phi \tag{4.3}$$

where ϕ_M is the maximum packing fraction and will be considered equal to 1, then $\psi = 1$. Therefore, equation 4.1 becomes:

$$E = E_M \left(\frac{1 + \phi}{1 - \frac{\phi}{C}} \right) \tag{4.4}$$

Where ϕ is equal to $1 - v_f$. v_f is defined volume fraction of the layer. Equation 4.4 becomes:

$$E_{eq} = E\left(\frac{v_f}{1 + \frac{1-v_f}{C}}\right) \tag{4.5}$$

The mixture law is defined as Voigt model and it is rational with volume fraction. It is defined as:

$$E = E_M(1 - \phi) \tag{4.6}$$

and it becomes after $v_f = 1 - \phi$ as:

$$E_{eq} = Ev_f \tag{4.7}$$

The Halpin-Tsai model is defined on equation 4.5 and the Voigt model is defined on equation 4.7.

5. MATHEMATICAL MODEL OF PCBs

The PCBs are modeled as multilayered sandwich plates. The plates are assumed incompressible and in-plane and transverse shear strains together with in-plane normal strains will be considered in the formulation. Layers are assumed to be perfectly bonded to each other, and linear analyzes are performed. The geometry and the deformations of the n-layered sandwich plate are depicted in Figure 5.1 and 5.2.

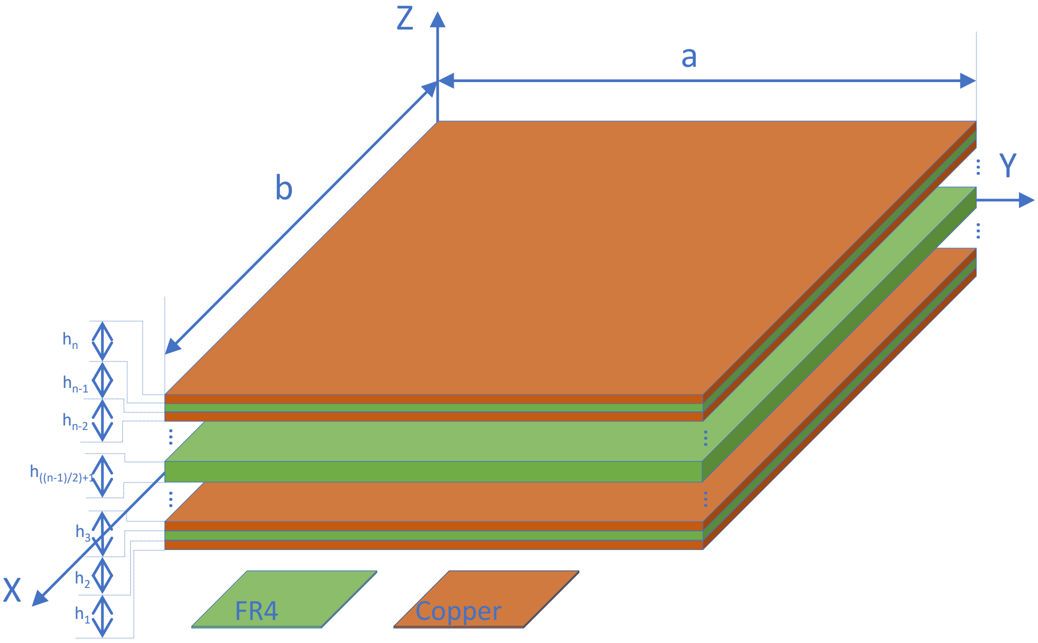

Figure 5.1 : Configuration of PCB, dimensions and the coordinate system.

The kinematic relations are:

$$
\begin{aligned}
U_k(x,y,z,t) &= u_k(x,y,t) + \frac{z^k}{h_k}\left[u_{k+1}(x,y,t) - u_k(x,y,t)\right] \\
V_k(x,y,z,t) &= v_k(x,y,t) + \frac{z^k}{h_k}\left[v_{k+1}(x,y,t) - v_k(x,y,t)\right] \quad ,k = 1,2,\ldots,n \\
W_k(x,y,z,t) &= w(x,y,t)
\end{aligned}
\tag{5.1}
$$

where, U_k, V_k and W_k are displacement field through k'th layer in x, y and z directions respectively.

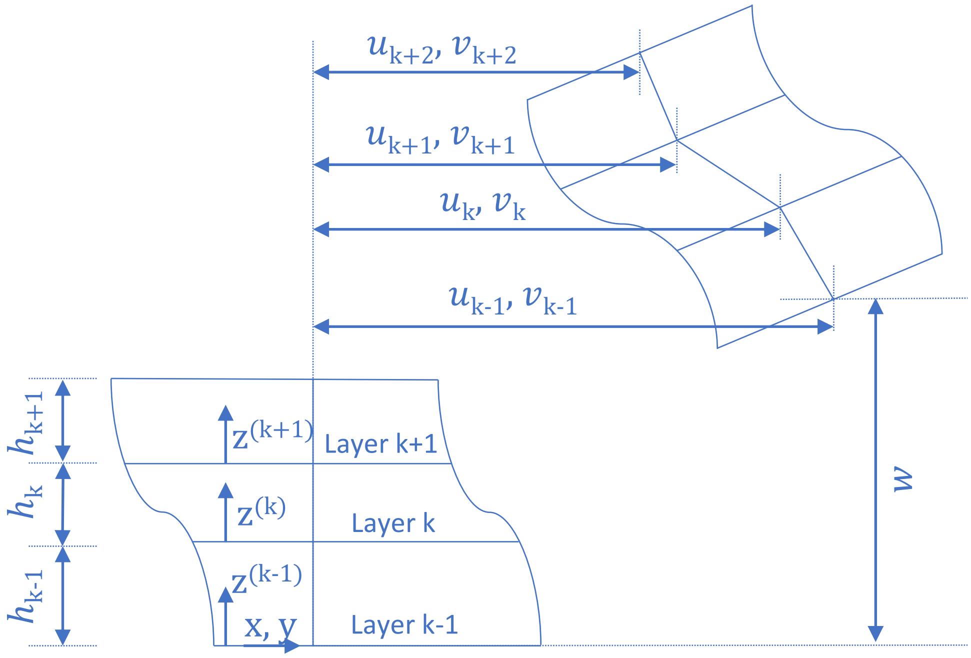

Figure 5.2 : Deformations of the layers.

The strain displacement relations are:

$$\begin{aligned}
\varepsilon_{xx}^k &= \frac{\partial u_k}{\partial x} + \frac{z^k}{h_k}\left(\frac{\partial u_{k+1}}{\partial x} - \frac{\partial u_k}{\partial x}\right) \\
\varepsilon_{yy}^k &= \frac{\partial v_k}{\partial y} + \frac{z^k}{h_k}\left(\frac{\partial v_{k+1}}{\partial y} - \frac{\partial v_k}{\partial y}\right) \\
\gamma_{xz}^k &= \frac{1}{h_k}(u_{k+1} - u_k) + \frac{\partial w}{\partial x} \qquad\qquad ,k = 1,2,\ldots,n \\
\gamma_{yz}^k &= \frac{1}{h_k}(v_{k+1} - v_k) + \frac{\partial w}{\partial y} \\
\gamma_{xy}^k &= \frac{\partial u_k}{\partial y} + \frac{z^k}{h_k}\left(\frac{\partial u_{k+1}}{\partial y} - \frac{\partial u_k}{\partial y}\right) + \frac{\partial v_k}{\partial x} + \frac{z^k}{h_k}\left(\frac{\partial v_{k+1}}{\partial x} - \frac{\partial v_k}{\partial x}\right)
\end{aligned} \tag{5.2}$$

The stress-strain relations for the isotropic copper and orthotropic FR-4 layers are presented, respectively, as follows:

$$\begin{Bmatrix} \sigma_{xx}^k \\ \sigma_{yy}^k \\ \tau_{xy}^k \\ \tau_{yz}^k \\ \tau_{xz}^k \end{Bmatrix} = \frac{E_k}{(1-v_k^2)} \begin{bmatrix} 1 & v_k & 0 & 0 & 0 \\ v_k & 1 & 0 & 0 & 0 \\ 0 & 0 & \frac{1-v_k}{2} & 0 & 0 \\ 0 & 0 & 0 & \frac{1-v_k}{2} & 0 \\ 0 & 0 & 0 & 0 & \frac{1-v_k}{2} \end{bmatrix} \begin{Bmatrix} \varepsilon_{xx}^k \\ \varepsilon_{yy}^k \\ \gamma_{xy}^k \\ \gamma_{yz}^k \\ \gamma_{xz}^k \end{Bmatrix} \quad ,k = 1,3,\ldots,n \tag{5.3}$$

Where E is the modulus of elasticity and υ is the Poisson's ratio. For the orthotropic FR-4 layers, we have:

$$\left\{\begin{array}{c}\sigma_{xx}^{k}\\ \sigma_{yy}^{k}\\ \tau_{xy}^{k}\\ \tau_{yz}^{k}\\ \tau_{xz}^{k}\end{array}\right\}=\left[\begin{array}{ccccc}Q_{11}^{k}&Q_{12}^{k}&Q_{16}^{k}&0&0\\ Q_{12}^{k}&Q_{22}^{k}&Q_{26}^{k}&0&0\\ Q_{16}^{k}&Q_{26}^{k}&Q_{66}^{k}&0&0\\ 0&0&0&Q_{44}^{k}&Q_{45}^{k}\\ 0&0&0&Q_{45}^{k}&Q_{55}^{k}\end{array}\right]\left\{\begin{array}{c}\varepsilon_{xx}^{k}\\ \varepsilon_{yy}^{k}\\ \gamma_{xy}^{k}\\ \gamma_{yz}^{k}\\ \gamma_{xz}^{k}\end{array}\right\} \quad ,k=2,4,\ldots,n-1 \tag{5.4}$$

where, $Q_{mn}^{(k)}$ are the transformed stiffness coefficients for the k'th layer that can be expressed in terms of the lamina stiffness coefficients in principal material coordinates as follows:

$$\begin{aligned}
\bar{Q}_{11}^{k}&=Q_{11}^{k}\cos^{4}\theta_{k}+2\left(Q_{12}^{k}+2Q_{66}^{k}\right)\sin^{2}\theta_{k}\cos^{2}\theta_{k}+Q_{22}^{k}\sin^{4}\theta_{k}\\
\bar{Q}_{12}^{k}&=\left(Q_{11}^{k}+Q_{22}^{k}-4Q_{66}^{k}\right)\sin^{2}\theta_{k}\cos^{2}\theta_{k}+Q_{12}^{k}\left(\sin^{4}\theta_{k}+\cos^{4}\theta_{k}\right)\\
\bar{Q}_{22}^{k}&=Q_{11}^{k}\sin^{4}\theta_{k}+2\left(Q_{12}^{k}+2Q_{66}^{k}\right)\sin^{2}\theta_{k}\cos^{2}\theta_{k}+Q_{22}^{k}\cos^{4}\theta_{k}\\
\bar{Q}_{16}^{k}&=\left(Q_{11}^{k}-Q_{12}^{k}-2Q_{66}^{k}\right)\sin_{\theta}\cos^{3}\theta_{k}+\left(Q_{12}^{k}-Q_{22}^{k}+2Q_{66}^{k}\right)\sin^{3}\theta_{k}\cos\theta_{k}\\
\bar{Q}_{26}^{k}&=\left(Q_{11}^{k}-Q_{12}^{k}-2Q_{66}^{k}\right)\sin^{3}\theta_{k}\cos\theta_{k}+\left(Q_{12}^{k}-Q_{22}^{k}+2Q_{66}^{k}\right)\sin\theta_{k}\cos^{3}\theta_{k}\\
\bar{Q}_{66}^{k}&=\left(Q_{11}^{k}+Q_{22}^{k}-2Q_{12}^{k}-2Q_{66}^{k}\right)\sin^{2}\theta_{k}\cos^{2}\theta_{k}+Q_{66}^{k}\left(\sin^{4}\theta_{k}+\cos^{4}\theta_{k}\right)\\
\bar{Q}_{44}^{k}&=Q_{44}^{k}\cos^{2}\theta_{k}+Q_{55}^{k}\sin^{2}\theta_{k}\\
\bar{Q}_{45}^{k}&=\left(Q_{55}^{k}-Q_{44}^{k}\right)\cos\theta_{k}\sin\theta_{k}\\
\bar{Q}_{55}^{k}&=Q_{55}^{k}\cos^{2}\theta_{k}+Q_{44}\sin^{2}\theta_{k}
\end{aligned} \tag{5.5}$$

where, θ_k is the angle of lamination of the k'th layer and Q_{mn}^{k} are related to the engineering constants as follows:

$$Q_{11}^{k}=\frac{E_{1}^{k}}{1-v_{12}v_{21}},Q_{12}^{k}=\frac{v_{12}E_{2}^{k}}{1-v_{12}v_{21}},Q_{22}^{k}=\frac{E_{2}^{k}}{1-v_{12}v_{21}},Q_{66}^{k}=G_{12},Q_{44}^{k}=G_{23},\\ Q_{55}^{k}=G_{13},v_{21}=\frac{E_{2}^{k}v_{12}}{E_{1}^{k}} \tag{5.6}$$

Hamilton's principle that will be used in deriving governing equations can be represented in the following general form:

$$\int_{t_1}^{t_2}\left[\int_{V}\rho\frac{\partial^{2}\vec{u}}{\partial t^{2}}.\delta\vec{u}dV-\left(\int_{V}\rho\vec{f}.\delta\vec{u}\,dV+\int_{S_2}\vec{t}.\delta\vec{u}dS-\int_{V}\sigma_{ij}\delta\varepsilon_{ij}dV\right)\right]dt=0 \tag{5.7}$$

Where $\vec{u}$ is the vector of displacement field, ρ is the density, $\vec{f}$ is the vector of body forces, $\vec{t}$ is the surface traction force vector, σ_{ij} are the stresses and ε_{ij} are the strains.

Hamilton's principle for the free vibrations of n-layered plate gives:

$$
\begin{aligned}
&\int_{t_1}^{t_2}\left[\sum_{k=1}^{n}\int_0^a\int_0^b\int_0^{h_k}\rho_k\left(\frac{\partial^2 U_k}{\partial t^2}\delta U_k+\frac{\partial^2 V_k}{\partial t^2}\delta V_k+\frac{\partial^2 W_k}{\partial t^2}\delta W_k\right)dz^k dydx\right]dt\\
&+\int_{t_1}^{t_2}\left[\sum_{k=1}^{n}\int_0^a\int_0^b\int_0^{h_k}\left(\sigma_{xx}^k\delta\varepsilon_{xx}^k+\sigma_{yy}^k\delta\varepsilon_{yy}^k+\tau_{xy}^k\delta\gamma_{xy}^k+\tau_{xz}^k\delta\gamma_{xz}^k\right.\right.\\
&\left.\left.+\tau_{yz}^k\delta\gamma_{yz}^k\right)dz^k dydx\right]dt=0
\end{aligned}
\tag{5.8}
$$

That leads to:

$$
\begin{aligned}
&\int_{t_1}^{t_2}\left[\sum_{k=1}^{n}\int_0^a\int_0^b\int_0^{h_k}\rho_k\left[\left(\frac{\partial^2 u_k}{\partial t^2}+\frac{z^k}{h_k}\frac{\partial^2 u_{k+1}}{\partial t^2}+\frac{z^k}{h_k}\frac{\partial^2 u_k}{\partial t^2}\right)\left(\delta u_k+\frac{z^k}{h_k}\delta u_{k+1}+\frac{z^k}{h_k}\delta u_k\right)\right.\right.\\
&\qquad+\left(\frac{\partial^2 v_k}{\partial t^2}+\frac{z^k}{h_k}\frac{\partial^2 v_{k+1}}{\partial t^2}+\frac{z^k}{h_k}\frac{\partial^2 v_k}{\partial t^2}\right)\left(\delta v_k+\frac{z^k}{h_k}\delta v_{k+1}+\frac{z^k}{h_k}\delta v_k\right)\\
&\qquad\left.\left.+\frac{\partial^2 w}{\partial t^2}\delta w\right]dz^k dydx\right]dt\\
&\qquad+\int_{t_1}^{t_2}\left[\sum_{k=1}^{n}\int_0^a\int_0^b\int_0^{h_k}\left\{\sigma_{xx}^k\left[\delta\frac{\partial u_k}{\partial x}+\frac{z^k}{h_k}\left(\delta\frac{\partial u_{k+1}}{\partial x}-\delta\frac{\partial u_k}{\partial x}\right)\right]\right.\right.\\
&\qquad+\sigma_{yy}^k\left[\delta\frac{\partial v_k}{\partial y}+\frac{z^k}{h_k}\left(\delta\frac{\partial v_{k+1}}{\partial y}-\delta\frac{\partial v_k}{\partial y}\right)\right]\\
&\qquad+\tau_{xy}^k\left[\delta\frac{\partial u_k}{\partial y}+\frac{z^k}{h_k}\left(\delta\frac{\partial u_{k+1}}{\partial y}-\delta\frac{\partial u_k}{\partial y}\right)+\delta\frac{\partial v_k}{\partial x}+\frac{z^k}{h_k}\left(\delta\frac{\partial v_{k+1}}{\partial x}\right.\right.\\
&\qquad\left.\left.-\delta\frac{\partial v_k}{\partial x}\right)\right]+\tau_{xz}^k\left[\frac{1}{h_k}\left(\delta u_{k+1}-\delta u_k\right)+\delta\frac{\partial w}{\partial x}\right]\\
&\qquad\left.\left.+\tau_{yz}^k\left[\frac{1}{h_k}\left(\delta v_{k+1}-\delta v_k\right)+\delta\frac{\partial w}{\partial y}\right]\right\}dz^k dydx\right]dt=0
\end{aligned}
\tag{5.9}
$$

Integration by parts gives the governing equations and boundary conditions as follows:

$$
\begin{aligned}
&\delta u_k : \frac{1}{6}\rho_{k-1}h_{k-1}\frac{\partial^2 u_{k-1}}{\partial t^2}+\frac{1}{3}\left(\rho_{k-1}h_{k-1}+\rho_k h_k\right)\frac{\partial^2 u_k}{\partial t^2}\\
&+\frac{1}{6}\rho_k h_k\frac{\partial^2 u_{k+1}}{\partial t^2}-\frac{\partial N_{xx}^k}{\partial x}+\frac{\partial M_{xx}^k}{\partial x}-\frac{\partial M_{xx}^{k-1}}{\partial x}-\frac{\partial Q_{xy}^k}{\partial y} \qquad ,k=1,\ldots,n+1\\
&+\frac{\partial T_{xy}^k}{\partial y}-\frac{\partial T_{xy}^{k-1}}{\partial y}-\frac{Q_{xz}^k}{h_k}+\frac{Q_{xz}^{k-1}}{h_{k-1}}=0\\
&\delta v_k : \frac{1}{6}\rho_{k-1}h_{k-1}\frac{\partial^2 v_{k-1}}{\partial t^2}+\frac{1}{3}\left(\rho_{k-1}h_{k-1}+\rho_k h_k\right)\frac{\partial^2 v_k}{\partial t^2}\\
&+\frac{1}{6}\rho_k h_k\frac{\partial^2 v_{k+1}}{\partial t^2}-\frac{\partial N_{yy}^k}{\partial y}+\frac{\partial M_{yy}^k}{\partial y}-\frac{\partial M_{yy}^{k-1}}{\partial y}-\frac{\partial Q_{xy}^k}{\partial x} \qquad ,k=1,\ldots,n+1\\
&+\frac{\partial T_{xy}^k}{\partial x}-\frac{\partial T_{xy}^{k-1}}{\partial x}-\frac{Q_{yz}^k}{h_k}+\frac{Q_{yz}^{k-1}}{h_{k-1}}=0\\
&\qquad\qquad \delta w : \left(\sum_{k=1}^{n}\rho_k h_k\right)\frac{\partial^2 w}{\partial t^2}-\sum_{k=1}^{n}\frac{\partial Q_{xz}^k}{\partial x}-\sum_{k=1}^{n}\frac{\partial Q_{yz}^k}{\partial y}=0
\end{aligned}
\tag{5.10}
$$

where the section force and moment components are as follows:

$$
\begin{aligned}
&N_{xx}^k=\int_0^{h_k}\sigma_{xx}^k dz^k, N_{yy}^k=\int_0^{h_k}\sigma_{yy}^k dz^k, Q_{xz}^k=\int_0^{h_k}\tau_{xz}^k dz^k, Q_{yz}^k\\
&=\int_0^{h_k}\tau_{yz}^k dz^k, Q_{xy}^k=\int_0^{h_k}\tau_{xy}^k dz^k\\
&M_{xx}^k=\int_0^{h_k}\left(\frac{z^k}{h_k}\right)\sigma_{xx}^k dz^k, M_{yy}^k=\int_0^{h_k}\left(\frac{z^k}{h_k}\right)\sigma_{yy}^k dz^k, T_{xy}^k=\int_0^{h_k}\left(\frac{z^k}{h_k}\right)\tau_{yy}^k dz^k
\end{aligned}
\tag{5.11}
$$

Note that ρ_k, h_k, N_{xx}^k, N_{yy}^k, Q_{xz}^k, Q_{yz}^k, Q_{xy}^k, M_{xx}^k, M_{yy}^k and T_{xy}^k are equal to zero for $k=0$ and $k=n+1$. In addition, open form of section forces and moments in equation 5.11 are as follows:

For copper layers (k=1, 3, ..., n):

$$
\begin{aligned}
N_{xx}^{k} &= \frac{E_k h_k}{2\left(1-\nu_k^2\right)}\left[\frac{\partial u_k}{\partial x}+\frac{\partial u_{k+1}}{\partial x}+\nu_k\left(\frac{\partial v_k}{\partial y}+\frac{\partial v_{k+1}}{\partial y}\right)\right]\\
N_{yy}^{k} &= \frac{E_k h_k}{2\left(1-\nu_k^2\right)}\left[\frac{\partial v_k}{\partial y}+\frac{\partial v_{k+1}}{\partial y}+\nu_k\left(\frac{\partial u_k}{\partial x}+\frac{\partial u_{k+1}}{\partial x}\right)\right]\\
Q_{xy}^{k} &= \frac{E_k h_k}{4\left(1+\nu_k\right)}\left(\frac{\partial u_k}{\partial y}+\frac{\partial u_{k+1}}{\partial y}+\frac{\partial v_k}{\partial x}+\frac{\partial v_{k+1}}{\partial x}\right)\\
Q_{xz}^{k} &= \frac{E_k h_k}{2\left(1+\nu_k\right)}\left[\frac{1}{h_k}\left(u_{k+1}-u_k\right)+\frac{\partial w}{\partial x}\right]\\
Q_{yz}^{k} &= \frac{E_k h_k}{2\left(1+\nu_k\right)}\left[\frac{1}{h_k}\left(v_{k+1}-v_k\right)+\frac{\partial w}{\partial y}\right]\\
M_{xx}^{k} &= \frac{E_k h_k}{6\left(1-\nu_k^2\right)}\left[\frac{\partial u_k}{\partial x}+2\frac{\partial u_{k+1}}{\partial x}+\nu_k\left(\frac{\partial v_k}{\partial y}+2\frac{\partial v_{k+1}}{\partial y}\right)\right]\\
M_{yy}^{k} &= \frac{E_k h_k}{6\left(1-\nu_k^2\right)}\left[\frac{\partial v_k}{\partial y}+2\frac{\partial v_{k+1}}{\partial y}+\nu_k\left(\frac{\partial u_k}{\partial x}+2\frac{\partial u_{k+1}}{\partial x}\right)\right]\\
T_{xy}^{k} &= \frac{E_k h_k}{12\left(1+\nu_k\right)}\left(\frac{\partial u_k}{\partial y}+2\frac{\partial u_{k+1}}{\partial y}+\frac{\partial v_k}{\partial x}+2\frac{\partial v_{k+1}}{\partial x}\right)
\end{aligned}
\tag{5.12}
$$

For FR-4 layers (k=2, 4, ..., n-1):

$$
\begin{aligned}
N_{xx}^{k} &= \frac{1}{2}h_k\left[\bar{Q}_{11}^{k}\left(\frac{\partial u_k}{\partial x}+\frac{\partial u_{k+1}}{\partial x}\right)+\bar{Q}_{12}^{k}\left(\frac{\partial v_k}{\partial y}+\frac{\partial v_{k+1}}{\partial y}\right)+\bar{Q}_{16}^{k}\left(\frac{\partial u_k}{\partial y}+\frac{\partial u_{k+1}}{\partial y}\right.\right.\\
&\left.\left.+\frac{\partial v_k}{\partial x}+\frac{\partial v_{k+1}}{\partial x}\right)\right]\\
N_{yy}^{k} &= \frac{1}{2}h_k\left[\bar{Q}_{12}^{k}\left(\frac{\partial u_k}{\partial x}+\frac{\partial u_{k+1}}{\partial x}\right)+\bar{Q}_{22}^{k}\left(\frac{\partial v_k}{\partial y}+\frac{\partial v_{k+1}}{\partial y}\right)+\bar{Q}_{26}^{k}\left(\frac{\partial u_k}{\partial y}+\frac{\partial u_{k+1}}{\partial y}\right.\right.\\
&\left.\left.+\frac{\partial v_k}{\partial x}+\frac{\partial v_{k+1}}{\partial x}\right)\right]\\
Q_{xy}^{k} &= \frac{1}{2}h_k\left[\bar{Q}_{16}^{k}\left(\frac{\partial u_k}{\partial x}+\frac{\partial u_{k+1}}{\partial x}\right)+\bar{Q}_{26}^{k}\left(\frac{\partial v_k}{\partial y}+\frac{\partial v_{k+1}}{\partial y}\right)+\bar{Q}_{66}^{k}\left(\frac{\partial u_k}{\partial y}+\frac{\partial u_{k+1}}{\partial y}\right.\right.\\
&\left.\left.+\frac{\partial v_k}{\partial x}+\frac{\partial v_{k+1}}{\partial x}\right)\right]\\
Q_{xz}^{k} &= \bar{Q}_{45}^{k}\left(h_k\frac{\partial w}{\partial y}-v_k+v_{k+1}\right)+\bar{Q}_{55}^{k}\left(h_k\frac{\partial w}{\partial x}-u_k+u_{k+1}\right)\\
Q_{yz}^{k} &= \bar{Q}_{44}^{k}\left(h_k\frac{\partial w}{\partial y}-v_k+v_{k+1}\right)+\bar{Q}_{45}^{k}\left(h_k\frac{\partial w}{\partial x}-u_k+u_{k+1}\right)\\
M_{xx}^{k} &= \frac{1}{6}h_k\left[\bar{Q}_{11}^{k}\left(\frac{\partial u_k}{\partial x}+2\frac{\partial u_{k+1}}{\partial x}\right)+\bar{Q}_{12}^{k}\left(\frac{\partial v_k}{\partial y}+2\frac{\partial v_{k+1}}{\partial y}\right)+\bar{Q}_{16}^{k}\left(\frac{\partial u_k}{\partial y}+2\frac{\partial u_{k+1}}{\partial y}\right.\right.\\
&\left.\left.+\frac{\partial v_k}{\partial x}+2\frac{\partial v_{k+1}}{\partial x}\right)\right]\\
M_{yy}^{k} &= \frac{1}{6}h_k\left[\bar{Q}_{12}^{k}\left(\frac{\partial u_k}{\partial x}+2\frac{\partial u_{k+1}}{\partial x}\right)+\bar{Q}_{22}^{k}\left(\frac{\partial v_k}{\partial y}+2\frac{\partial v_{k+1}}{\partial y}\right)+\bar{Q}_{26}^{k}\left(\frac{\partial u_k}{\partial y}+2\frac{\partial u_{k+1}}{\partial y}\right.\right.\\
&\left.\left.+\frac{\partial v_k}{\partial x}+2\frac{\partial v_{k+1}}{\partial x}\right)\right]\\
T_{xy}^{k} &= \frac{1}{6}h_k\left[\bar{Q}_{16}^{k}\left(\frac{\partial u_k}{\partial x}+2\frac{\partial u_{k+1}}{\partial x}\right)+\bar{Q}_{26}^{k}\left(\frac{\partial v_k}{\partial y}+2\frac{\partial v_{k+1}}{\partial y}\right)+\bar{Q}_{66}^{k}\left(\frac{\partial u_k}{\partial y}+2\frac{\partial u_{k+1}}{\partial y}\right.\right.\\
&\left.\left.+\frac{\partial v_k}{\partial x}+2\frac{\partial v_{k+1}}{\partial x}\right)\right]
\end{aligned}
\tag{5.13}
$$

And the boundary conditions are:

$$
\left.
\begin{aligned}
&\left(N_{xx}^{k}-M_{xx}^{k}+M_{xx}^{k-1}\right)\delta u_k\Big|_{x=0}^{a}=0\\
&\left(N_{yy}^{k}-M_{yy}^{k}+M_{yy}^{k-1}\right)\delta v_k\Big|_{y=0}^{b}=0\\
&\left(Q_{xy}^{k}-T_{xy}^{k}+T_{xy}^{k-1}\right)\delta u_k\Big|_{y=0}^{b}=0\\
&\left(Q_{xy}^{k}-T_{xy}^{k}+T_{xy}^{k-1}\right)\delta v_k\Big|_{x=0}^{a}=0\\
&Q_{xz}^{k}\delta w\Big|_{x=0}^{a}=0\\
&Q_{yz}^{k}\delta w\Big|_{y=0}^{b}=0
\end{aligned}
\right. \quad ,k=1,2,\ldots,n+1
\tag{5.14}
$$

In total, we have 2n+3 equations as presented in equation 5.10 and 2n+3 dependent variables.

The purpose of this study is to obtain accurate natural frequencies of PCBs without using detailed models that require lots of computational effort. There are voids inside layers of PCBs and current approach depends on homogenization of elastic properties of layers using Halpin Tsai model [48]. Also, Chapter 4 explains the derivation of the elastic properties equations. Therefore, elastic properties of copper and FR-4 layers will be assumed in the following form:

$$E_k = \frac{v_f^k}{1+\frac{1-v_f^k}{C_{copper}}} E_{copper} \quad ,k = 1,3\ldots,n \tag{5.15}$$

$$E_1^k = \frac{v_f^k}{1+\frac{1-v_f^k}{C_{FR-4}}} E_{1,FR-4} \quad and \quad E_2^k = \frac{v_f^k}{1+\frac{1-v_f^k}{C_{FR-4}}} E_{2,FR-4} \quad ,k = 2,4\ldots,n-1 \tag{5.16}$$

Note that the Poisson's ratio is assumed independent of the volume fraction for both copper and FR-4 layers.

Assuming harmonic vibrations of the PCBs, the displacements are:

$$\begin{aligned}
u_k(x,y,t) &= \bar{u}_k(x,y)e^{i\omega t} \\
v_k(x,y,t) &= \bar{v}_k(x,y)e^{i\omega t} \quad ,k = 1,2,\ldots,n \\
w(x,y,t) &= \bar{w}(x,y)e^{i\omega t}
\end{aligned} \tag{5.17}$$

Then, the governing equations become:

$$\begin{aligned}
&-\frac{\partial N_{xx}^k}{\partial x} + \frac{\partial M_{xx}^k}{\partial x} - \frac{\partial M_{xx}^{k-1}}{\partial x} - \frac{\partial Q_{xy}^k}{\partial y} + \frac{\partial T_{xy}^k}{\partial y} - \frac{\partial T_{xy}^{k-1}}{\partial y} \\
&-\frac{Q_{xz}^k}{h_k} + \frac{Q_{xz}^{k-1}}{h_{k-1}} = \omega^2 \left[\frac{1}{6}\rho_{k-1}h_{k-1}\bar{u}_{k-1}\right. \qquad ,k = 1,\ldots,n+1 \\
&\left.+\frac{1}{3}\left(\rho_{k-1}h_{k-1} + \rho_k h_k\right)\bar{u}_k + \frac{1}{6}\rho_k h_k \bar{u}_{k+1}\right] \\
&-\frac{\partial N_{yy}^k}{\partial y} + \frac{\partial M_{yy}^k}{\partial y} - \frac{\partial M_{yy}^{k-1}}{\partial y} - \frac{\partial Q_{xy}^k}{\partial x} + \frac{\partial T_{xy}^k}{\partial x} - \frac{\partial T_{xy}^{k-1}}{\partial x} \\
&-\frac{Q_{yz}^k}{h_k} + \frac{Q_{yz}^{k-1}}{h_{k-1}} = \omega^2 \left[\frac{1}{6}\rho_{k-1}h_{k-1}\bar{v}_{k-1}\right. \qquad ,k = 1,\ldots,n+1 \\
&\left.+\frac{1}{3}\left(\rho_{k-1}h_{k-1} + \rho_k h_k\right)\bar{v}_k + \frac{1}{6}\rho_k h_k \bar{v}_{k+1}\right] \\
&\qquad -\sum_{k=1}^{n}\frac{\partial Q_{xz}^k}{\partial x} - \sum_{k=1}^{n}\frac{\partial Q_{yz}^k}{\partial y} = \omega^2\left(\sum_{k=1}^{n}\rho_k h_k\right)\bar{w}
\end{aligned} \tag{5.18}$$

6. DIFFERENTIAL QUADRATURE METHOD AND MODELS

In this chapter, the Differential Quadrature Method (DQM) is explained, and the models utilized are presented.

6.1 Method

The governing differential equation system presented in equation 5.18 is discretized by the differential quadrature method. This method depends on Lagrange interpolating polynomials and the partial derivatives of a function $f(x,y)$ with respect to spatial coordinates are represented as a weighted sum of function points:

$$\frac{\partial^p f}{\partial x^p}(x_i,y_j) = \sum_{k=1}^{N} c_{ik}^{(p)} f(x_k,y_j) \tag{6.1}$$

$$\frac{\partial^r f}{\partial y^r}(x_i,y_j) = \sum_{m=1}^{M} d_{jm}^{(r)} f(x_i,y_m) \tag{6.2}$$

where, N and M are the number of grid points in x and y directions respectively and c_{ik} and d_{jm} are weighting coefficients are calculated for the first order derivatives as follows [50]:

$$c_{ik}^{(1)} = \begin{cases} \frac{\bar{M}_x^{(1)}(x_i)}{(x_i-x_k)\bar{M}_x^{(1)}(x_k)} & \text{for } i \neq k \text{ and } i,k = 1,2,\ldots,N \\ -\sum_{s=1,s\neq i}^{N} c_{is}^{(1)} & \text{for } i = k \text{ and } i,k = 1,2,\ldots,N \end{cases} \tag{6.3}$$

$$d_{jm}^{(1)} = \begin{cases} \frac{\bar{M}_y^{(1)}(y_j)}{(y_j-y_m)\bar{M}_y^{(1)}(y_m)} & \text{for } j \neq m \text{ and } j,m = 1,2,\ldots,M \\ -\sum_{s=1,s\neq j}^{M} d_{js}^{(1)} & \text{for } j = m \text{ and } j,m = 1,2,\ldots,M \end{cases} \tag{6.4}$$

With

$$\bar{M}_x(x) = \prod_{s=1}^{N}(x-x_s) \text{ and } \bar{M}_y(y) = \prod_{s=1}^{M}(y-y_s) \tag{6.5}$$

And

$$\bar{M}_x^{(1)}(x_i) = \prod_{s=1,s\neq i}^{N}(x_i-x_s) \text{ and } \bar{M}_y^{(1)}\left(y_j\right) = \prod_{s=1,s\neq j}^{M}\left(y_j-y_s\right) \tag{6.6}$$

For higher order coefficients we have:

$$c_{ik}^{(p)} = \begin{cases} p\left(c_{ii}^{(p-1)}c_{ik}^{(1)} - \frac{c_{ik}^{(p-1)}}{x_i - x_k}\right) & \text{for } i \neq k \text{ and } i,k = 1,2,\ldots,N \\ -\sum_{s=1,s\neq i}^{N} c_{is}^{(p)} & \text{for } i = k \text{ and } i,k = 1,2,\ldots,N \end{cases} \tag{6.7}$$

$$d_{jm}^{(r)} = \begin{cases} r\left(d_{jj}^{(r-1)}d_{jm}^{(1)} - \frac{d_{jm}^{(r-1)}}{y_j - y_m}\right) & \text{for } j \neq m \text{ and } j,m = 1,2,\ldots,M \\ -\sum_{s=1,s\neq i}^{M} d_{js}^{(r)} & \text{for } j = m \text{ and } j,m = 1,2,\ldots,M \end{cases} \tag{6.8}$$

It is well known that a grid distribution denser on the boundaries give much better results compared to an equispaced distribution, therefore, the Chebyshev-Gauss-Lobatto distribution will be used to determine the grid points:

$$x_i = a\left[1 - cos\left(\frac{i-1}{N-1}\pi\right)\right], \quad i = 1,2,\ldots,N \tag{6.9}$$

$$y_j = b\left[1 - cos\left(\frac{j-1}{M-1}\pi\right)\right], \quad j = 1,2,\ldots,M \tag{6.10}$$

6.2 Models

In this section, DQM models which solved for optimization and validation are shown following figures.

2-Layer PCB-001, 2-Layer PCB-002, 4-Layer PCB-001, and 4-Layer PCB-002 models are used for optimization. And the Chebyshev-Gauss-Lobatto distribution are seen on the grid data. Three of remained PCB models are used for validation. All dimensions of PCB models are shown in Table 3.9. 2-Layer PCB-001 model's grid distribution is shown in Figure 6.1.

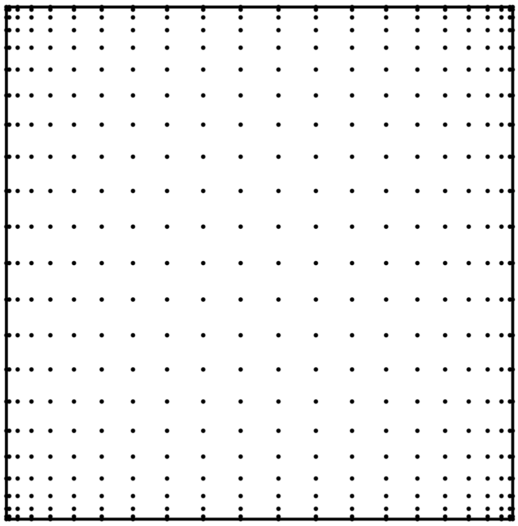

Figure 6.1 : Grid distribution of 2-Layer PCB-001 DQM model.

2-Layer PCB-002 model's grid distribution is shown in Figure 6.2.

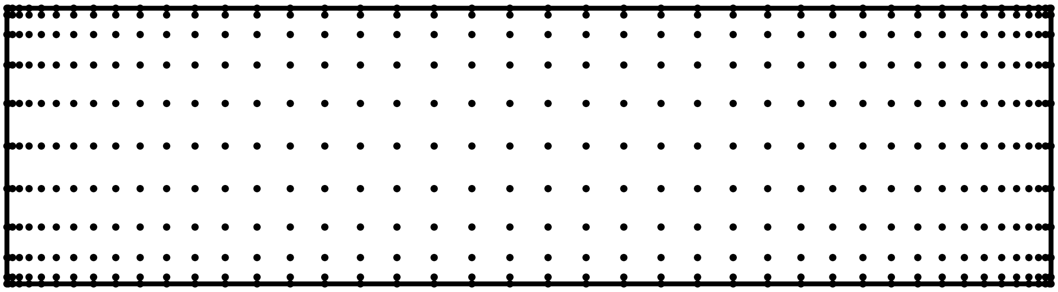

Figure 6.2 : Grid distribution of 2-Layer PCB-002 DQM model.

4-Layer PCB-001 model's grid distribution is shown in Figure 6.3.

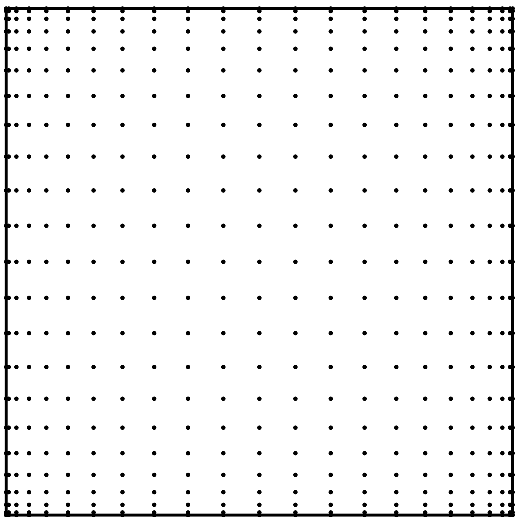

Figure 6.3 : Grid distribution of 4-Layer PCB-001 DQM model.

4-Layer PCB-002 model's grid distribution is shown in Figure 6.4.

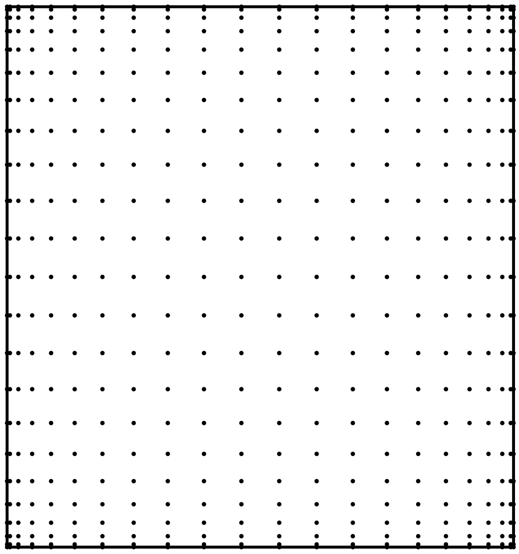

Figure 6.4 : Grid distribution of 4-Layer PCB-002 DQM model.

6-Layer PCB-001 model's grid distribution is shown in Figure 6.5.

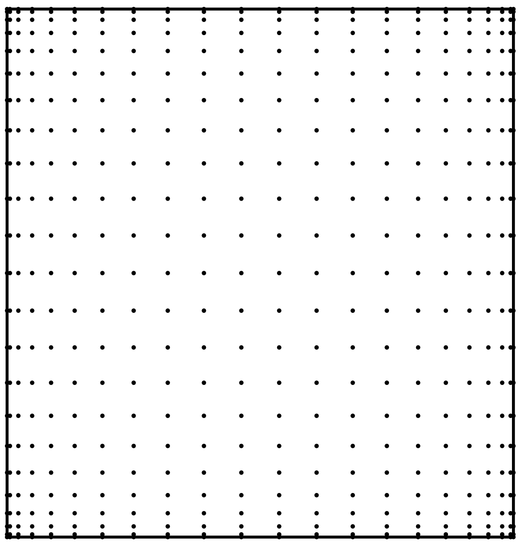

Figure 6.5 : Grid distribution of 6-Layer PCB-001 DQM model.

6-Layer PCB-002 model's grid distribution is shown in Figure 6.6.

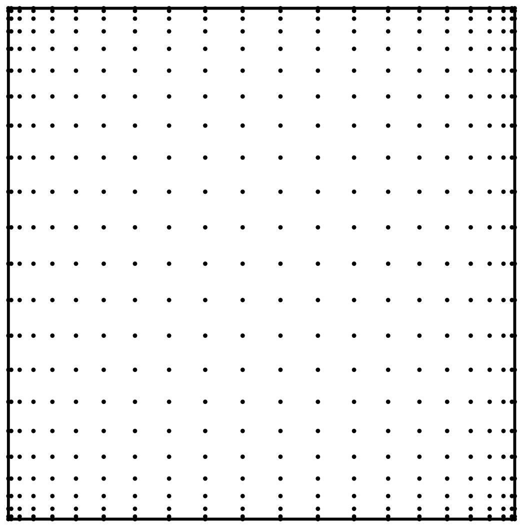

Figure 6.6 : Grid distribution of 6-Layer PCB-002 DQM model.

8-Layer PCB-001 model's grid distribution is shown in Figure 6.7.

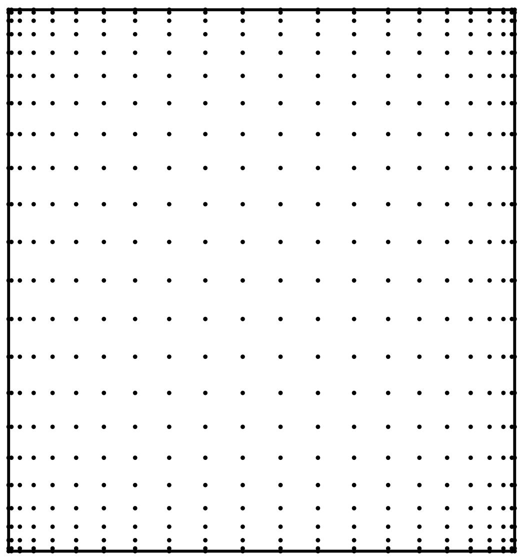

Figure 6.7 : Grid distribution of 8-Layer PCB-001 DQM model.

All edges are fixed for all models.

7. OPTIMIZATION

The optimization problem is selected to minimize the sum of normalized root mean squared deviation between DQM and FEM results for the first n number of modes calculated for m number of different PCB models:

$$\min_{x} f = \sum_{j=1}^{m} \sqrt{\frac{1}{n} \sum_{i=1}^{n} \left(\frac{\omega_i^{FEM_j} - \omega_i^{DQM_j}}{\omega_i^{FEM_j}} \right)^2} \tag{7.1}$$

And x is the vector of decision variables:

$$x = \{C_{FR-4}, C_{copper}\} \tag{7.2}$$

Since there are only two parameters, the optimization problem is solved by brute force approach. The objective function in equation 7.1 is solved for possible values of design parameters in equation 7.2 and obtained plot is shown in Figure 7.1. The minimum value of the objective function is found to be f=0.103124 at $C_{FR-4} = \infty$ and C_{copper}=2.505 as indicated by a red dot in Figure 7.1. Variation of the material properties by volume fraction of copper and FR-4 corresponding to these optimal parameters are presented in Figure 7.2. On the other hand, Voigt model assumes a linear variation between elastic properties and volume fraction as follows:

$$E_k = v_f^k E_{copper}, \quad k = 1, 3, \ldots, n \tag{7.3}$$

$$E_1^k = v_f^k E_{1,FR-4} \quad \text{and} \quad E_2^k = v_f^k E_{2,FR-4}, \quad k = 2, 4, \ldots, n-1 \tag{7.4}$$

This model is a special case of the Halpin-Tsai model for $C \rightarrow \infty$. Actually, the calculated optimal material coefficient $C_{FR-4} = \infty$ indicates that variation of FR-4 elastic properties obey Voigt model, nevertheless, the same thing does not apply to copper.

The objective function using the Voigt model is calculated as f=0.108121, which is $\approx$%5 larger compared to the result obtained with the Halpin-Tsai model (f=0.103124).

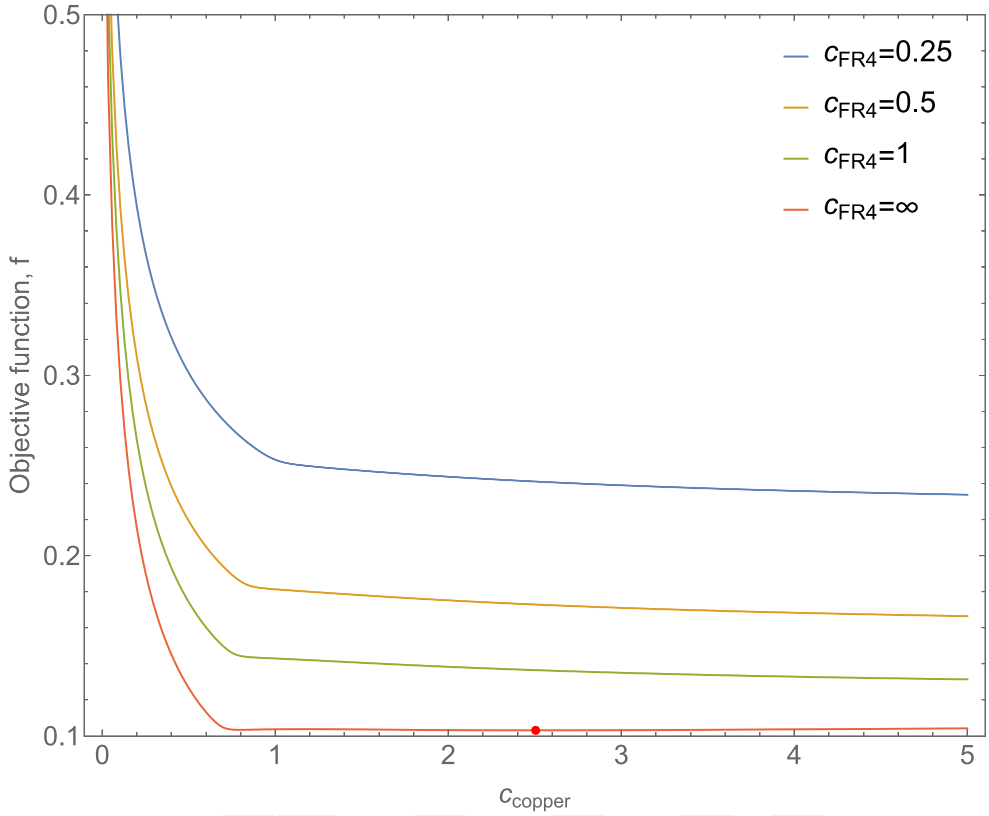

Figure 7.1 : Variation of the objective function with design parameters.

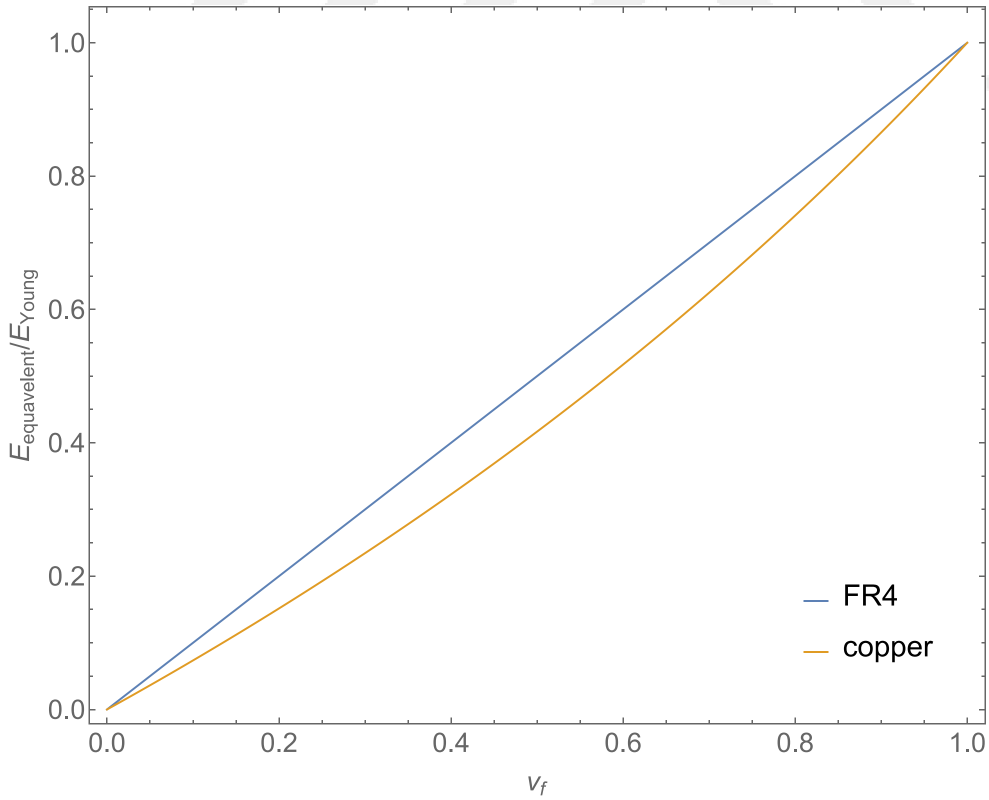

Figure 7.2 : Variation of the material properties by volume fraction of copper and FR-4.

8. RESULTS AND DISCUSSIONS

In this chapter, validation cases are shown. Detailed FEM analysis and equivalent model analysis are compared. Equivalent model analyses were performed using the DQM for several cases, while one analysis was conducted using FEA.

8.1 Results of Detailed FEM And Equivalent Model DQM Analyses

In this section, FEM analysis results and modified material models' DQM analyses results are represented. The mode shapes of the first six modes and their values are given in Figures 8.1 to Figures 8.7.

The detailed solution of FEM analysis that contains different mesh sizes is shown in Table 1 to Table 8 which defines the first six mode results. Each of the models has more than one result. The mesh size of each model starts from 1.00 mm. The second mesh size is 0.50 mm. If one more solution is needed, the third mesh size is 0.25 mm. Each model solved a more precise mesh model until the average difference between mesh sizes was less than 1.00%.

Results of FEM detailed modal analyses and DQM equivalent material model's modal analyses are represented in following figures. Results are included mode shapes and their frequencies. Firstly, results of 2-Layer PCB-001, 2-Layer PCB-002, 4-Layer PCB-001, and 4-Layer PCB-002 are represented in Figure 8.1, Figure 8.2, Figure 8.3, Figure 8.4. Those are optimization cases results.

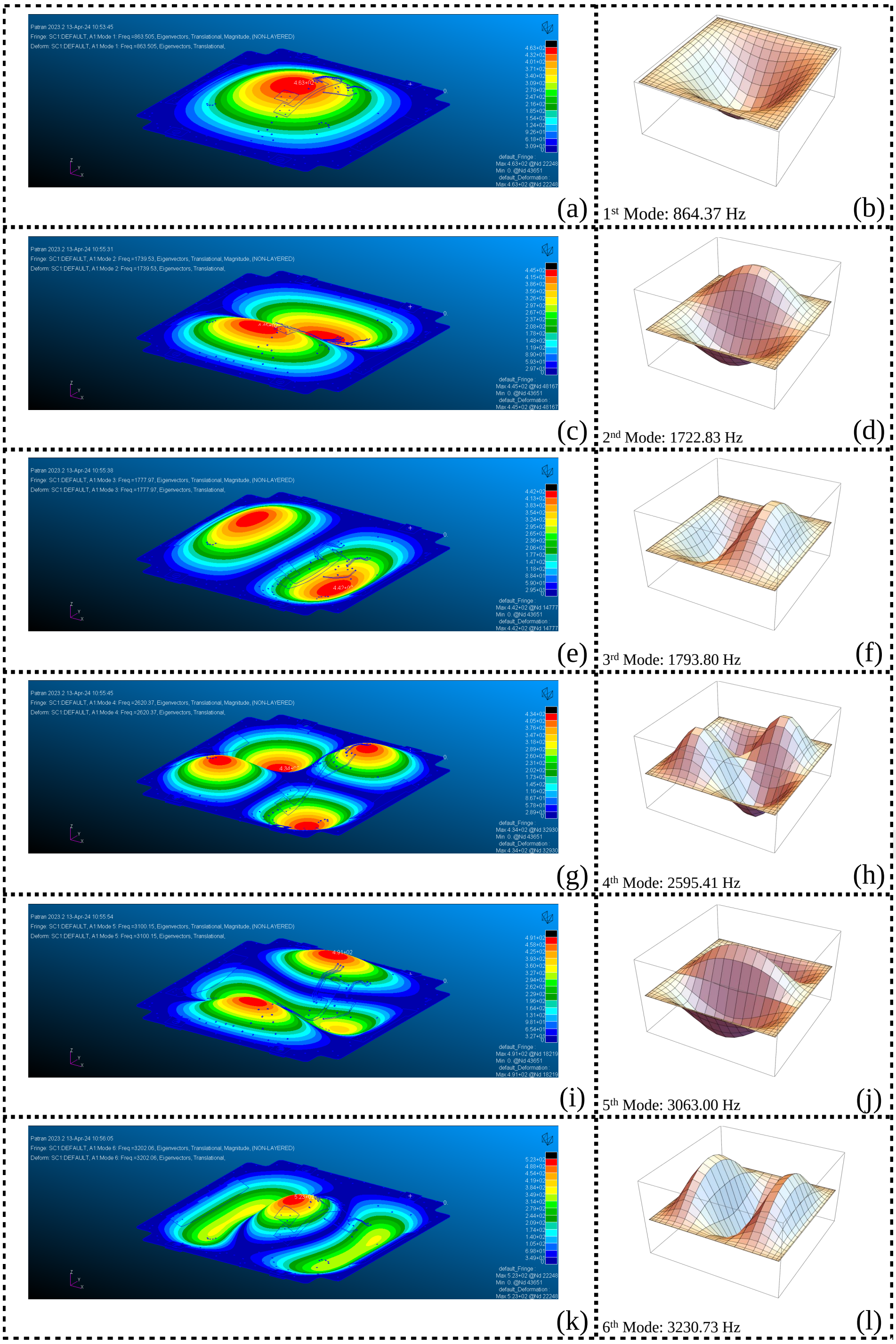

Figure 8.1 : 2-Layer PCB-001's detailed FEM and DQM analyses results mode shapes and frequencies; First modes: (a) 863.505 Hz. (b) 864.37 Hz. Second modes: (c) 1739.53 Hz. (d) 1722.83 Hz. Third modes: (e) 1777.97 Hz. (f) 1793.80 Hz. Forth modes: (g) 2620.37 Hz. (h) 2595.41 Hz. Fifth modes: (i) 3100.15 Hz. (j) 3063.00 Hz. Sixth modes: (k) 3202.06 Hz. (l) 3230.73 Hz.

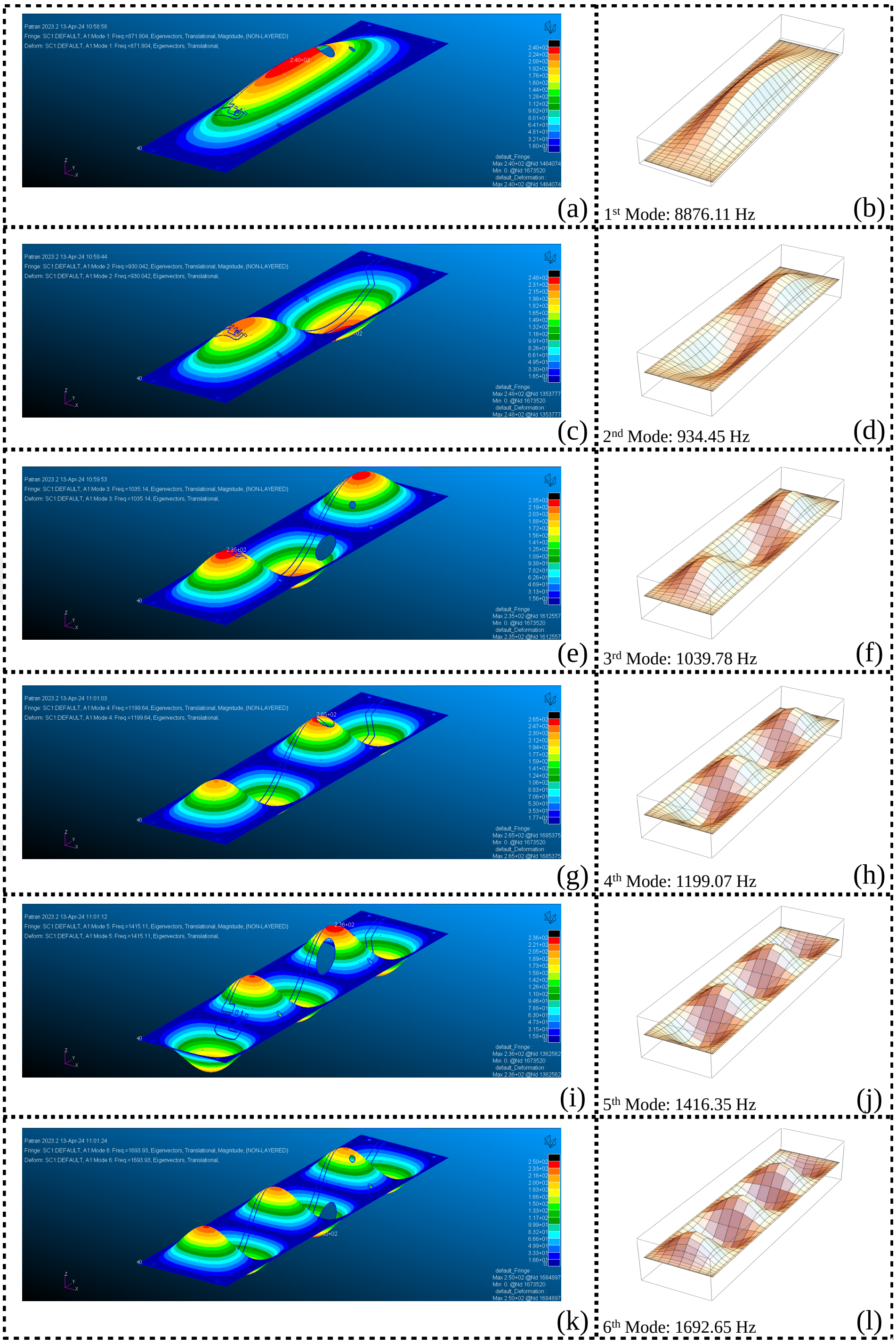

Figure 8.2 : 2-Layer PCB-002's detailed FEM and DQM analyses results mode shapes and frequencies; First modes: (a) 871.804 Hz. (b) 876.11 Hz. Second modes: (c) 930.042 Hz. (d) 934.45 Hz. Third modes: (e) 1035.14 Hz. (f) 1039.78 Hz. Forth modes: (g) 1199.64 Hz. (h) 1199.07 Hz. Fifth modes: (i) 1415.11 Hz. (j) 1416.35 Hz. Sixth modes: (k) 1693.93 Hz. (l) 1692.65 Hz.

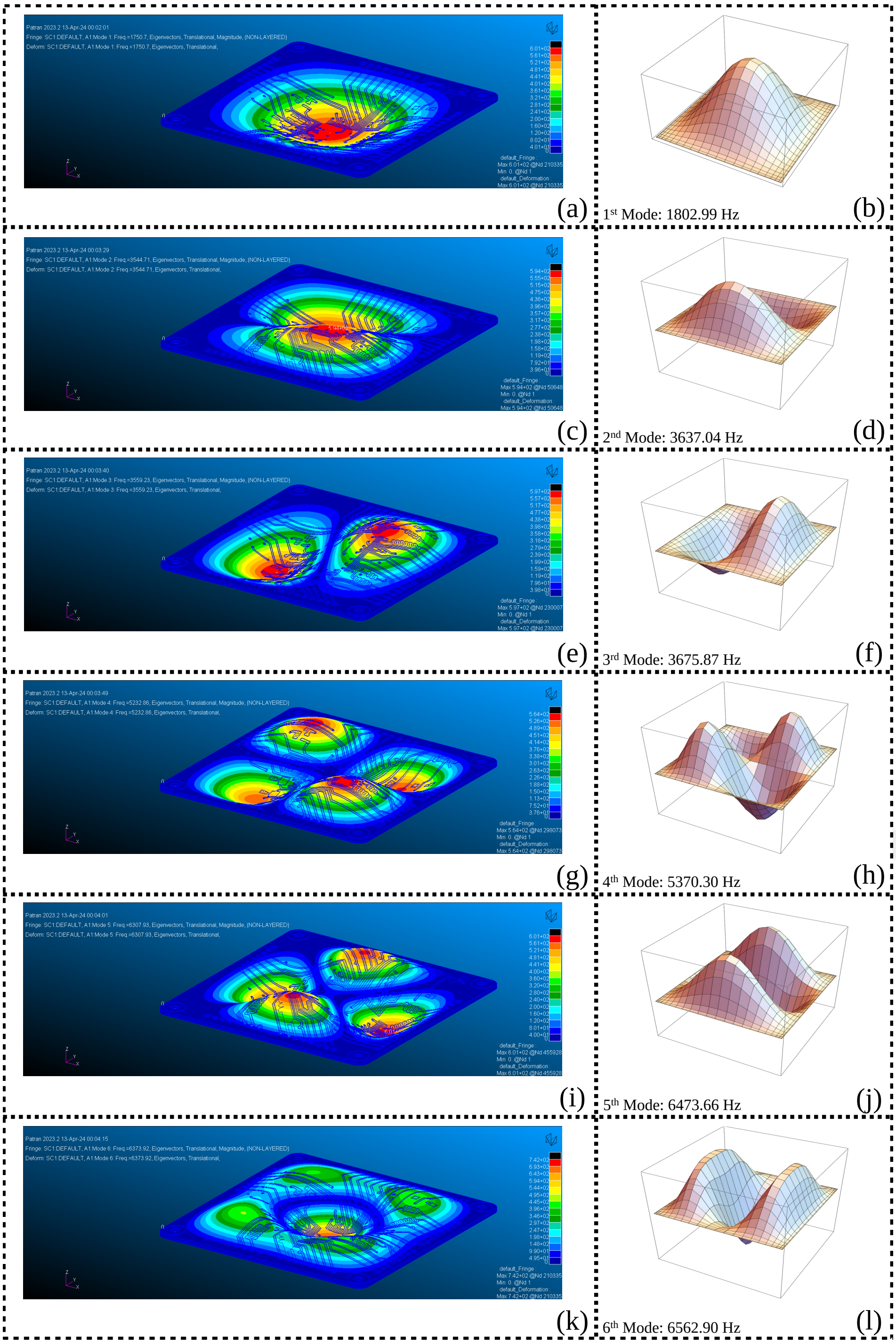

Figure 8.3 : 4-Layer PCB-001's detailed FEM and DQM analyses results mode shapes and frequencies; First modes: (a) 1750.7 Hz. (b) 1802.99 Hz. Second modes: (c) 3544.71 Hz. (d) 3637.04 Hz. Third modes: (e) 3559.23 Hz. (f) 3675.87 Hz. Forth modes: (g) 5232.86 Hz. (h) 5370.30 Hz. Fifth modes: (i) 6307.93 Hz. (j) 6473.66 Hz. Sixth modes: (k) 6373.92 Hz. (l) 6562.90 Hz.

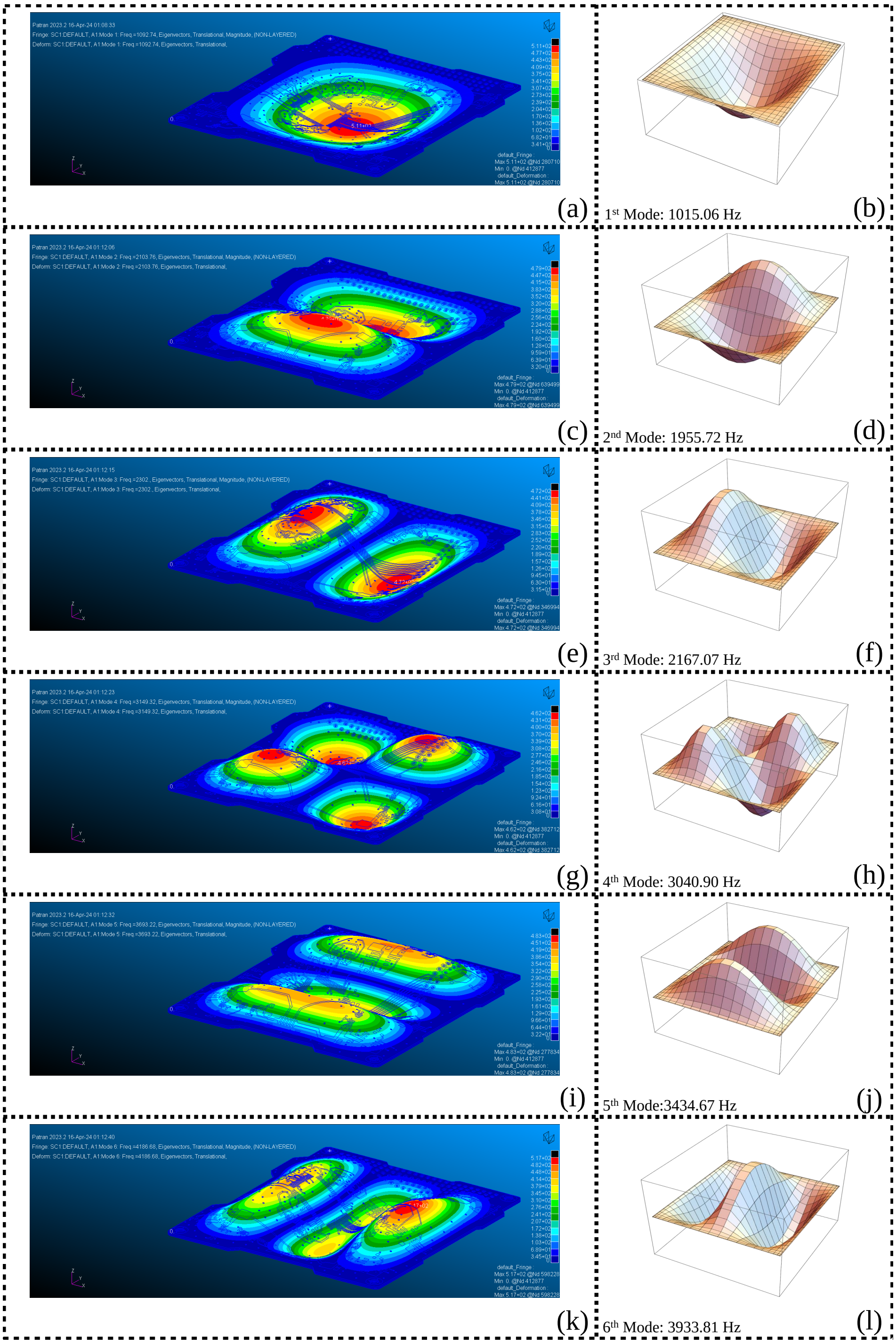

Figure 8.4 : 4-Layer PCB-002's detailed FEM and DQM analyses results mode shapes and frequencies; First modes: (a) 1092.74 Hz. (b) 1015.06 Hz. Second modes: (c) 2103.76 Hz. (d) 1955.72 Hz. Third modes: (e) 2302.00 Hz. (f) 2167.07 Hz. Forth modes: (g) 3149.32 Hz. (h) 3040.90 Hz. Fifth modes: (i) 3693.22 Hz. (j) 3434.67 Hz. Sixth modes: (k) 4186.68 Hz. (l) 3933.81 Hz.

Results of validation cases those are 6-Layer PCB-001, 6-Layer PCB-002, and 8-Layer PCB-001 are represented starting from Figure 8.5 to Figure 8.7.

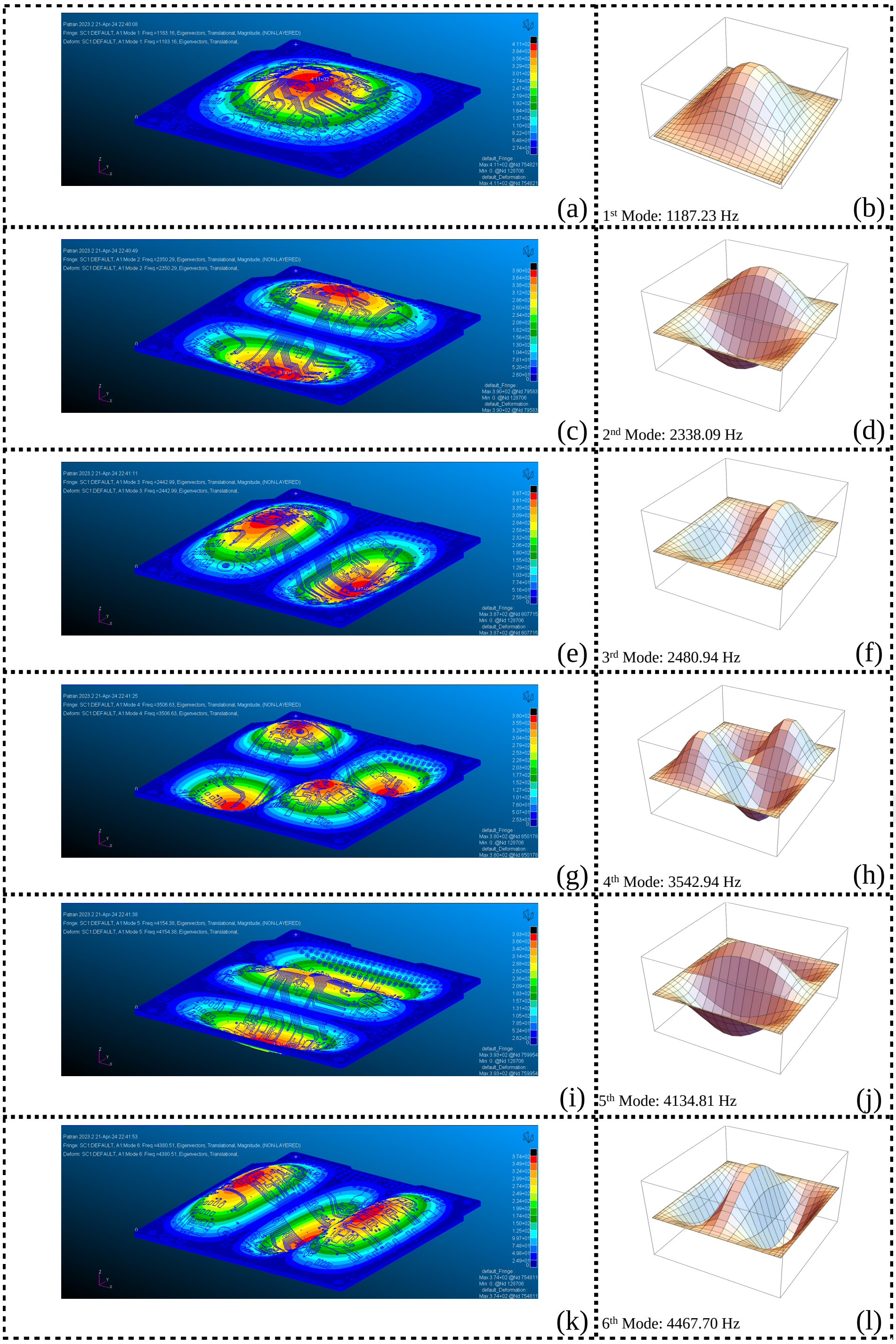

Figure 8.5 : 6-Layer PCB-001's detailed FEM and DQM analyses results mode shapes and frequencies; First modes: (a) 1183.16 Hz. (b) 1187.23 Hz. Second modes: (c) 2350.29 Hz. (d) 2338.09 Hz. Third modes: (e) 2442.99 Hz. (f) 2480.94 Hz. Forth modes: (g) 3506.63 Hz. (h) 3542.94 Hz. Fifth modes: (i) 4154.38 Hz. (j) 4134.81 Hz. Sixth modes: (k) 4380.51 Hz. (l) 4467.70 Hz.

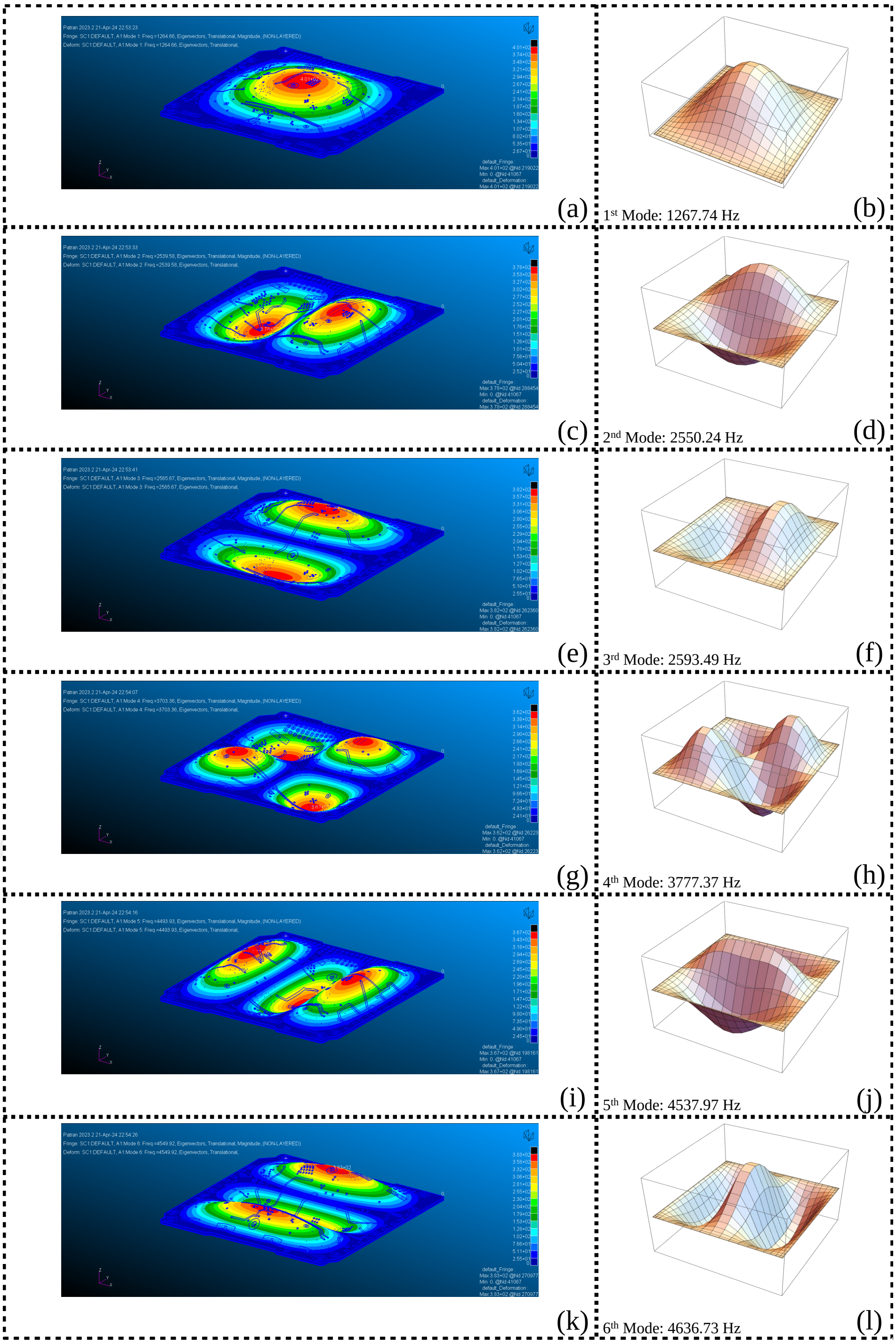

Figure 8.6 : 6-Layer PCB-002's detailed FEM and DQM analyses results mode shapes and frequencies; First modes: (a) 1264.66 Hz. (b) 1267.74 Hz. Second modes: (c) 2539.58 Hz. (d) 2550.24 Hz. Third modes: (e) 2565.67 Hz. (f) 2593.49 Hz. Forth modes: (g) 3703.36 Hz. (h) 3777.37 Hz. Fifth modes: (i) 4493.96 Hz. (j) 4537.37 Hz. Sixth modes: (k) 4549.92 Hz. (l) 4636.73 Hz.

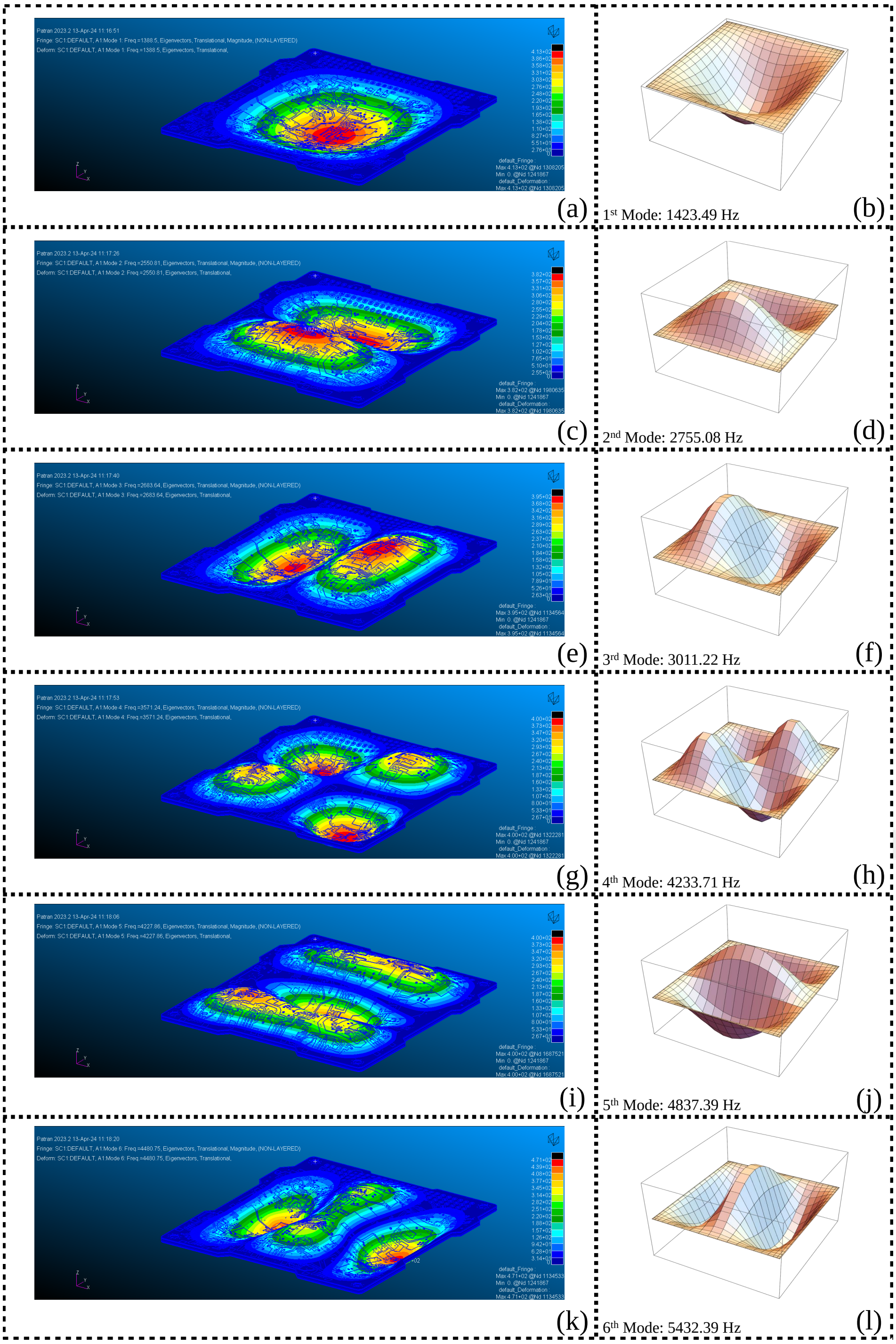

Figure 8.7 : 8-Layer PCB-001's detailed FEM and DQM analyses results mode shapes and frequencies; First modes: (a) 1388.50 Hz. (b) 1423.49 Hz. Second modes: (c) 2550.81 Hz. (d) 2755.08 Hz. Third modes: (e) 2683.64 Hz. (f) 3011.22 Hz. Forth modes: (g) 3571.24 Hz. (h) 4233.71 Hz. Fifth modes: (i) 4227.86 Hz. (j) 4837.39 Hz. Sixth modes: (k) 4480.75 Hz. (l) 5432.39 Hz.

Each model's results of values are represented in Table 9 to 15.

8.2 8-Layer Model-002 PCB Validation via FEM Analysis

In this section, 8-Layer Model-002 PCB validate according to detailed FEM model analysis.

8.2.1 Material and properties of validation model

The PCB modelled according to Table 8.1. All volume fractions are used to find equivalent material model constant. All layers equivalent material properties divided by un-voided Young's Modulus are represented on the table at last column as E_{eq}/E. These constants are achieved by using their material constant that was found at optimization section. E_{eq}/E is calculated by using equation 4.5. It is explained at Chapter 4. The average of the volume fraction is calculated as weighted according to thickness. It is around 0.837. According to this constant values, mechanical elastic properties are calculated and used elastic properties are represented at Table 17 and 18.

Table 8.1 : Equivalent Material information of 8-Layer PCB-002 validation model.

Layer Number	Material	Thickness, mm	Volume Fraction	E_{eq}/E
1	$Copper_1$	0.035	0.915	0.88
2	$FR\text{-}4_1$	0.107	0.996	1.00
3	$Copper_3$	0.018	0.924	0.90
4	$FR\text{-}4_1$	0.107	0.996	1.00
5	$Copper_5$	0.035	0.908	0.88
6	$FR\text{-}4_1$	0.071	0.996	1.00
7	$Copper_7$	0.035	0.071	0.05
8	$FR\text{-}4_1$	0.720	0.996	1.00
9	$Copper_9$	0.035	0.030	0.02
10	$FR\text{-}4_1$	0.071	0.996	1.00
11	$Copper_{11}$	0.035	0.902	0.87
12	$FR\text{-}4_1$	0.107	0.996	1.00
13	$Copper_{13}$	0.018	0.914	0.88
14	$FR\text{-}4_1$	0.107	0.996	1.00
15	$Copper_{15}$	0.035	0.923	0.90
Average	-	-	0.837	-

8.2.2 Boundary condition and contacts of validation model

All edges of the model are clamped. The boundary conditions is shown in Figure 8.8.

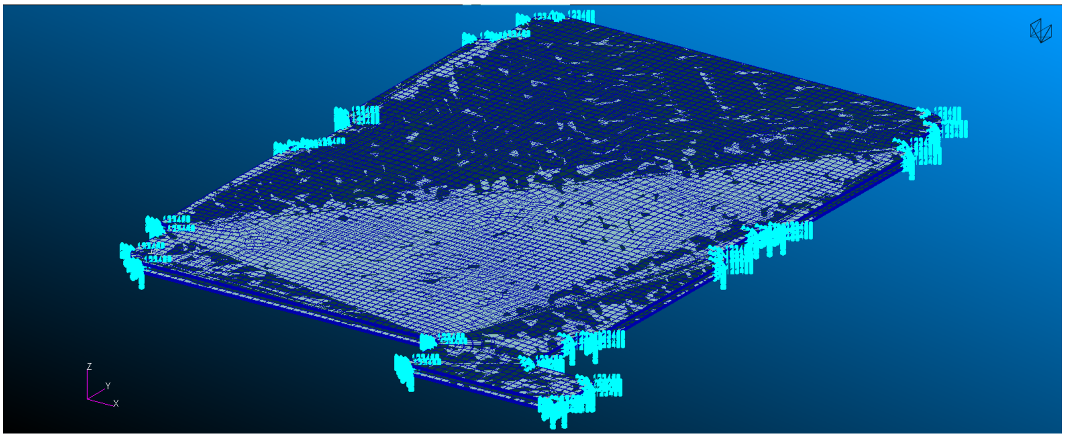

Figure 8.8 : 8-Layer PCB-002's validation case boundary condition model is shown.

8.2.3 Mesh information of 8-Layer PCB-002 validation model

The model (mesh size: 1.00 mm) is meshed with 81652 quad elements. The mesh model information is shown in Table 8.2 and its visual is shown in Figure 8.9.

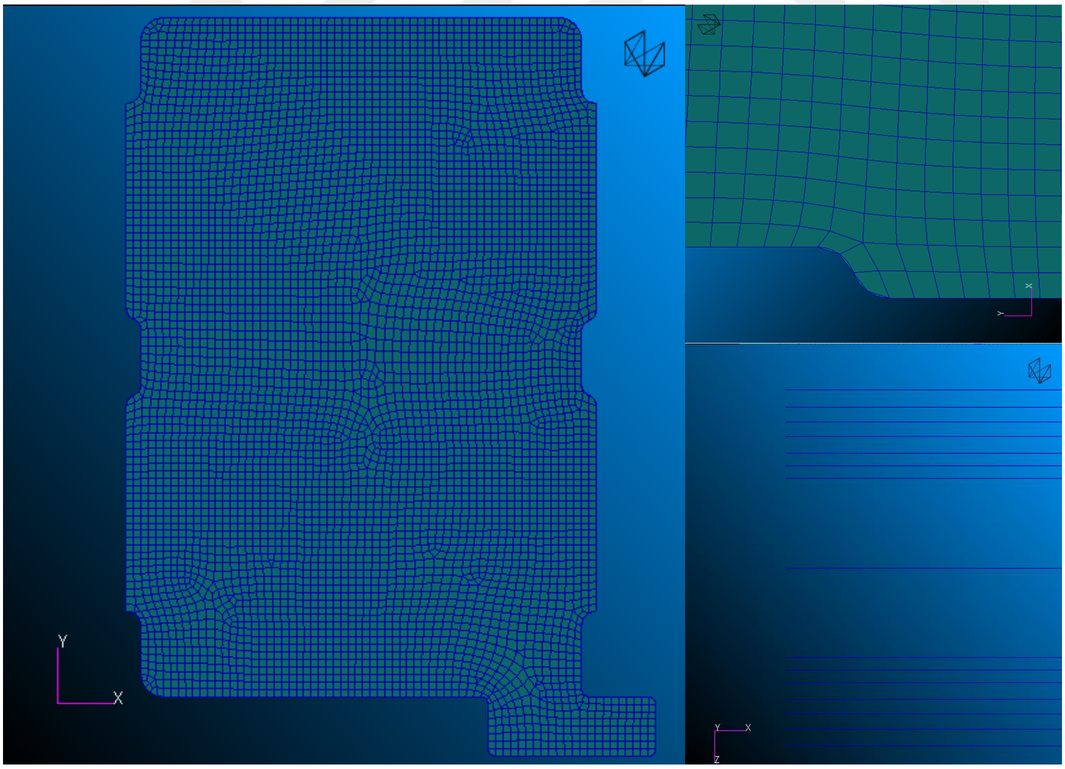

Figure 8.9 : 8-Layer PCB-002's validation mesh model is shown.

Table 8.2 : 8-Layer PCB-002's validation case mesh properties information is shown.

Property	Failed Quantity	Worst Case	Criteria
Aspect Ratio	0	Max=1.96	5
Skew Angle	0	Min=49.24	30
Normal Offset	0	Max=0.	0.15
Tangent Offset	0	Max=0.	0.15
Jacobian Ratio	0	Max=3.21	-
Jacobian Zero	0	Min=0.06	-
Taper	4	Max=0.52	0.5
Warp Angle	0	Max=0.	0.05

8.2.4 Result of 8-Layer PCB-002 validation model

The 8-Layer PCB-002 model's two different material is compared. The first analysis is a detailed FEM analysis. The second is a suggested equivalent model according to Halpin-Tsai. The third one is Voigt model is generally used as a composite element. All result values are shown in Table 16. Mode shapes and details of results of models those are detailed model, and Halpin-Tsai equivalent model are shown in Figure 8.10.

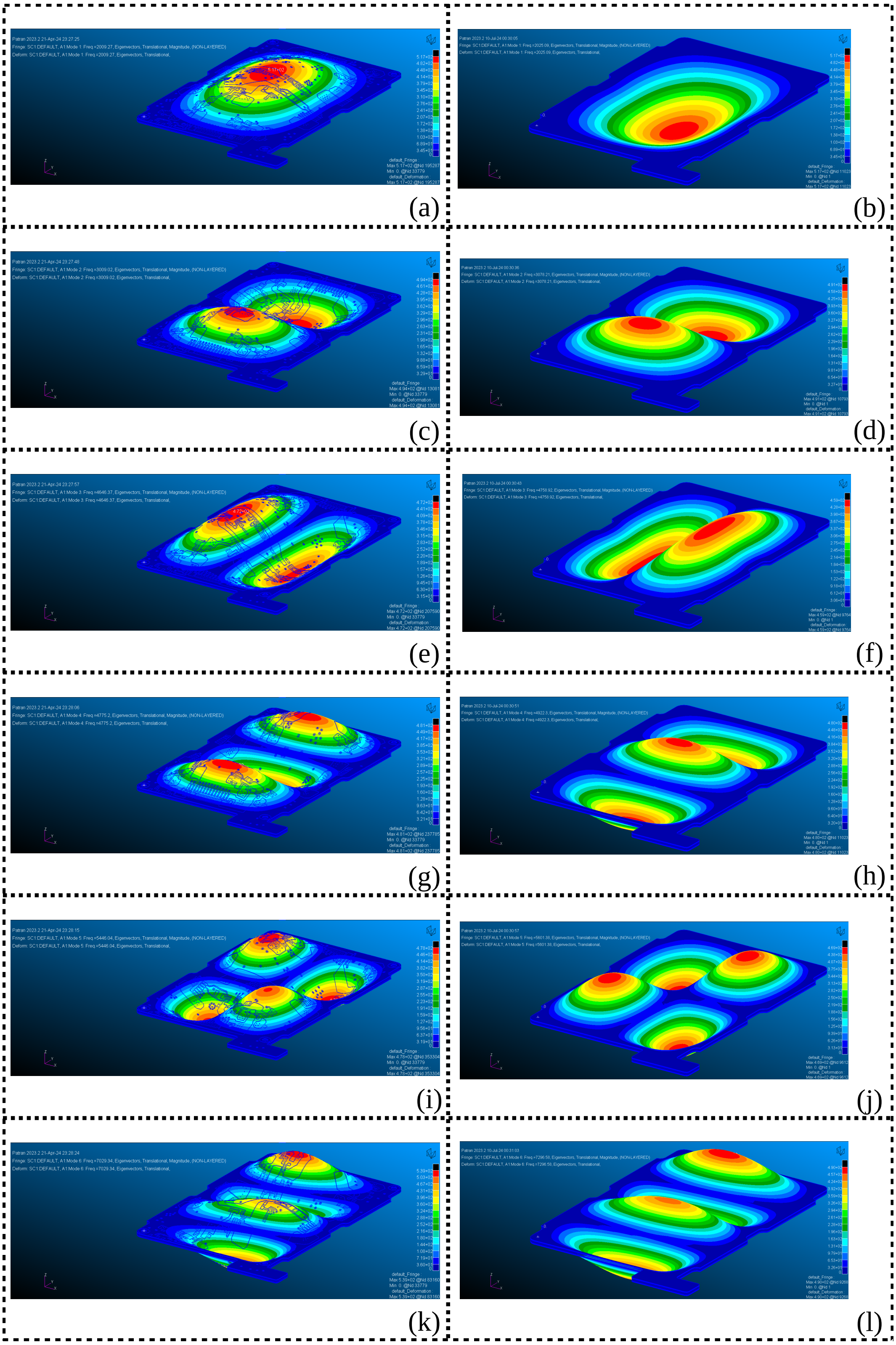

Figure 8.10 : 8-Layer PCB-002's detailed FEM and Equivalent FEM analyses results mode shapes and frequencies; First modes: (a) 2009.27 Hz. (b) 2025.09 Hz. Second modes: (c) 3009.02 Hz. (d) 3078.21 Hz. Third modes: (e) 4646.37 Hz. (f) 4758.92 Hz. Forth modes: (g) 4775.20 Hz. (h) 4922.30 Hz. Fifth modes: (i) 5446.04 Hz. (j) 5601.38 Hz. Sixth modes: (k) 7029.34 Hz. (l) 7296.58 Hz.

8.3 Discussion

Eight PCBs' results are represented in this chapter. All of them validation results those are difference between FEA detailed analysis and equivalent model analysis are represented in the graph in Figure 8.11.

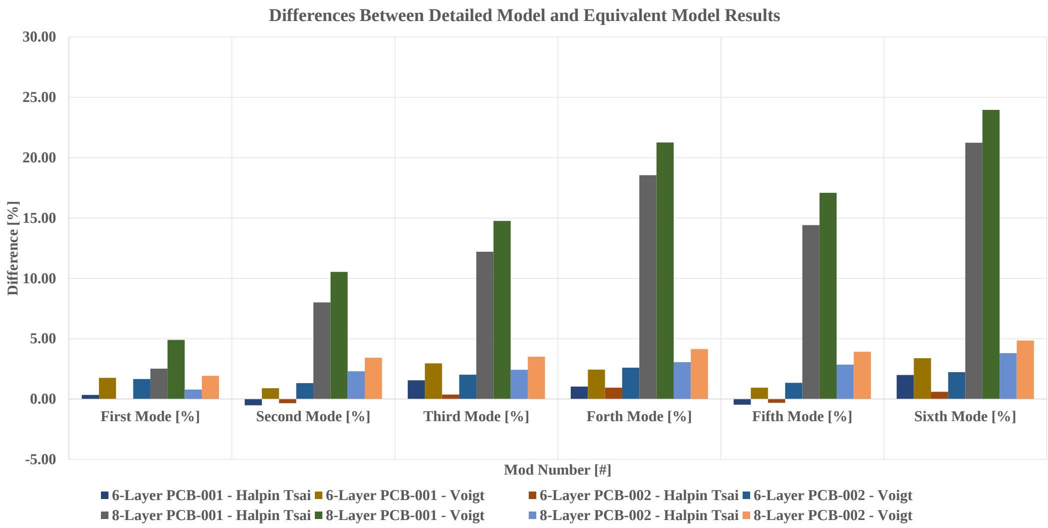

Figure 8.11 : Differences of FEM detailed modal analysis and validation analysis results with modeled equivalent material models.

Firstly, results show that equivalent material model is good representative for doing analysis instead of use detailed model PCBs. Average of the difference between detailed model and equivalent model is for all models 3.47%. This value is obtained for seven PCBs. The last validation is done different from others for 8-Layer PCB-002 because of its shape. Because of that, results comparing is separated from others. Its average of difference between detailed and equivalent model that is based Halpin-Tsai model is 2.54%. The difference between the results of the detailed model and the equivalent model is small compared to the time consumed in modeling. This provides a significant advantage for modeling an equivalent PCB instead of a detailed model.

9. CONCLUSIONS

The study suggests that equivalent models are a viable approach for FEA modeling of PCBs. While it is crucial to consider the detailed geometry of PCBs in the analysis, equivalent models offer a good balance, capturing the essential features for accurate results while reducing computational time and cost compared to detailed models. In the final validation case that was applied on the 8-Layer PCB-002 the equivalent material model is used. It shows that the results of the detailed model and the equivalent model have a small difference relative to the time saved. The maximum difference of the Halpin-Tsai model is 3.80%, and its average difference is 2.54%. When all models results are compared according to the Halpin-Tsai and Voigt models, the Halpin-Tsai model is more accurate than the Voigt model, with their differences being around 3% compared to detailed model. While the detailed model analysis of the 8-Layer PCB-002 took 28,695 seconds on a 24-CPU computer, the equivalent model analysis took 1,583 seconds on a 12-CPU computer. The consumed time decreased by approximately 94.48%.

According to the study, the elastic equivalent model can be used safely for FEA analysis. Future work can begin with expanding the database for optimization. There are two ways to expand the database. Firstly, more PCBs can be added to the database and modeled on high-performance computers. Secondly, the natural frequencies of the PCBs can be determined through testing and included in the database. Another area of study is expanding the optimization data. The optimization process currently takes too much time due to the high number of processes required to obtain results.

REFERENCES

[1] **Grout, I.**, (2008). PCB Design, Digital Systems Design with FPGAs and CPLDs, Elsevier, pp.123–176, <https://linkinghub.elsevier.com/retrieve/pii/B9780750683975000039>.

[2] **URL-1**, n-ART EPS Electric Power Subsystem, <https://gumush.com.tr/product/n-art-eps/>, date retrieved: 28.04.2024.

[3] **URL-2**, NEMA, <https://www.nema.org/>, date retrieved: 14.07.2024.

[4] **URL-3**, PCBWay, <https://www.pcbway.com/blog/Engineering_Technical/Basic_PCB_Materials.html>, date retrieved: 14.07.2024.

[5] **Nakahara, H.**, (2016). Classification of Printed Wiring Boards, **C.F. Coombs Jr. and H.T. Holden**, editors, Printed Circuits Handbook, McGraw-Hill Education, New York, 7th edition edition, pp.19–21, <https://www.accessengineeringlibrary.com/content/book/9780071833950/toc-chapter/chapter2/section/section3>.

[6] **URL-4**, IPC Simple Standards Tree 2024, <https://www.ipc.org/media/9160/download>, date retrieved: 21.04.2024.

[7] **URL-5**, ECSS Disciplines, <https://ecss.nl/standards/ecss-document-tree-and-status/>, date retrieved: 28.04.2024.

[8] **URL-6**, ECSS Q-70 Discipline, <https://ecss.nl/wp-content/uploads/2022/11/ECSS-Q-70-Branch(7Nov2022).png>, date retrieved: 28.04.2024.

[9] **Di Mauro, G.**, **Lawn, M. and Bevilacqua, R.** (2018). Survey on Guidance Navigation and Control Requirements for Spacecraft Formation-Flying Missions, *Journal of Guidance, Control, and Dynamics*, *41*(3), 581–602, <https://arc.aiaa.org/doi/10.2514/1.G002868>.

[10] **URL-7**, CubeSat Design Specification Rev. 14.1, <https://static1.squarespace.com/static/5418c831e4b0fa4ecac1bacd/t/62193b7fc9e72e0053f00910/1645820809779/CDS+REV14_1+2022-02-09.pdf>, date retrieved: 28.04.2024.

[11] **URL-8**, PocketQube Standard, <https://static1.squarespace.com/static/53d7dcdce4b07a1cdbbc08a4/t/5b34c395352f5303fcec6f45/1530184648111/PocketQube+Standard+issue+1+-+Published.pdf>, date retrieved: 28.04.2024.

[12] **URL-9**, KILICSAT 3U CubeSat, <https://www.nanosats.eu/sat/kilicsat>, date retrieved: 14.07.2024.

[13] **URL-10**, BeEagleSat 2U CubeSat, <https://usttl.itu.edu.tr/>, date retrieved: 28.04.2024.

[14] **URL-11**, BDSAT 1U CubeSat, <https://space.skyrocket.de/doc_sdat/bdsat.htm>, date retrieved: 28.04.2024.

[15] **URL-12**, SPACEBEE 0.25U CubeSat, <https://airandspace.si.edu/collection-media/NASM-B227F439DA492_005>, date retrieved: 28.04.2024.

[16] **URL-13**, FOSSASAT-1 1P PocketQube, <https://fossa.systems/our-history/>, date retrieved: 28.04.2024.

[17] **URL-14**, FOSSASAT-2 2P PocketQube, <https://github.com/FOSSASystems/FOSSASAT-2?tab=readme-ov-file>, date retrieved: 28.04.2024.

[18] **URL-15**, DELFI-PQ 3P PocketQube, <https://www.tudelft.nl/stories/articles/de-geboorte-van-de-minisatelliet-delfipq>, date retrieved: 28.04.2024.

[19] **URL-16**, MRC-100 2P PocketQube, <https://gnd.bme.hu/mrc100/>, date retrieved: 28.04.2024.

[20] **Pitarresi, J.** (1990). Modeling of printed circuit cards subject to vibration, *IEEE International Symposium on Circuits and Systems*, IEEE, pp.2104–2107, <http://ieeexplore.ieee.org/document/112213/>.

[21] **Bhavsar, N.R.**, **Shinde, H.P.**, **Bhat, M.**, **Pune, C. and Specialist, T.** (2014). Determination of Mechanical Properties of PCB, *International Journal on Mechanical Engineering and Robotics*, *2*(4), 23–27, <http://www.irdindia.in/journal_ijmer/pdf/vol2_iss4/6.pdf>.

[22] **Chippalkatti, V.S.**, **Biradar, R.C.**, **Chandrashekar, B.K. and Joteppa, S.** (2021). Estimation of equivalent mechanical properties of multi-layered PCBs based on FEA, vibration testing and analytical calculation, *AIP Conference Proceedings*, American Institute of Physics Inc., p.090020, <https://pubs.aip.org/aip/acp/article/1000800>.

[23] **Gharaibeh, M.** (2022). Identification of printed circuit boards mechanical properties using response surface methods, *Microelectronics International*, *39*(1), 38–47.

[24] **Gharaibeh, M.A.** (2024). An artificial intelligence-based approach for identifying the in-plane orthotropic mechanical properties of electronic circuit boards, *The Journal of Strain Analysis for Engineering Design*, *0*(0), 0–0, <https://journals.sagepub.com/doi/10.1177/03093247241240832>.

[25] **Morettini, G.**, **Staffa, A.**, **Mancini, E.**, **Dionigi, M.**, **Cianetti, F. and Braccesi, C.** (2022). Simplified Fe Modeling of the PyCubed PCB Complete with Components for CubeSat Missions, *Journal of Space Safety Engineering*, *9*(3), 328–340.

[26] **Wei, H. and Xu, L.** (2017). Research on dynamic model of printed circuit board based on finite element method, *AIP Conference Proceedings*, volume1864, American Institute of Physics Inc., p.020082, <https://pubs.aip.org/aip/acp/article/628748>.

[27] **Bell, J.**, **Redmond, L.**, **Carpenter, K. and de la Croix, J.P.** (2022). Finite Element Modeling of Rigid-Flex PCBs for Dynamic Environments, *Journal of Microelectronics and Electronic Packaging*, *19*(1), 25–38, <https://jmep.scholasticahq.com/article/37450>.

[28] **Fuchs, P.**, **Pinter, G. and Tonjec, M.** (2012). Determination of the orthotropic material properties of individual layers of printed circuit boards, *Microelectronics Reliability*, *52*(11), 2723–2730, <https://linkinghub.elsevier.com/retrieve/pii/S0026271412001461>.

[29] **Tunhøvd Haugan, E. and Dalsjø, P.** (2014). Characterization of the material properties of two FR4 printed circuit board laminates, **Technical Report**, Norwegian Defence Research Establishment.

[30] **Guoquan, R.**, **Ben, L.**, **Dongwei, L. and Yingqi, J.** (2015). Modal Analysis of the Printed Circuit Board Based on Finite Element Method, *Proceedings of the 2014 International Conference on Computer Science and Electronic Technology*, Atlantis Press, pp.150–154, <https://www.atlantis-press.com/article/16300>.

[31] **Lim, G.H.** (2000). Vibration Analysis of a Printed Circuit Board, *Ph.D. thesis*, Aston University.

[32] **Dash, P.K.**, **Thraza, M.M. and Babithakodavanla** (2018). Modelling and Simulation of Effect of Component Stiffness on Dynamic Behaviour of Printed Circuit Board, *International Journal of Mechanical and Production Engineering Research and Development*, *8*(2), 307–314, <http://tjprc.org/publishpapers/2-67-1519874463-34.IJMPERDAPR201834.pdf>.

[33] **Al-Araji, Z.H.**, **Swaikat, N.A.**, **Muratov, A. and Turetsky, A.V.** (2019). Modeling and Experimental Research of Vibration N Properties of A Multi-Layer Printed Circuit Board, *2019 4th Scientific International Conference Najaf (SICN)*, IEEE, IRAQ, pp.43–47, <https://ieeexplore.ieee.org/document/9019364/>.

[34] **Bachoo, R.**, **Balliram, S. and Bridge, J.** (2020). Experimental and Numerical Vibration Analysis of Printed Circuit Boards, *Proceedings of the International Conference on Emerging Trends in Engineering & Technology (IConETech-2020)*, Faculty of Engineering, The University of the West Indies, St. Augustine, pp.719–729, <http://conferences.sta.uwi.edu/iconetech2020/Abstract-RBachoo.php>.

[35] **Amy, R.A.** (2009). Efficient Design of Spacecraft Electronics to Satisfy Launch Vibration Requirements, *Ph.D. thesis*, University of Southampton, <https://eprints.soton.ac.uk/73512/1/Thesis.pdf>.

[36] **Tinca, I.E.**, **Ailinei, I.I. and Davidescu, A.** (2022). Printed Circuit Board Orthotropic Material Calibration for Static and Dynamic Loading, *2022 IEEE 9th Electronics System-Integration Technology Conference (ESTC)*, IEEE, pp.194–202, <https://ieeexplore.ieee.org/document/9939509/>.

[37] **Zhang, B.**, **Ding, H. and Sheng, X.** (2008). Modal analysis of board-level electronic package, *Microelectronic Engineering*, *85*(3), 610–620, <https://linkinghub.elsevier.com/retrieve/pii/S0167931707007368>.

[38] **Zhang, B.**, **Liu, P.k.**, **Ding, H. and Cao, W.** (2010). Modeling of board-level package by Finite Element Analysis and laser interferometer measurements, *Microelectronics Reliability*, *50*(7), 1021–1027, <https://linkinghub.elsevier.com/retrieve/pii/S0026271410001290>.

[39] **Mukind, T.W.** (2022). Investigation of the mechanical properties of printed circuit boards for nanosatellite, *Ph.D. thesis*, Cape Peninsula University of Technology, Bellville, <https://etd.cput.ac.za/handle/20.500.11838/3717>.

[40] **Fontana, F.**, **Chiocca, A.**, **Sgamma, M.**, **Bucchi, F. and Frendo, F.** (2023). Numerical-experimental Characterization of the Dynamic Behavior of PCB for the Fatigue Analysis of PCBa, *Procedia Structural Integrity*, *47*, 757–764.

[41] **Lall, P.**, **Islam, M.**, **Singh, N.**, **Suhling, J. and Darveaux, R.** (2004). Model for BGA and CSP Reliability in Automotive Underhood Applications, *IEEE Transactions on Components and Packaging Technologies*, *27*(3), 585–593, <http://ieeexplore.ieee.org/document/1331556/>.

[42] **URL-17**, Altium Designer - PCB Design Software, <https://www.altium.com/altium-designer>, date retrieved: 28.04.2024.

[43] **URL-18**, CATIA - CAD Modelling Software, <https://www.3ds.com/products/catia>, date retrieved: 28.04.2024.

[44] **URL-19**, Ansys SpaceClaim - CAD Software, <https://www.ansys.com/products/3d-design/ansys-spaceclaim>, date retrieved: 28.04.2024.

[45] **URL-20**, PATRAN - FEM Software, <https://hexagon.com/products/patran>, date retrieved: 28.04.2024.

[46] **URL-21**, MSC NASTRAN - FEM Software, <https://hexagon.com/products/product-groups/computer-aided-engineering-software/msc-nastran>, date retrieved: 28.04.2024.

[47] **URL-22**, (2021), Mechanical Products, Ansys, <https://www.ansys.com/resource-center/webinar/ansys-2021-r2-whats-new-with-ansys-mechanical>, date retrieved: 13.07.2024.

[48] **Tognana, S.**, **Pomarico, M.**, **Montecinos, S. and Salgueiro, W.** (2023). Application of composite material models to determine the Young's modulus of the grid pattern of partially infilled 3D printed samples, *Engineering Research Express*, *5*(4), 045049, <https://iopscience.iop.org/article/10.1088/2631-8695/ad0929>.

[49] **Kerner, E.H.** (1956). The Elastic and Thermo-elastic Properties of Composite Media, *Proceedings of the Physical Society. Section B*, *69*(8), 808–813, <https://iopscience.iop.org/article/10.1088/0370-1301/69/8/305>.

[50] **Arikoglu, A. and Ozkol, I.** (2012). Vibration Analysis of Composite Sandwich Plates by the Generalized Differential Quadrature Method, *AIAA Journal*, *50*(3), 620–630, <https://arc.aiaa.org/doi/10.2514/1.J051287>.

APPENDICES

APPENDIX A : FEM Analysis Results
APPENDIX B : Optimization and Validation Results
APPENDIX C : Equivalent Material Elastic Properties of 8-Layer PCB-002

APPENDIX A :FEM Analysis Results

Table 1 : 2-Layer PCB-001's results of modal analysis.

Mesh Size, mm	1^{st} Mode, Hz	2^{nd} Mode, Hz	3^{rd} Mode, Hz	4^{th} Mode, Hz	5^{th} Mode, Hz	6^{th} Mode, Hz
1.00[1]	869.03	1749.78	1788.71	2639.40	3117.08	3218.90
0.50[2]	863.51	1739.53	1777.97	2620.37	3100.15	3202.06

Table 2 : 2-Layer PCB-002's results of modal analysis.

Mesh Size, mm	1^{st} Mode, Hz	2^{nd} Mode, Hz	3^{rd} Mode, Hz	4^{th} Mode, Hz	5^{th} Mode, Hz	6^{th} Mode, Hz
1.00[3]	886.93	947.12	1055.13	1225.14	1447.72	1735.80
0.50[4]	872.40	930.96	1036.52	1202.04	1418.70	1698.93
0.25[5]	871.80	930.04	1035.14	1199.64	1415.11	1693.93

Table 3 : 4-Layer PCB-001's results of modal analysis.

Mesh Size, mm	1^{st} Mode, Hz	2^{nd} Mode, Hz	3^{rd} Mode, Hz	4^{th} Mode, Hz	5^{th} Mode, Hz	6^{th} Mode, Hz
1.00[6]	1829.10	3703.51	3721.32	5466.22	6560.90	6634.38
0.50[7]	1762.16	3562.20	3571.67	5247.88	6320.61	6388.35
0.25[8]	1750.70	3544.71	3559.23	5232.86	6307.93	6373.92

[1]Solved by using a computer has 6 cores 32GB RAM in 78 seconds.
[2]Solved by using a computer has 6 cores 32GB RAM in 262 seconds.
[3]Solved by using a computer has 6 cores 32GB RAM in 1453 seconds.
[4]Solved by using a computer has 6 cores 32GB RAM in 12437 seconds.
[5]Solved by using a computer has 12 cores 64GB RAM in 91902 seconds.

Table 4 : 4-Layer PCB-002's results of modal analysis.

Mesh Size, mm	1^{st} Mode, Hz	2^{nd} Mode, Hz	3^{rd} Mode, Hz	4^{th} Mode, Hz	5^{th} Mode, Hz	6^{th} Mode, Hz
1.00[9]	1112.63	2128.22	2334.53	3176.69	3714.68	4213.20
0.50[10]	1093.56	2102.57	2297.49	3141.20	3682.77	4169.60
0.25[11]	1092.74	2103.76	2302.00	3149.32	3693.22	4186.68

Table 5 : 6-Layer PCB-001's results of modal analysis.

Mesh Size, mm	1^{st} Mode, Hz	2^{nd} Mode, Hz	3^{rd} Mode, Hz	4^{th} Mode, Hz	5^{th} Mode, Hz	6^{th} Mode, Hz
1.00[12]	1221.37	2410.26	2484.88	3542.92	4206.42	4373.13
0.50[13]	1181.71	2337.08	2423.25	3467.07	4103.54	4314.20
0.25[14]	1183.16	2350.29	2442.99	3506.63	4154.38	4380.51

[6] Solved by using a computer has 6 cores 32GB RAM in 3197 seconds.
[7] Solved by using a computer has 6 cores 32GB RAM in 14027 seconds.
[8] Solved by using a computer has 6 cores 32GB RAM in 126670 seconds.
[9] Solved by using a computer has 6 cores 32GB RAM in 212 seconds.
[10] Solved by using a computer has 6 cores 32GB RAM in 1009 seconds.
[11] Solved by using a computer has 6 cores 32GB RAM in 8964 seconds.
[12] Solved by using a computer has 6 cores 32GB RAM in 6270 seconds.
[13] Solved by using a computer has 12 cores 64GB RAM in 31219 seconds.
[14] Solved by using a computer has 12 cores 64GB RAM in 240606 seconds.
[15] Solved by using a computer has 6 cores 32GB RAM in 2615 seconds.
[16] Solved by using a computer has 12 cores 64GB RAM in 31721 seconds.
[17] Solved by using a computer has 12 cores 64GB RAM in 321265 seconds.

Table 6 : 6-Layer PCB-002's results of modal analysis.

Mesh Size, mm	1^{st} Mode, Hz	2^{nd} Mode, Hz	3^{rd} Mode, Hz	4^{th} Mode, Hz	5^{th} Mode, Hz	6^{th} Mode, Hz
1.00[15]	1287.75	2551.94	2602.97	3717.97	4455.96	4587.13
0.50[16]	1264.66	2539.58	2565.67	3703.36	4493.93	4549.92
0.25[17]	1267.84	2559.14	2583.81	3742.18	4552.23	4608.98

Table 7 : 8-Layer PCB-001's results of modal analysis.

Mesh Size, mm	1^{st} Mode, Hz	2^{nd} Mode, Hz	3^{rd} Mode, Hz	4^{th} Mode, Hz	5^{th} Mode, Hz	6^{th} Mode, Hz
1.00[18]	1392.45	2530.91	2674.23	3544.88	4153.65	4451.52
0.50[19]	1388.50	2550.81	2683.64	3571.24	4227.86	4480.75

Table 8 : 8-Layer PCB-002's results of modal analysis.

Mesh Size, mm	1^{st} Mode, Hz	2^{nd} Mode, Hz	3^{rd} Mode, Hz	4^{th} Mode, Hz	5^{th} Mode, Hz	6^{th} Mode, Hz
1.00[20]	2071.31	3062.08	4672.39	4816.39	5487.42	7003.99
0.50[21]	2009.27	3009.02	4646.37	4776.20	5446.04	7029.34

[18] Solved by using a computer has 6 cores 32GB RAM in 9595 seconds.
[19] Solved by using a computer has 12 cores 64GB RAM in 91010 seconds.
[20] Solved by using a computer has 6 cores 32GB RAM in 4917 seconds.
[21] Solved by using a computer has 12 cores 64GB RAM in 28695 seconds.

APPENDIX B : Optimization and Validation Results

Table 9 : 2-Layer PCB-001's modal results differences between detailed FEM and Halpin-Tsai model DQM.

Mode Number	Detailed Model [Hz]	Halpin-Tsai Model [Hz]	Difference [%]
1^{st}	863.51	864.37	0.10
2^{nd}	1739.53	1722.83	-0.96
3^{rd}	1777.97	1793.80	0.89
4^{th}	2620.37	2595.41	-0.95
5^{th}	3100.15	3063.00	-1.20
6^{th}	3202.06	3230.73	0.90
Average	-	-	0.83

Table 10 : 2-Layer PCB-002's modal results differences between detailed FEM and Halpin-Tsai model DQM.

Mode Number	Detailed Model [Hz]	Halpin-Tsai Model [Hz]	Difference [%]
1^{st}	871.80	876.11	0.49
2^{nd}	930.04	934.45	0.47
3^{rd}	1035.14	1039.78	0.45
4^{th}	1199.64	1199.07	-0.05
5^{th}	1415.11	1416.35	0.09
6^{th}	1693.93	1692.65	-0.08
Average	-	-	0.27

Table 11 : 4-Layer PCB-001's modal results differences between detailed FEM and Halpin-Tsai model DQM.

Mode Number	Detailed Model [Hz]	Halpin-Tsai Model [Hz]	Difference [%]
1^{st}	1750.70	1802.99	2.99
2^{nd}	3544.71	3637.04	2.60
3^{rd}	3559.23	3675.87	3.28
4^{th}	5232.86	5370.30	2.63
5^{th}	6307.93	6473.66	2.63
6^{th}	6373.92	6562.90	2.96
Average	-	-	2.85

Table 12 : 4-Layer PCB-002's modal results differences between detailed FEM and Halpin-Tsai model DQM.

Mode Number	Detailed Model [Hz]	Halpin-Tsai Model [Hz]	Difference [%]
1^{st}	1092.74	1015.06	-7.11
2^{nd}	2103.76	1955.72	-7.04
3^{rd}	2302.00	2167.07	-5.86
4^{th}	3149.32	3040.90	-3.44
5^{th}	3693.22	3434.67	-7.00
6^{th}	4186.68	3933.81	-6.04
Average	-	-	6.08

Table 13 : 6-Layer PCB-001's modal results differences between detailed FEM and Halpin-Tsai and Voigt models DQM.

Mode Number	Detailed Model [Hz]	Halpin-Tsai Model [Hz]	Difference [%]	Voigt Model [Hz]	Difference [%]
1^{st}	1183.16	1187.23	0.34	1203.98	1.76
2^{nd}	2350.29	2338.09	-0.52	2371.34	0.90
3^{rd}	2442.99	2480.94	1.55	2515.27	2.96
4^{th}	3506.63	3542.94	1.04	3592.18	2.44
5^{th}	4154.38	4134.81	-0.47	4193.50	0.94
6^{th}	4380.51	4467.70	1.99	4528.66	3.38
Average	-	-	0.99	-	2.06

Table 14 : 6-Layer PCB-002's modal results differences between detailed FEM and Halpin-Tsai and Voigt models DQM.

Mode Number	Detailed Model [Hz]	Halpin-Tsai Model [Hz]	Difference [%]	Voigt Model [Hz]	Difference [%]
1^{st}	1267.84	1267.74	-0.01	1288.94	1.66
2^{nd}	2559.14	2550.24	-0.35	2593.02	1.32
3^{rd}	2583.81	2593.49	0.37	2636.03	2.02
4^{th}	3742.18	3777.37	0.94	3839.41	2.60
5^{th}	4552.23	4537.97	-0.31	4613.61	1.35
6^{th}	4608.98	4636.73	0.60	4711.65	2.23
Average	-	-	0.43	-	1.86

Table 15 : 8-Layer PCB-001's modal results differences between detailed FEM and Halpin-Tsai and Voigt models DQM.

Mode Number	Detailed Model [Hz]	Halpin-Tsai Model [Hz]	Difference [%]	Voigt Model [Hz]	Difference [%]
1^{st}	1388.50	1423.49	2.52	1456.47	4.90
2^{nd}	2550.81	2755.08	8.01	2819.40	10.53
3^{rd}	2683.64	3011.22	12.21	3079.61	14.75
4^{th}	3571.24	4233.71	18.55	4330.26	21.25
5^{th}	4227.86	4837.39	14.42	4950.13	17.08
6^{th}	4480.75	5432.39	21.24	5553.97	23.95
Average	-	-	12.82	-	15.41

Table 16 : 8-Layer PCB-002's modal results differences between detailed FEM and Halpin-Tsai and Voigt models FEM.

Mode Number	Detailed Model [Hz]	Halpin-Tsai Model [Hz]	Difference [%]	Voigt Model [Hz]	Difference [%]
1^{st}	2009.27	2025.09	0.79	2047.92	1.92
2^{nd}	3009.02	3078.21	2.30	3111.93	3.42
3^{rd}	4646.37	4758.92	2.42	4809.41	3.51
4^{th}	4776.20	4922.30	3.06	4974.27	4.15
5^{th}	5446.04	5601.38	2.85	5659.62	3.92
6^{th}	7029.34	7296.58	3.80	7370.15	4.85
Average	-	-	2.54	-	3.63

APPENDIX C : Equivalent Material Elastic Properties of 8-Layer PCB-002

Table 17 : 8-Layer PCB-002's equivalence material properties for copper layers.

Properties	$Copper_1$	$Copper_3$	$Copper_5$	$Copper_7$	$Copper_9$	$Copper_{11}$	$Copper_{13}$	$Copper_{15}$
E $[MPa]$	111442.95	112935.74	110276.42	6545.47	2679.84	109305.82	111316.25	112791.24
G $[MPa]$	41428.47	41983.41	40994.82	2433.25	996.22	40634.01	41381.37	41929.70
ρ $[kg/m^3]$	8178.49	8259.17	8115.05	636.75	263.86	8062.00	8171.62	8251.39
v	0.345	0.345	0.345	0.345	0.345	0.345	0.345	0.345

Table 18 : 8-Layer PCB-002's equivalence material properties for FR-4 layers.

Properties	FR-$4_{Alllayers}$
$E_{11}[MPa]$	20324.58
$E_{22}[MPa]$	18331.97
$G_{12}[MPa]$	9165.99
$G_{23}[MPa]$	8368.94
$G_{13}[MPa]$	6575.60
$\rho[kg/m^3]$	1892.98
v_{11}	0.11

CURRICULUM VITAE

Name SURNAME: Erdinç YAKUT

EDUCATION:

- **B.Sc.:** 2014, Istanbul Technical University, Faculty of Aeronautical and Astronautical Engineering, Department of Astronautical Engineering

PROFESSIONAL EXPERIENCE AND REWARDS:

- **Mechanical Systems Supervisor**
  GUMUSH AeroSpace
  Aug 2016 - Present (8 years)
  - Responsible for the mechanical systems of satellites
  - Experienced in design, analysis, production, integration, testing, and launch preparations.
  - Projects involved:
    - n-ART a-IoT / Aug 2022 - Present
    - KILIÇSAT 3U-CubeSat / Nov 2018 - Sep 2023 / Launched in Apr 2023
    - SSS-2B 3U-CubeSat / Sep 2015 - Jun 2023 / Launched in Apr 2023
    - ASELSAT 3U-CubeSat / Jan 2016 - Jan 2021 / Launched in Jan 2021
    - TURKSAT 6A-TTR Subsystem Mechanical and Thermal Design / Feb 2016 - Dec 2019 / Launched in July 2024

- **Research and Development Mechanical Engineer**
  Aug 2014 - Aug 2016 (2 years, 1 month)
  - Contributed to BeEagleSat 2U-CubeSat (QB50) / Jan 2014 - Apr 2017 / Launched in Apr 2017
  - Contributed to HAVELSAT 2U-CubeSat (QB50) / Jan 2014 - Apr 2017 / Launched in Apr 2017

- **Assistant Mechanical Engineer**
  Jun 2012 - Aug 2014 (2 years, 3 months)
  - Contributed to TURKSAT-3USAT / Jun 2012 - Apr 2013 / Launched in Apr 2013

PUBLICATIONS, PRESENTATIONS AND PATENTS ON THE THESIS:

- **Yakut E.**, **Arıkoğlu A.** (2024). Determining Equivalent Mechanical Properties of Printed Circuit Board for Preliminary Design Modelling of CubeSat. International Graduate Research Symposium, May 8-10, 2024 Istanbul, Turkey.

OTHER PUBLICATIONS, PRESENTATIONS AND PATENTS:

- **Uludag**, **S.**, **Yakut**, **E.**, **Speretta**, **S.**, **Radu**, **S.**, **Chronas Foteinakis**, **N.**, **Bouwmeester**, **J.**, **Menicucci**, **A.**,& **Gill**, **E.**, Getting the Delfi-PQ Ready for Multiple Launch Options. In Proceedings of the International Symposium on Space Technology and Science, Fukui (Japan), June 15th-21st, 2019 Article 2019-f-08
- **A.R. Aslan**, **A.Y. Ozyildirim**, **M. Suer**, **O. Sarı**, **M.E. Bas**, **E. Yakut**, **M.S. Uludag**, **B. Karabulut**, **M.D. Aksulu**, **E. Erdogan**, **S. Turkoglu**, **M. Karatas**, **C. Cenik**, ASELSAT: High Resolution High Speed Cubesat, 7th Nanosatellite Symposium, Varna, Bulgaria, 18-23 October 2016
- **A.R. Aslan**, **B. Karabulut**, **M.S. Uludag**, **M.E. Bas**, **E. Yakut**, **M.D. Aksulu**, **S. Turkoglu**, **M. Karatas**, **C. Cenik**, **M. Suer**, **İ. Arslan**, **K. Arslankoz**, BEAGLESAT and HAVELSAT: Two 2U CubeSat's for QB50, 7th Nanosatellite Symposium, Varna, Bulgaria, 18-23 October 2016.
- **Yakut**, **E.**, **Çilden**, **D.**, **Oran**, **C.**, **Erdogan**, **E.**, Meteorological Observations and Establishing a Base for Future Mars Missions, 11th International Planetary Probe Workshop, Pasadena, California, USA, 16-20 June 2014.
- **A. Rustem Aslan**, **Mengu Cho**, **M. Sevket Uludag**, **Bogac Karabulut**, **M. Erdem Bas**, **M. Deniz Aksulu**, **Mustafa Karatas**, **Erdinc Yakut**, **Murat Suer**, **Baris Dinc**, The Integration and Testing of UBAKUSAT, 3rd IAA Conference On University Satellite Missions And Cubesat Workshop, Rome, Italy, 30 November – 05 December 2015
- **E. Yakut**, **M. Suer**, **M.S. Uludag**, **E. Bas**, **S. Turkoglu**, **A.R. Aslan**, **A. Hacıoglu**, **M. Çelebi**, **M.E. Aydemir**, **S. Basturk**, **A. Telli**, **S. Gokcebag**, QB50 - BeEagleSat Inner - Outer Design Details and ADCS Testing-Integration, 7th European CubeSat Symposium, Liège, Belgium, 9 – 11 September 2015
- **A. Rustem Aslan**, **Mansur Celebi**, **Ahmet Sofyalı**, **Sibel Türkoglu**, **M. Sevket Uludag**, **I. Eray Akyol**, **M. Deniz Aksulu**, **Erdinc Yakut**, **Murat Süer**, **Serhan Gökçebag**, **M. Erdem Bas**, The Integration and Testing of BeEagleSat, 30th International Symposium on Space Technology and Science, Kobe-Hyogo Japan, (30th ISTS)(6th NSAT) , 4-10 July 2015
- **Süer**, **M.**, **Yakut**, **E.**, **Oran**, **C.** & **Aslan**, **A.R.**, NART – Nano Küp Uydular için Boyutlandırılabilir Modüler Uydu Yapısı Alt Sistemi, V. Ulusal Havacılık ve Uzay Konferansı, September 2014., Kayseri, Turkey.
- **Demet Çilden**, **Erdinç Yakut**, **Cem Oran**, CubeSat Technology on Titan Exploration, 10th International Planetary Probe Workshop, San Jose, California, USA, 17 - 21 June 2013.
- **Aslan**, **R.**, **Yagci**, **H.B.**, **Umit**, **M.E.**, **Sofyalı**, **A.**, **Bas**, **M.E.**, **Uludag**, **M.S.**, **Ozen**, **O.E.**, **Aksulu**, **M.D.**, **Yakut**, **E.**, **Oran**, **C.**, **Suer**, **M.**, **Akyol**, **I.E.**, **Ecevit**, **A.B.**, **Ersoz**, **M.S.**, **Öz**, **I.**, **Gulgonul**, **S.**, **Dinc**, **B.**, **Dengiz**, **T.**,Development of a LEO Communication CubeSat, 6th International Conference Series on Recent Advances in Space Technologies-RAST, June 2013